ISRAPS
Bulletin

ISRAPS

Guest Editor
Dr. Sriram Kanvah

A Publication of
Indian Society for
Radiation and Photochemical Sciences

Message from the President and Secretary, ISRAPS

Dear ISRAPS members,

Greetings from the ISRAPS Executive Council!

We take this opportunity to acknowledge the contribution of all the members who have participated in organizing various activities of ISRAPS.

Now, as the world crawls out of the pandemic situation, we are finally starting to see the return of in-person events. Keeping with this trend, we are trying to arrange the discussion meetings and symposia in hybrid mode. Recently, we have successfully organized ISRAPS One-day Seminar (hybrid mode) on "Societal Applications of Radiation Chemistry" on June 10, 2022, at North- Eastern Hill University (NEHU), Shillong.

ISRAPS also brings out bulletin which is an important medium for dissemination of information on frontier research in the field of Radiation and Photochemistry. This edition is a collection of articles about the recent developments in the field of photochemistry from the eminent speakers invited to National Symposium on Radiation and Photochemistry (NSRP-2021), which was held virtually at IIT Gandhinagar during June 25-26, 2021. The Executive council of ISRAPS takes this opportunity to thank the authors for making this issue very informative. We would also like to thank Prof. Sriram Kanvah Gundimeda, the Guest Editor of this issue, for his efforts to bring out a scientifically rich bulletin.

We would also like to inform ISRAPS members about the forthcoming NSRP-2023 under the ISRAPS flagship. NSRP-2023 will be held during 5-7 January 2023 at BITS Pilani, K. K. Birla Campus, Goa. We request all the researchers in this field to join hands to make it a grand success.

Finally, on behalf of the ISRAPS executive council, we wish to express our sincere gratitude to all the members of ISRAPS for their continued support and encouragement in carrying out the activities of the society. We also look forward to your valuable suggestions and active participation in the forthcoming events of ISRAPS.

Dr. Awadhesh Kumar
President

Dr. (Mrs.) J. Mohanty
Secretary

ISRAPS

INDIAN SOCIETY FOR RADIATION AND PHOTOCHEMICAL SCIENCES (ISRAPS)

EXECUTIVE COUNCIL (2021-2023)

President

Dr. Awadhesh Kumar

Vice-Presidents

Prof. C. T. Aravindakumar

Prof. A. S. Kumbhar

Secretary

Dr. (Mrs.) J. Mohanty

Jt. Secretary

Dr. P. Mathi

Treasurer

Dr. Atanu Barik

Executive Members

Dr. N. Choudhury	Dr. G. R. Dey	Prof. K. R. Genwa
Prof. S. K. Gundimeda	Dr. Virendra Kumar	Dr. M. Kumbhakar
Dr. M. C. Rath	Dr. (Mrs.) S. Sen Gupta	Dr. P. Sharma
Dr. V. S. Tripathi	Dr. P. D. Naik	Dr. A. C. Bhasikuttan

Co-opted Members

Prof. Santosh Chidangil	Prof. Anindya Datta	Dr. S. Dutta Choudhury
Prof. J. P. Mittal	Dr. D. B. Naik	Dr. C. N. Patra
Dr. R. Puspalata	Dr. S. K. Sarkar	Prof. K. K. Sharma
Prof. A. K. Singh	Dr. Avesh K. Tyagi	Prof. S. Wategaonkar

Web Master

Dr. Abhishek Das

Contact details:

C/o Radiation & Photochemistry Division

Bhabha Atomic Research Centre, Mumbai-400085

E-mail: israps.secretary@gmail.com

Telephone:(022)- 25593771/25592668/25590302

Editor's Desk...

Light-induced processes have attracted immense attention across interdisciplinary research areas involving chemistry, materials science, and the biological domain. Indian Society of Radiation and Photochemical Sciences (ISRAPS) aims to foster research in these domains by organizing several symposia, workshops, and meetings. In 2021, we organized National Symposium on Radiation and Photochemistry (NSRP) virtually, where several eminent scientists have delivered excellent scientific deliberations. Continuing the rich tradition of ISRAPS to bring forth a special issue after every national or international meeting, I am honored to guest-edit a special issue ISRAPS bulletin-2021 containing articles on contemporary research areas in the field of radiation and photochemical sciences. The current issue has five articles. The first article discusses the synthesis, photophysical and electrochemical properties of diketopyrrolopyrroles substituted with electron-donating groups and could provide avenues for developing newer organic materials for organic electronic applications. The second article discusses the commonly available sensing strategies for detecting Heparin, an anionic polysaccharide, and a widely used anticoagulant during surgical procedures. The third article discusses the photophysical properties, particularly the preferential solvation of 5-amino quinoline in binary solvent mixtures, and highlights various solute-solvent interactions. The fourth article summarizes the understanding of exciton diffusion and deactivation pathways in phenyl and phenylethynyl derivatives of anthracene. The article also discusses the substituent-dependent formation of the excimer state or dissociation to the triplet pair state. Finally, the last article discusses various fluorescence sensors with coumarin scaffolds to detect various ionic analytes of environmental relevance. On behalf of ISRAPS, I sincerely acknowledge the cooperation from all the contributing authors on this issue. I take this opportunity to thank ISRAPS for giving me the guest editorial responsibility.

Dr. Sriram Kanvah *obtained his Ph.D. in Chemistry from the Indian Institute of Technology Bombay, Mumbai. He was a post-doctoral fellow with Prof. Gary Schuster at Georgia Institute of Technology Atlanta and worked as a research-intellectual property analyst at General Electric Company Bangalore. After that, he joined IIT-Gandhinagar, Discipline of Chemistry, in Dec 2009. His groups research interests are in synthesizing and developing photoresponsive systems for organic electronics, biological imaging, and chemosensing applications. So far their research group graduated 7 PhD students and guided dissertation projects of several MSc students. Apart from the research, Sriram gives several lecture-demos to school students and teachers to promote science awareness..*

Contents

Donor Functionalized bis(thienyl)diketopyrrolopyrroles: Photophysical and Electrochemical properties

Faizal Khan[+], Yogajivan Rout[+], Rajneesh Misra*

(*[+]Authors contributed equally*)
Department of Chemistry, Indian Institute of Technology Indore, Indore- 453552, India
* Email: rajneeshmisra@iiti.ac.in

Abstract

Diketopyrrolopyrrole (DPP) is a π-conjugated bicyclic bis(lactam) ring, having strong electron accepting nature and exceptional photochemical and thermal stability. The modification of donor functionalized DPPs with tetracyanoethylene (TCNE) results in improved acceptor strength and the resultant molecular system shows absorption in the near infra-red region. The 1,1,4,4-tetracyanobutadiene (TCBD) functionalized DPPs show applications in organic photovoltaic, nonlinear optics, and bio-imaging. In this article, we have discussed about the synthesis of donor–acceptor based DPP chromophores and, the effect of various donor/acceptor moieties on the photophysical and electrochemical properties.

Introduction

The organic small molecules with absorption in the visible to near-infrared (vis-NIR) region have attracted considerable research interest owing to their potential applications in organic photovoltaics (OPVs), dye sensitized solar cells (DSSCs), nonlinear optics (NLOs), organic light emitting diodes (OLEDs), and organic field effect transistor (OFETs).[1-3] The π-conjugated organic chromophores are an interesting class of materials, which can be easily synthesized and absorb light in vis-NIR region. Diketopyrrolopyrrole (DPP) has attracted great deal of attention in last few years due to its strong electron accepting nature, exceptional photochemical, thermal stabilities, and applications in materials chemistry.[4,5] In 1974, DPP was first discovered by Farnum *et al.* and further its synthetic procedure was modified by Iqbal, Cassar, and Rochat in the early 1980s. [6, 7] DPP is considered as an important class of pigments used in paints, inks and plastics owing to their excellent shades and better ambient stability.[8] DPP dyes are generally insoluble in most of the organic solvents due to strong intermolecular H-bonding and π–π stacking interactions between the lactam rings.

[9] The solubility of DPPs can be improved in organic solvents by easy functionalization of the N-atoms with long linear or branched alkyl side chains.[10] The optoelectronic properties of the DPPs can be tailored by substituting DPP with various donor units at 3- and 6- positions.[11] Our group is involved in the design and synthesis of donor functionalized DPP derivatives in which thienyl-DPP was used as a central core unit as thiophene is a good electron donor and makes less dihedral angle with the DPP core which enhances the electronic communication in the molecular system. A number of electron donor moieties (phenothiazine, triphenylamine, ferrocene and carbazole) were incorporated to 3- and 6- positions of DPP core. Another component tetracyanoethylene (TCNE) was used as an additional electron withdrawing unit.[12] The incorporation of TCNE to electron donor functionalized DPPs significantly improves the electron accepting strength and photonic properties of the obtained materials. In this article, we present the highlights from our recent work on different electron donor functionalized DPP derivatives.

1. Tetracyanobutadiene incorporated phenothiazine-bis(thienyl) diketopyrrolopyrrole dyad systems

The optoelectronic properties of the DPPs can be tailored by substituting DPP with various donor functionalities at 3- and 6- positions. The monobromo and dibromo substituted DPPs were reacted with ethynyl phenothiazine through Sonogashira cross coupling reaction to synthesize **1** and **2** (Chart 1). [13] The ethynyl linkage of **1** and **2** was further functionalized with tetracyanoethylene (TCNE) through the [2+2] cycloaddition-retroelectrocyclization reactions to form tetracyanobutadiene (TCBD) bridged DPP-phenothiazine **3** and **4**. The photophysical, computational and electrochemical properties of **1–4** were investigated.

The electronic absorption spectra of acetylene bridged DPPs **1** and **2** display absorption bands at 584, 549 nm and 626, 585 nm, respectively (Figure 1). The high energy band corresponds to the π→π* transition of the DPP core, whereas the low energy band is originated from intramolecular interactions between the donor and acceptor units. The TCBD bridged DPPs **3** and **4** show absorption maxima in lower energy and higher energy regions at 689, 635 nm and 746, 684 nm respectively corresponding to the intramolecular interactions between the phenothiazine donor

and DPP-TCBD conjugate acceptor units, and π→π* transition of the DPP-TCBD conjugate moiety. The incorporation of a supplementary acceptor (TCBD) to the acetylene bridged DPPs **1** and **2** significantly alters the absorption and a bathochromic shift of 105 nm and 120 nm were observed in the absorption maxima of **3** and **4** (Figure 1).
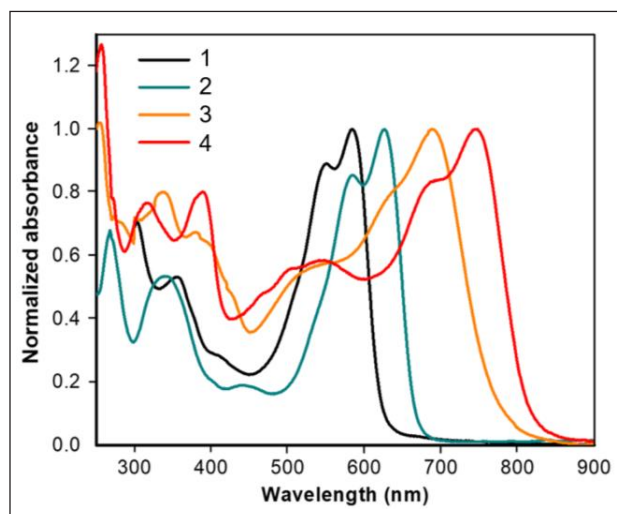

Figure 1. *Normalized absorption spectra of DPPs **1–4** recorded in dichloromethane solution.*

The unsymmetrically substituted DPP **1** exhibits three reversible oxidations at +0.42V, +0.73V and +0.91V, respectively whereas, the symmetrically substituted DPP **2** exhibits two
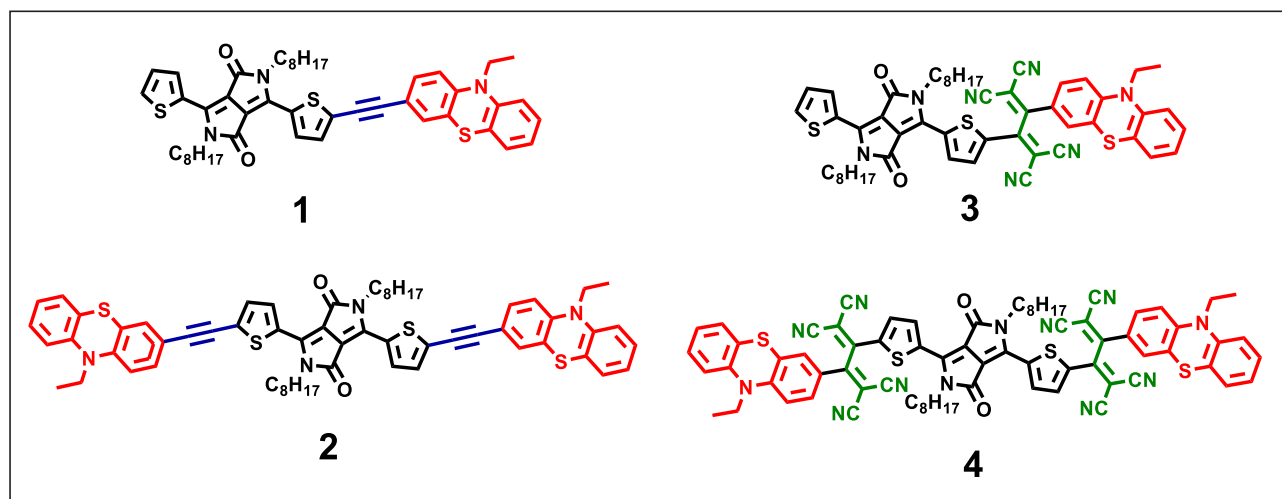

Chart 1. *Chemical structures of the phenothiazine functionalized bis(thienyl)diketopyrrolopyrrole derivatives **1–4**.*

oxidation potentials at +0.71V and +0.93V (Figure 2a). The incorporation of TCBD to ethyne bridged **1** hardens the oxidation, and the DPP **3** shows the first oxidation potential at +0.41V, whereas the second and third oxidation potential were anodically shifted by 260 mV and 180 mV and appeared at +0.99V and +1.09V, respectively. The DPP **4** shows two oxidation potentials at +0.97V and +1.21V. The ethyne bridged **1** and TCBD bridged **3** exhibit two and four reduction potentials in their voltammograms. The reduction potentials of **1** was identified by DPV at -0.89V and -1.13V corresponding to the DPP moiety whereas the reduction potentials of **3** was identified at -1.38V and -0.81V corresponding to the DPP moiety and the two additional reduction potentials at -0.50V and -0.30V were observed, which was attributed to the reduction of TCBD moiety. The DPP **2** exhibits two reduction potentials at -0.94V and -1.49V and two oxidation potentials at +0.71V and +0.93V. The DPP **4** shows two oxidation potentials at +0.97V and +1.21V and four reduction potentials at -0.19V, -0.28V, -0.66V and -1.52V.

The optimized geometries of acetylene bridged DPPs **1** and **2** show that the electron density in HOMO is mainly localized on the DPP moiety and acetylene bridge, and some part is localized on the phenothiazine moiety. On the other hand, electron density in LUMO energy level is mainly concentrated on the DPP core indicating its electron acceptor nature (Figure 2b). The di-substitution of DPP core by ethynyl phenothiazine lowers the HOMO–LUMO gap in **2** (2.11 eV) compared to mono-substitution in **1** (2.28 eV). The TD-DFT studies on TCBD bridged **3** and **4** indicated that the absorption peak originated due to the transfer of electron density from donor (phenothiazine) to the acceptors (DPP and TCBD). The incorporation of TCBD in acetylene based DPPs disturbs the molecular planarity and results in the twisted conformations of **3** and **4**. The incorporation of TCBD stabilizes the HOMO and LUMO energy levels and the degree of stabilization of LUMO level was more, which resulted in further lowering of HOMO–LUMO gap in **3** (1.96 eV) and **4** (1.62 eV).

2. Tetracyanobutadiene incorporated triphenylamine-bis(thienyl) diketopyrrolopyrrole dyad systems

The diketopyrrolopyrrole has been identified as a potential electron acceptor, when combined with an electron donor, it forms a donor–acceptor molecular system. Furthermore, strong donor–acceptor (D–A) interactions between the DPP core and adjacent thiophene moieties result in strongly hybridized frontier molecular orbitals in diketopyrrolopyrrole-based systems. We functionalized DPP with
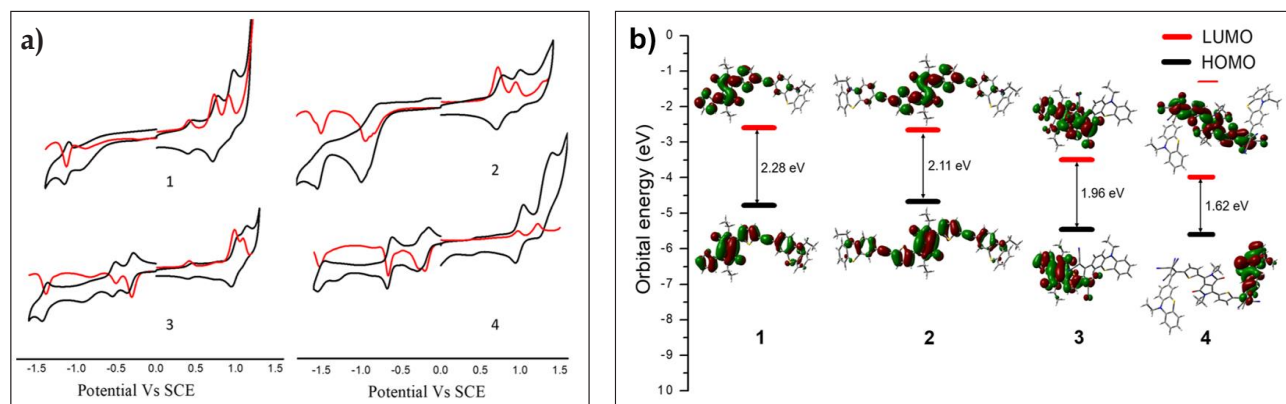

Figure 2. *(a) Cyclic voltammograms (black line) and differential pulse voltammograms (red line) of DPPs **1–4** recorded in 0.1 M Bu$_4$NPF$_6$ solution in dichloromethane at 100 mV s^{-1} scan rate, versus SCE at 25 °C, (b) Frontier Molecular Orbitals and energy level diagram of DPPs **1–4**.*
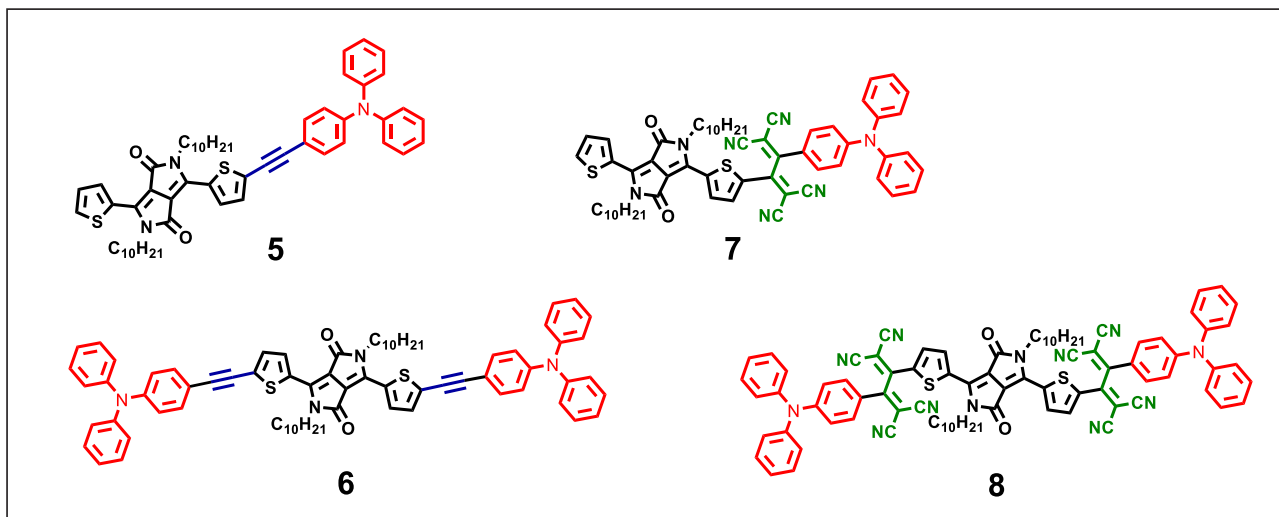
Chart 2. *Chemical structures of triphenylamine functionalized bis(thienyl)diketopyrrolopyrrole derivatives* **5–8**.

another donor triphenylamine, to see its effect on the photophysical properties of the resultant DPP materials. The monobromo and dibromo DPPs were reacted with ethynyl triphenylamine through Sonogashira cross coupling reaction, to synthesize DPP **5** and **6** (Chart 2).[14] The ethynyl bridged compounds **5** and **6** were reacted with TCNE through [2+2] cycloaddition retroelectrocyclization reaction to synthesize DPP **7** and **8**.

Figure 3 shows the electronic absorption spectra of DPPs **5** and **6** in the UV-visible region from 300–750 nm. The shorter wavelength absorption bands (below 500 nm) and longer wavelength absorption bands (510–750 nm) correspond to the π–π* transition and

intramolecular charge transfer (ICT) from TPA to DPP, respectively. The absorption spectra of these DPPs in thin films are red shifted as compared to their solutions. This suggested that the DPP molecules have more planar conjugated backbone in solid state as compared to solution.

The optical absorption spectra of DPP **7** and **8** in a dilute tetrahydrofuran solution and in thin film cast from tetrahydrofuran is shown in Figure 3. The absorption bands of **7** (λ_{max} = 476 nm) and **8** (λ_{max} = 480 nm) in the shorter wavelength region are attributed to the π-π* transition and are similar, whereas the absorption bands of **7** (λ_{max} = 683 nm) and **8** (λ_{max} = 738 nm) in the longer wavelength region are attributed to intramolecular charge transfer (ICT) between donor and acceptor
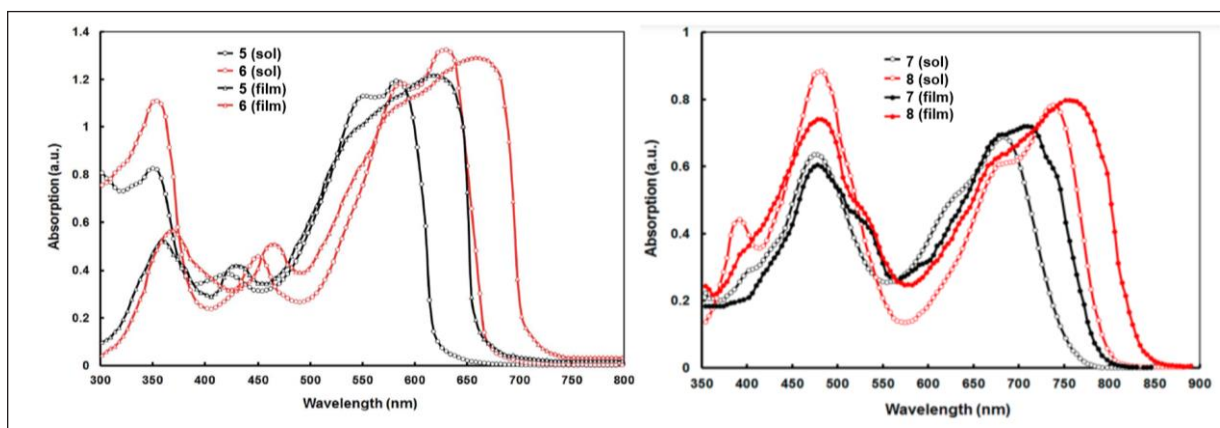

Figure 3. *Absorption spectra of DPPs* **5–8** *recorded in tetrahydrofuran solution and in thin films.*
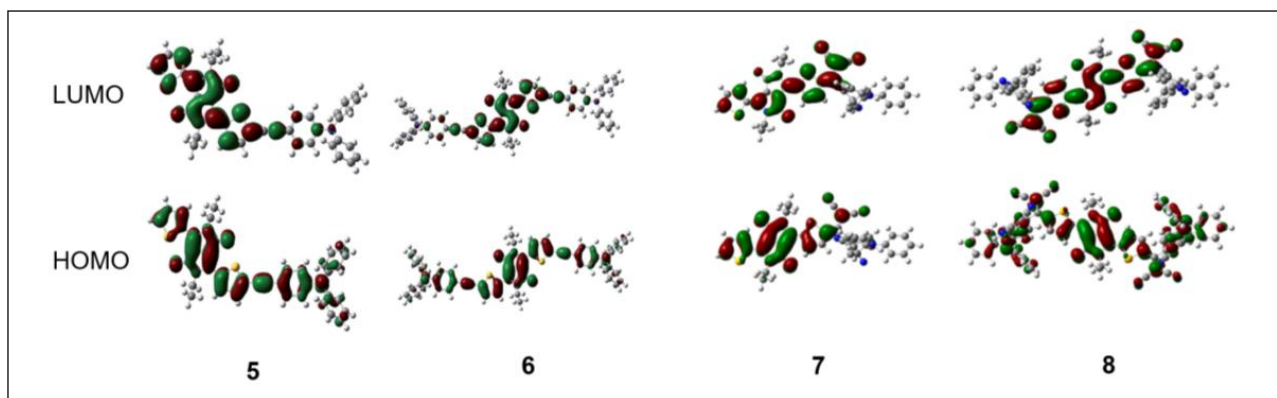
Figure 4. *Frontier molecular orbital pictures of triphenylamine substituted DPPs* **5–8** *showing localization of electron density in HOMO and LUMO energy levels.*

moieties present in the molecules. The red shift in the ICT band of **8** as compared to **7** suggested stronger D-A interaction in DPP **8** caused by the presence of two TCBD units.

The DFT studies show that the electron density on HOMO for both the DPPs is distributed throughout the molecule, whereas the LUMOs is mainly concentrated on the DPP unit. The localization of LUMO on the DPP core indicated its acceptor nature. The typical donor–acceptor (D–A) interaction and charge transfer from TPA to DPP is depicted in Figure 4. In unsymmetrical DPP **7,** the LUMO is concentrated on the DPP-TCBD conjugate moiety. The DPP **7** exhibits ICT transition which was originated due to the transition from HOMO-1→LUMO. In DPP **8**, the HOMO is distributed over the entire molecule, while HOMO-2 is distributed over the two triphenylamine donor units. The HOMO-2→LUMO and HOMO→LUMO transitions in **8** at the long wavelength region corresponds to charge transfer from donor TPA to TCBD-DPP conjugate acceptor units.

DPP **5** and **6** exhibits four oxidation potentials in their cyclic voltammograms and have nearly identical first oxidation potentials. Two reduction waves in the CV and DPV of **5** and **6** correspond to the formation of mono and dianion. There are three oxidation waves in the TCBD-substituted unsymmetrical DPP **7**, but only two in the symmetrical DPP **8**. The di-TCBD bridged DPP
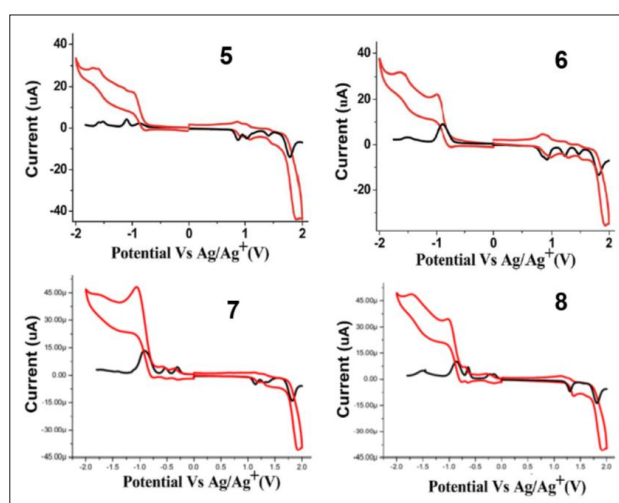

Figure 5. *Cyclic voltammetry (red line) and differential pulse voltammetry (black line) of DPPs* **5–8** *recorded in 0.1 M Bu_4NPF_6 solution in dichloromethane at 100 mV s^{-1} scan rate, versus Ag/Ag$^+$ at 25 °C.*

8 show higher first oxidation potential as compared to the mono-TCBD bridged DPP **7**, indicating that TCBD causes harder oxidation. The unsymmetrical and symmetrical TCBD derivatives (**7** and **8**) have four reduction waves, two of which correspond to the TCBD unit and two correspond to the DPP unit (Figure 5).

3. Metal functionalized bis(thienyl) diketopyrrolopyrrole

The redox chemistry and formation of electron transfer complexes in metal functionalized systems make them to be used in a variety of optoelectronic applications. We developed

and synthesized a cobalt-based bis(thienyl) diketopyrrolopyrrole to investigate the effect of metal on the photonic and electrochemical properties. The di-ethynyl diketopyrrolopyrrole reacts with cyclopentadienyl cobalt (I) dicarbonyl and sulphur in degassed toluene to produce the cobalt-dithiolene functionalized DPP **9** (Chart 3).[15]
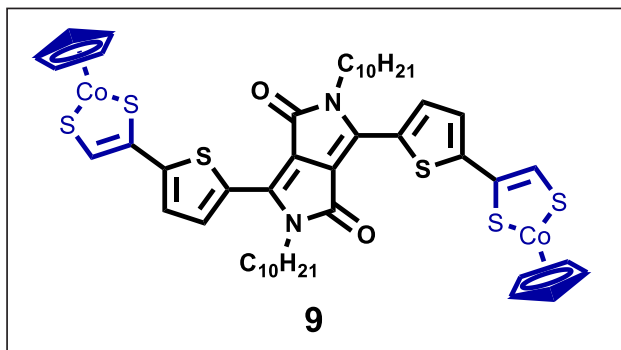

Chart 3. *Chemical structure of cobalt-based bis(thienyl) diketopyrrolopyrrole derivative* **9**.

The DPP **9** shows two absorption bands, one in the visible region at 620 nm and another in the NIR region at 820 nm (Figure 6a). The CV and DPV voltammograms of **9** show two oxidation waves in which the first oxidation at 0.61V was due to the cobalt oxidation and second oxidation at 0.78V was due to the thiophene moiety (Figure 6b). DFT calculation revealed localization of HOMO on the central DPP core while LUMO

is localized over the cobalt-di-thiophene ring as shown in Figure 6c.

4. bis(thienyl)diketopyrrolopyrrole dimers

We synthesized two dimers of DPP, **10** and **11** that contained vinyl and acetylene bridges between the two DPP units with a D-A-D-π-D-A-D structure and investigated their optical and electrochemical properties.[16] The DPPs **10** and **11** were synthesised *via* the Stille coupling reactions of monobromo DPP with a half equivalent of bis(tributylstannyl)ethene and bis(tributylstannyl)acetylene, respectively (Chart 4).
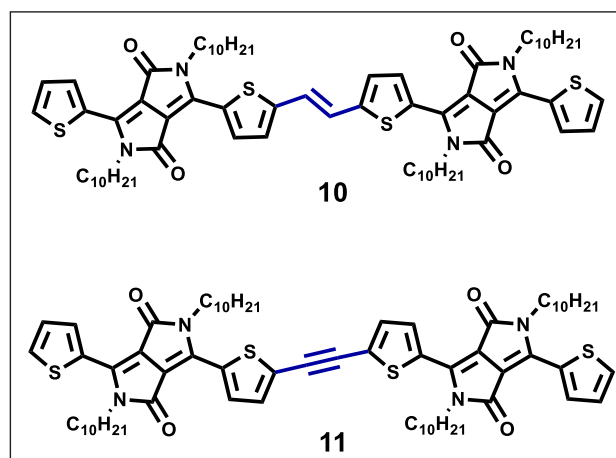
Chart 4. *Chemical structure of bis(thienyl) diketopyrrolopyrrole dimers* **10** *and* **11**.

Figure 6. *(a) Normalized absorption spectra of DPP* **9** *recorded in dichloromethane solution (b) Cyclic voltammetry (red line) and differential pulse voltammetry (black line) of DPP* **9** *recorded in 0.1 M Bu$_4$NPF$_6$ solution in dichloromethane at 100 mV s^{-1} scan rate, versus Ag/Ag$^+$ at 25 °C; and (c) Frontier molecular orbitals of* **9** *showing localization of electron density in HOMO and LUMO energy levels.*

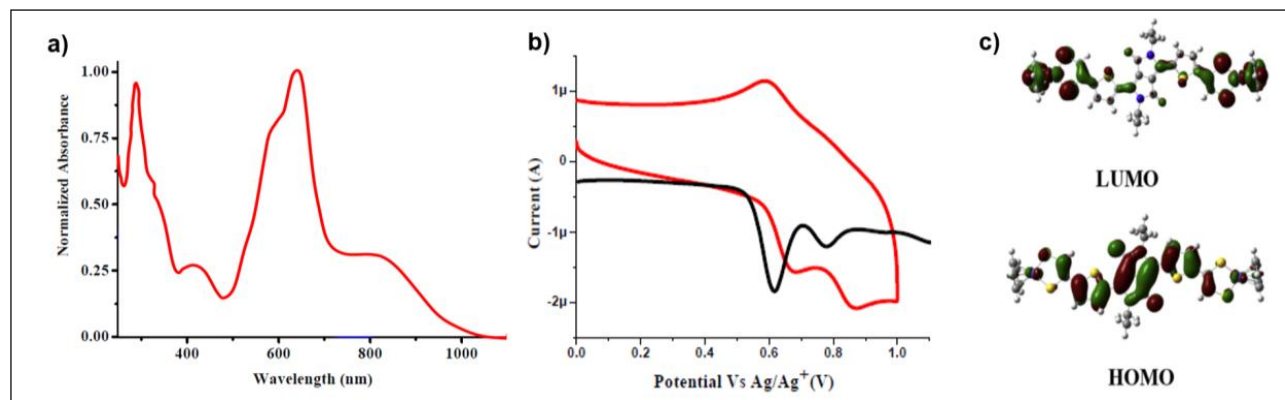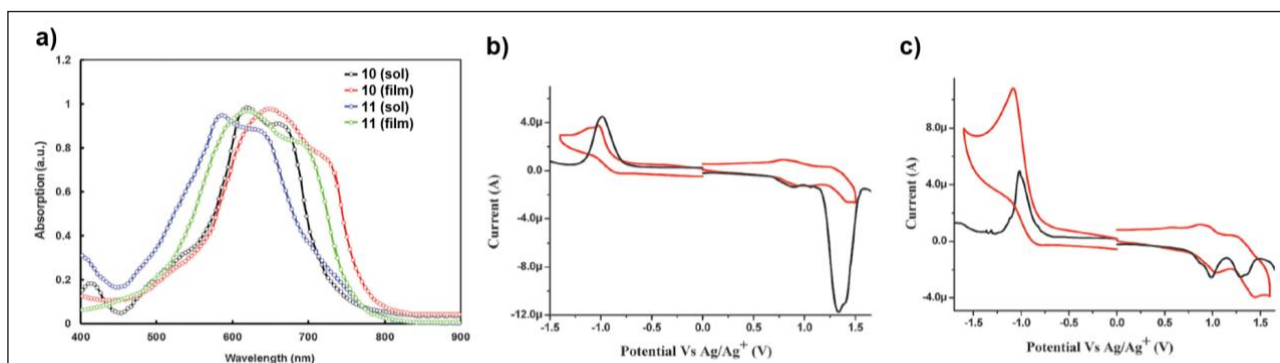**Figure 7**. *(a) Normalized absorption spectra of DPP* **10** *and* **11** *recorded in chloroform solution and in thin films. Cyclic voltammetry (red line) and differential pulse voltammetry (black line) of (b)* **10** *and (c)* **11** *recorded in 0.1 M Bu_4NPF_6 solution in dichloromethane at 100 mV s^{-1} scan rate, versus Ag/Ag$^+$ at 25 °C.*

Figure 7a shows the normalized electronic absorption spectra of DPP dimers **10** and **11** in chloroform and in thin films. The absorption maxima of **10** and **11** in the solution was observed at 618 nm and 584 nm, respectively due to the ICT transition. In thin films, the absorption spectra of DPP **10** and **11** show strong absorption over the entire wavelength range of 500–850 nm. The absorption spectra of the thin film were similar to those in solution, but the absorption maxima value was redshifted, and the peak was widened, implying strong π–π intermolecular interactions in the solid state, resulting in enhanced π-electron delocalization across the molecular backbone.

The DPPs **10** and **11** show one reduction wave corresponding to the DPP core and two oxidation waves, corresponding to the unsymmetrical thiophene moieties (Figure 7b and c). The reduction wave associated with the DPP core was observed at -0.99 V in **10** and at -1.01 V in **11**. For DPPs **10** and **11**, the oxidation waves were observed at 0.89 V and 1.34 V and 0.99 V and 1.29 V, respectively.

5. Tetracyanobutadiene incorporated ferrocene-bis(thienyl)diketopyrrolopyrrole systems

Mono and di-ferrocenyl substituted DPP derivatives **12** and **13** were synthesized by the Sonogashira cross-coupling reactions of ethynyl ferrocene with monobromo and dibromo DPPs. The DPPs **12** and **13** were reacted with 1 and 2 equivalents of tetracyanoethylene through the [2+2] cycloaddition-retroelectrocyclization reactions at room temperature to give unsymmetrically and symmetrically substituted DPPs **14** and **15** (Chart 5).[17]

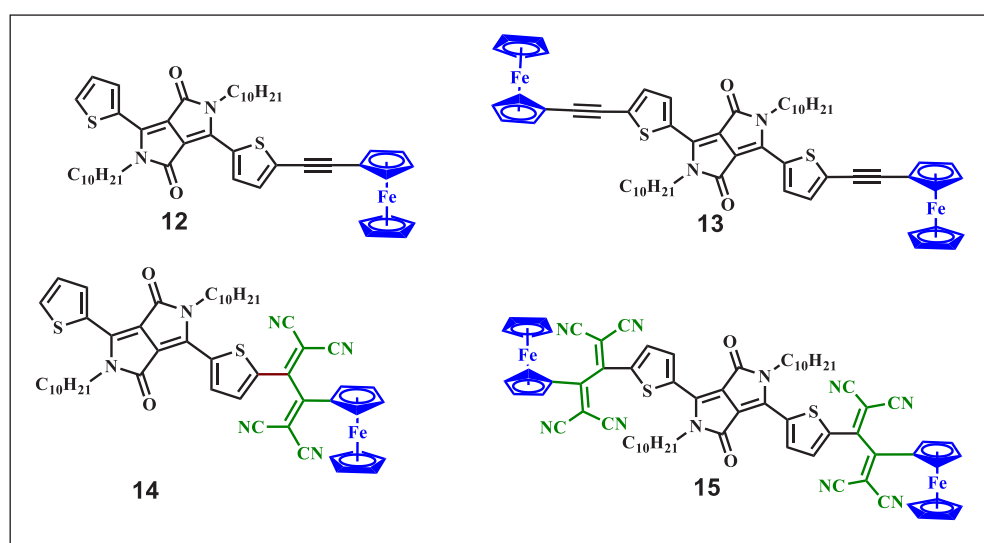The DPPs **12–15** show two absorption bands in their absorption spectra as shown in Figure 8.

Chart 5. *Chemical structures of ferrocenyl functionalized bis(thienyl)diketopyrrolopyrrole derivatives* **12–15**.

The absorption band in the lower wavelengths correspond to the π→π* transition, which is localized over the DPP unit, whereas the intense absorption bands at longer wavelength region is attributed to ICT transition from ferrocene to DPP core. The di-TCBD substituted DPP **15** showed redshift with broad absorption band compared to the DPPs **12–14** due to the presence of strong cyano based acceptor in both side of DPP unit.
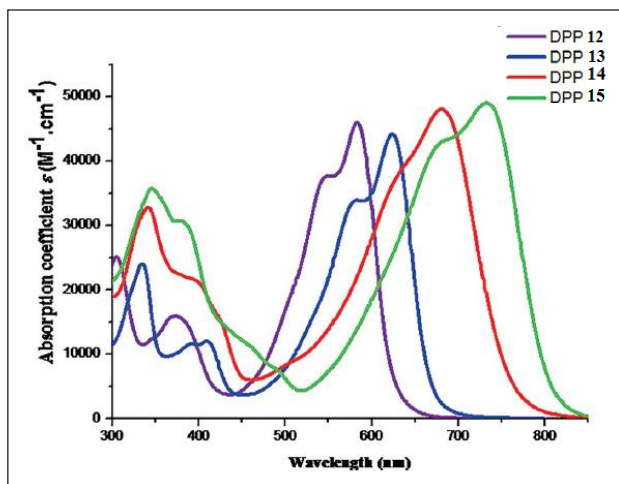

Figure 8. *Absorption spectra of DPP* **12–15** *recorded in dichloromethane solution.*

The thermal properties of DPPs **12–15** reveal that the DPPs exhibit good thermal stability (Figure 9). On increasing the π-electron conjugation the thermal stability increases due to which the symmetrical DPPs **13** and **15** show better thermal stability compared to unsymmetrical DPPs **12** and **14**.

In the electrochemical study, DPP **12** and its TCBD derivative DPP **14** show three oxidation waves, one for ferrocenyl unit and other two for the two different thiophene moieties (*i.e.*, the terminal thiophene and the thiophene adjacent to the
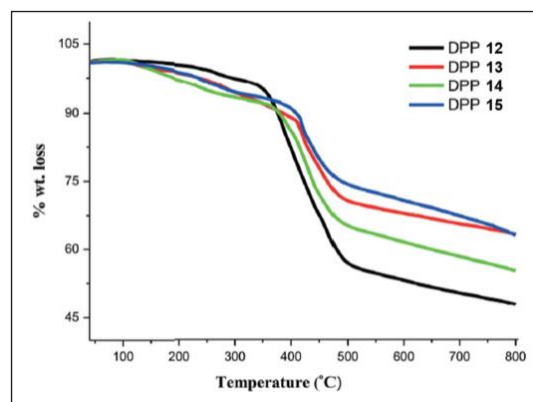
Figure 9. *Thermogravimetric analysis of DPPs* **12–15** *measured at a heating rate of 10 °C min⁻¹ under nitrogen.*

ferrocene unit, Figure 10). The DPP **13** and TCBD functionalized DPP **15** show two oxidation waves, one corresponds to the thiophene and the other one is attributed to the ferrocene moiety. After incorporation of TCBD unit the oxidation potential of ferrocene unit shifted from 0.60 V in DPP **12** to 0.96 V in DPP **14** and from 0.61 V in DPP **13** to 0.97 V in DPP **15**. The DPPs **12** and **13** showed two reduction waves for the DPP unit of the ferrocenyl-DPPs, which is attributed to mono and dianion formation, whereas DPPs **14** and **15**
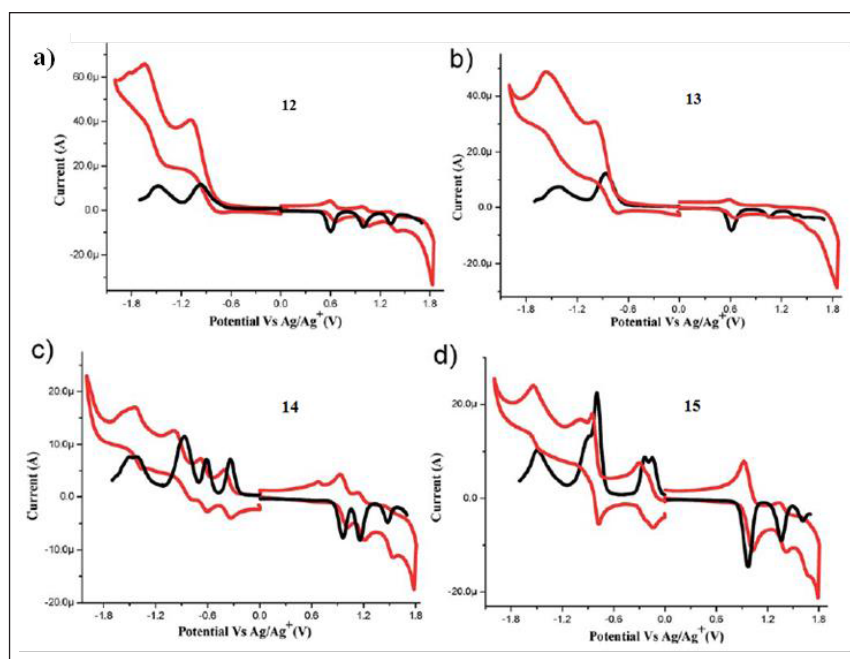
Figure 10. *Cyclic voltammetry (red line) and differential pulse voltammetry (black line) of (a)* **12***, (b)* **13***, (c)* **14***, and (d)* **15** *recorded in 0.1 M Bu₄NPF₆ solution in dichloromethane at 100 mV s⁻¹ scan rate, versus Ag/Ag⁺ at 25 °C.*
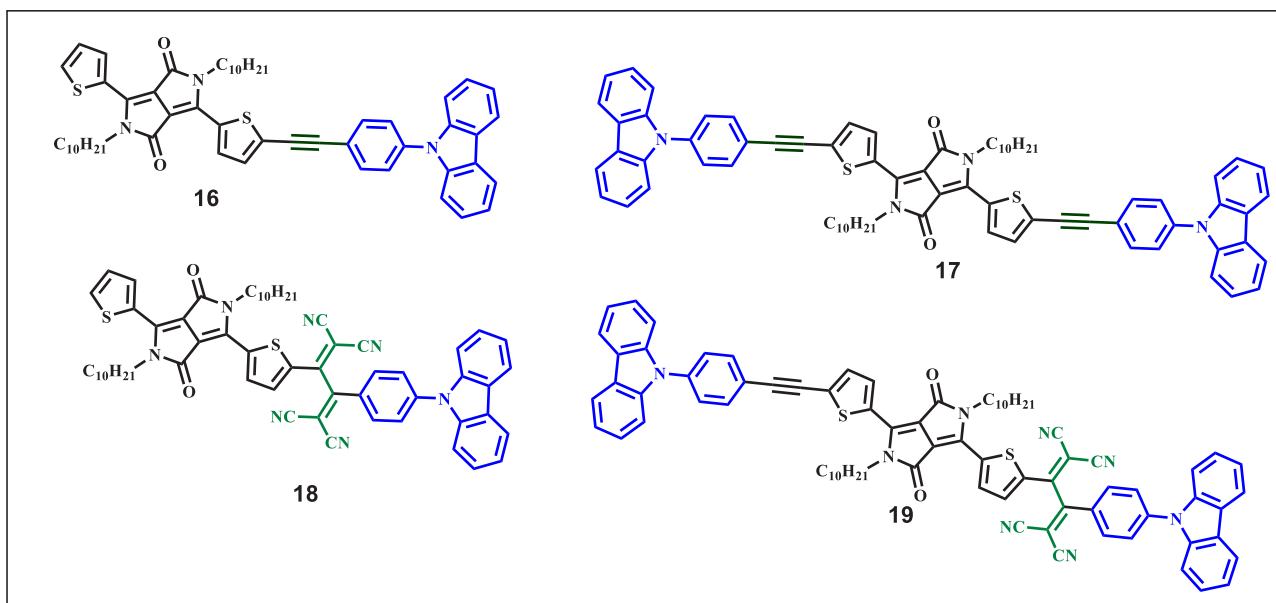
Chart 6. *Chemical structures of carbazole functionalized bis(thienyl)diketopyrrolopyrrole derivatives* **16–19**.

showed four reduction waves out of which the first two corresponds to the TCBD unit and the other two attributed to the DPP unit.

6. Tetracyanobutadiene incorporated carbazole-bis(thienyl)diketopyrrolopyrrole dyad systems

Further we have synthesized mono and di-carbazole based derivatives DPP **16** and **17** by the Pd-catalyzed Sonogashira cross-coupling reaction.[18] The DPP **16** and **17** were reacted with excess amount of TCNE at 135 °C in microwave irradiation for 4 h through [2+2] cycloaddition–retroelectrocyclization resulted in TCBD substituted DPPs **18** and **19** (Chart 6).

The carbazole functionalized derivatives DPP **16** and **17** showed two absorption bands in the visible region around 550–620 nm, in which the absorption band in the lower wavelength region corresponds to π→π* transitions and the absorption bands at higher wavelength region is attributed to the ICT transitions.

The TCBD bridged DPPs **18** and **19** show a bathochromic shift of 115 nm and 110 nm in their absorption spectra (Figure 11) as compared to their precursors, ethynyl bridged DPPs **16** and **17** due to the presence of cyano based TCBD
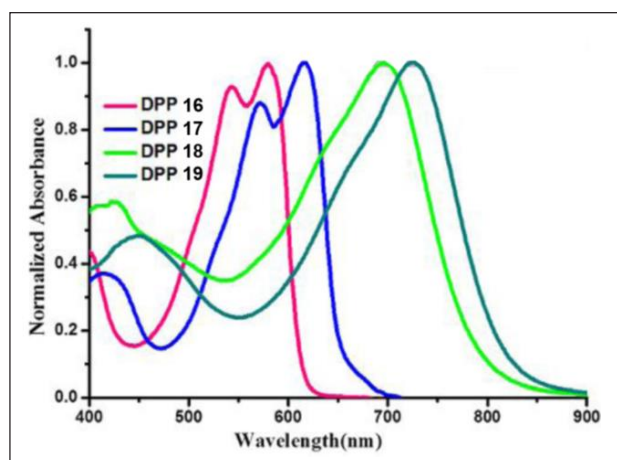
Figure 11. *Normalized absorption spectra of DPPs* **16–19** *recorded in dichloromethane.*

acceptor units. The DPPs **18** and **19** show a single absorption band around 695 and 726 nm, attributed to ICT transitions. The optical bandgap follows the trend **19>18>17>16**, indicating that the TCBD derivatives (**18** and **19**) show low HOMO–LUMO gap. The ethynyl bridged DPPs **16** and **17** are emissive in nature, whereas the TCBD based DPPs **18** and **19** are non-emissive due to the strong donor-acceptor interaction, which quenches the fluorescence. The thermal properties for DPPs **16–19** show decomposition temperatures at 333 °C, 398 °C, 266 °C and 329 °C, respectively (Figure 12). The DPP **16** and **17**
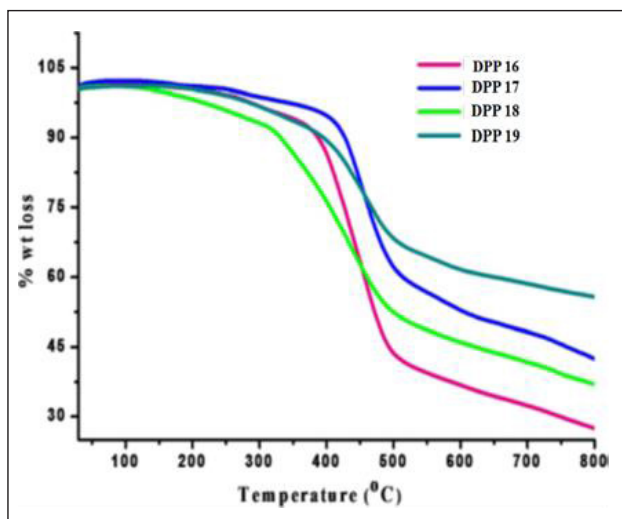
Figure 12. *Thermogravimetric analysis of DPPs* **16–19** *measured at a heating rate of 10 °C min⁻¹ under a nitrogen atmosphere.*

showed low HOMO–LUMO band gap compared to ethyne-bridged DPPs **16** and **17**.

Conclusions

In summary, this article describes various strategies used for the development of small molecules based on diketopyrrolopyrroles along with their photophysical, computational and electrochemical properties. The variation of the donor/acceptor strength results in significant tuning of the HOMO–LUMO gap. The incorporation of cyano-based TCBD acceptor units in ethyne bridged DPPs resulted in the extension of the absorption towards the NIR region. The main synthetic techniques used to synthesize the push-pull functionalized DPP derivatives include Sonogashira and Stille cross-
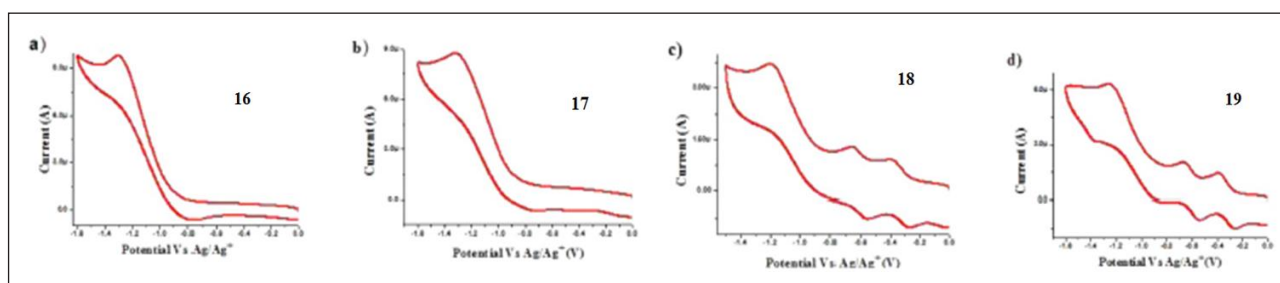

Figure 13. *Cyclic voltammograms of DPP (a)* **16***, (b)* **17***, (c)* **18***, and (d)* **19** *recorded in 0.1 M Bu₄NPF₆ solution in dichloromethane at 100 mV s⁻¹ scan rate, versus Ag/Ag⁺ at 25 °C.*

showed better thermal stability compared to their TCBD functionalized derivatives DPP **18** and DPP **19**.

The electrochemical properties of carbazole functionalized DPPs **16–19** explained that all derivatives showed multi redox waves due to presence of various donor and acceptor (carbazole, thiophene, TCBD and DPP) units (Figure 13). In the anodic side, DPPs **16–19** showed two oxidation waves due to the thiophene and carbazole moieties. In the cathodic side, first two reduction waves for DPP **18** and **19** corresponds to the TCBD unit and the next reduction waves were attributed to the DPP unit. The DPPs **16** and **17** exhibit two reduction waves due to the DPP moiety. The electrochemical results explained that the TCBD functionalized DPPs **18** and **19**

coupling reactions, and [2+2] cycloaddition-retroelectrocyclization reactions. Several donor units, including triphenylamine, phenothiazine, carbazole, ferrocene, and cobaltocene, were attached at the 3- and 6- positions of bis(thiophen-2-yl)diketopyrrolopyrrole to improve the donor-acceptor interactions and enhance the photophysical properties of these derivatives. The absorption spectra of ethyne bridged donor-DPP systems exhibit absorption in the UV-visible region and the incorporation of 1,1,4,4-tetracyanobutadiene (TCBD) moiety significantly shifts the absorption to near infrared region. Metal functionalization of DPP shifts its absorption to the NIR region, and the cobaltocene based derivative of DPP (**9**) exhibits an absorption band at 820 nm in its

absorption spectra. The electrochemical studies reveal additional low voltage waves in the cyclic voltammograms of TCBD based systems (**3**, **4**, **7**, **8**, **14**, **15**, **18**, and **19**). The photophysical and computational study indicates that inserting the strong electron-deficient moieties improves the intramolecular charge transfer (ICT) and lowers the HOMO-LUMO gap dramatically, for all the derivatives. We hope that this article represents substantial information about the synthesis of DPP derivatives and provides a new pathway for their application in optoelectronics.

Acknowledgements

References

1. Liu, Q.; Bottle, S. E.; Sonar, P. Developments of Diketopyrrolopyrrole-Dye-Based Organic Semiconductors for a Wide Range of Applications in Electronics. *Adv. Mater.* **2020**, 32, 1903882.

2. Tang, A.; Zhan, C.; Yao, J.; Zhou, E. Design of Diketopyrrolopyrrole (DPP)-Based Small Molecules for Organic-Solar-Cell Applications. *Adv. Mater.* **2017**, 29 (2), 1600013.

3. Kato, S.; Diederich, F. Non-Planar Push–Pull Chromophores. Chem. Commun. 2010, 46 (12), 1994. b) Bureš, F. Fundamental Aspects of Property Tuning in Push–Pull Molecules. *RSC Adv* **2014**, 4 (102), 58826–58851.

4. Zhao, C.; Guo, Y.; Zhang, Y.; Yan, N.; You, S.; Li, W. Diketopyrrolopyrrole-Based Conjugated Materials for Non-Fullerene Organic Solar Cells. *J. Mater. Chem. A* **2019**, 7 (17), 10174–10199.

5. Cai, Y.; Liang, P.; Tang, Q.; Si, W.; Chen, P.; Zhang, Q.; Dong, X. Diketopyrrolopyrrole-Based Photosensitizers Conjugated with Chemotherapeutic Agents for Multimodal Tumor Therapy. *ACS Appl. Mater. Interfaces* **2017**, 9 (36), 30398–30405.

6. Farnum DG, Mehta G, Moore GG, Siegal FP. Attempted reformatskii reaction of benzonitrile, 1, 4-diketo-3, 6-diphenylpyrrolo [3, 4-C] pyrrole. A lactam analogue of pentalene. *Tetrahedron Letters*. **1974**, 15, 2549-52.

7. (a) Iqbal, A.; Cassar, L. (CIBA-GEIGY AG). EP61426, 1982. (b) Rochat, A. C.; Cassar, L.; Iqbal, A. (CIBA-GEIGY AG). EP94911, 1983.

8. Faulkner EB, Schwartz RJ, editors. High performance pigments. John Wiley & Sons; **2009** Mar 9.

9. Woo, C. H.; Beaujuge, P. M.; Holcombe, T. W.; Lee, O. P.; Fréchet, J. M. J. Incorporation of Furan into Low Band-Gap Polymers for Efficient Solar Cells. *J. Am. Chem. Soc.* **2010**, 132 (44), 15547–15549.

10. Grzybowski, M.; Gryko, D. T. Diketopyrrolopyrroles: Synthesis, Reactivity, and Optical Properties. *Adv. Opt. Mater*. **2015**, 3 (3), 280–320.

11. Goswami, S.; Winkel, R. W.; Alarousu, E.; Ghiviriga, I.; Mohammed, O. F.; Schanze, K. S. Photophysics of Organometallic Platinum(II) Derivatives of the Diketopyrrolopyrrole Chromophore. *J. Phys. Chem. A* **2014**, 118 (50), 11735–11743.

12. Michinobu, T.; May, J. C.; Lim, J. H.; Boudon, C.; Gisselbrecht, J.-P.; Seiler, P.; Gross, M.; Biaggio, I.; Diederich, F. A New Class of Organic Donor–Acceptor Molecules with Large Third-Order Optical Nonlinearities. *Chem Commun* **2005**, No. 6, 737–739.

13. Khan F, Jang Y, Patil Y, Misra R, D'Souza F. Photoinduced Charge Separation Prompted Intervalence Charge Transfer in a Bis (thienyl) diketopyrrolopyrrole Bridged Donor-TCBD Push-Pull System. *Angewandte Chemie International Edition*. **2021**, 6, 20518-27.

14. a) Patil Y, Misra R, Chen FC, Keshtov ML, Sharma GD. Symmetrical and unsymmetrical triphenylamine based diketopyrrolopyrroles and their use as donors for solution processed bulk heterojunction organic solar cells. RSC advances. 2016;6(102):99685-94. b) Patil Y, Misra R, Keshtov ML, Sharma GD. 1, 1, 4, 4-Tetracyanobuta-1, 3-diene Substituted Diketopyrrolopyrroles: An Acceptor for Solution Processable Organic Bulk Heterojunction Solar Cells. *The Journal of Physical Chemistry C.* **2016**, 31, 120, 6324-35.

15. Patil Y, Shinde J, Misra R. Near-infrared absorbing metal functionalized diketopyrrolopyrroles. *Journal of Organometallic Chemistry*. **2017**, 1, 48-53.

16. Patil Y, Misra R, Sharma A, Sharma GD. D–A–D–π–D–A–D type diketopyrrolopyrrole based small molecule electron donors for bulk heterojunction organic solar cells. *Physical Chemistry Chemical Physics*. **2016**, 18, 16950-7.

17. a) Patil Y, Jadhav T, Dhokale B, Misra R. Tuning of the HOMO–LUMO gap of symmetrical and unsymmetrical ferrocenyl-substituted diketopyrrolopyrroles. *Eur. J. Org. Chem*. 2016, 733-8. b) Patil Y, Popli C, Misra R. Near-infrared absorbing tetracyanobutadiene-bridged diketopyrrolopyrroles. *New Journal of Chemistry*. **2018**, 42, 3892-9.

18. Patil Y, Jadhav T, Dhokale B, Misra R. Design and Synthesis of Low HOMO–LUMO Gap N-Phenylcarbazole-Substituted Diketopyrrolopyrroles. *Asian Journal of Organic Chemistry*. **2016**, 5, 1008-14.

Prof. Rajneesh Misra is currently working as a professor at the Department of Chemistry, Indian Institute of Technology Indore (IIT Indore). He obtained his master's degree from the University of Gorakhpur, India, in 2001. He moved to the Indian Institute of Technology Kanpur for his Ph.D. in chemical sciences, in 2007. After two successive postdoctoral stays at the Georgia Institute of Technology, Atlanta, USA, from 2007 to 2008, and Kyoto University, Japan, from 2008 to 2009, he joined IIT Indore, India, in 2009, as an assistant professor. His research interests lie in the areas of organic photonics and organic electronics.

Yogajivan Rout has completed his Ph.D. in Chemical sciences from Indian Institute of Technology (IIT) Indore in 2021, under the supervision of Prof. Rajneesh Misra. He received his Master of Science (M.Sc.) degree from the Pondicherry Central University in the year 2015 and Bachelor of Science (B.Sc.) degree from Ravenshaw University in the year 2013. At IIT Indore, his research focused on the design and synthesis of push–pull functionalized chromophores for optoelectronic applications.

Faizal Khan is currently a Ph.D. scholar at the Indian Institute of Technology (IIT) Indore, working under the supervision of Prof. Rajneesh Misra. He received his Bachelor of Science (B.Sc.) in 2013 and Master of Science (M.Sc.) in 2015 from St. Andrew's College, Gorakhpur. His research at IIT Indore focuses on the design and synthesis of organic mechanochromic luminogens.

An overview of commercially available fluorescent probes for Heparin sensing

Shrishti P. Pandey[a] and Prabhat K. Singh[b,c]*

[a]*Amity Institute of Biotechnology, Amity University, Mumbai-Pune Expressway, Bhatan, Panvel, Mumbai, 410206, INDIA*
[b]*Radiation & Photochemistry Division, Bhabha Atomic Research Centre, Mumbai 400 085, INDIA*
[c]*Homi Bhabha National Institute, Anushaktinagar, Mumbai-400085, INDIA*
*Authors for correspondence: Email: prabhatk@barc.gov.in; prabhatsingh988@gmail.com

Abstract

Heparin is the most negatively charged bio-macromolecule, and is a popularly used blood anticoagulant. The currently practised assays for Heparin monitoring are indirect measurements subject to their own limitations and variations. In this regard, considering the advantageous characteristics of fluorescence sensing, such as, high sensitivity, easy operation, flexibility to a range of assay conditions, and comparatively rapid detection, a variety of optical probe molecules are being utilized for Heparin sensing. Herein, we provide a brief overview on some of the fluorescent probe molecules explored by our research group. The potential of Thioflavin-T, Pseudoisocyanine and YOPRO-1 as potential fluorophores for the development of rapid and simple Heparin detection protocols have been summarized in this article.

1. Introduction

Heparin is a highly sulfated, linear glycosaminoglycan that possesses the highest anionic charge among all the biological macromolecules.[1] Heparin is widely used in surgical procedures as a blood anticoagulant, as well in the treatment of various thrombotic diseases. Heparin binds to antithrombin with a very strong affinity, and enhances the activity of antithrombin in the mechanism of blood clot formation.[2] Precisely, antithrombin inactivates the activity of thrombin, which is involved in the process of blood clotting. The addition of Heparin accelerates the activity of antithrombin, resulting into blood anticoagulation activity. [3] However, Heparin overdose in the blood can lead to various fatal complications, such as, hemorrhages, thrombocytopenia, and hyperkalemia. [4-5] The prescribed therapeutic doses of Heparin are 2–8 U/mL (17–67 μM) during cardiovascular surgery and 0.2–1.2 U/mL(1.7–10 μM) for long-term postoperative care.[6-7] In cases of Heparin overdose, a well-known and the only medically approved antidote of Heparin, Protamine, is used to reverse the activity of Heparin. Protamine is a cationic protein having an isoelectric point of 13.8 and interacts through strong electrostatic interactions with Heparin, thereby reversing its activity. Thus, it is imperative to monitor the level of Heparin in the blood during and after surgery. Considering the importance of Heparin as a widely used blood anticoagulant, there has been a constant effort for developing sensing systems for the detection of Heparin.

A wide array of techniques, have been utilized for the effective detection of Heparin, which include, electrochemical methods, [8] ion-exchange chromatography, [9] colorimetry, [10-12] fluorimetry, [13-18] and capillary electrophoresis [19]. Among the already reported methods, fluorescence based methods for the detection of any bioanalyte are considered to be particularly advantageous, because they offer very high sensitivity, moreover, it is an easy read-out technique which is widely utilized in the field of clinical diagnosis. [20-21] In addition,

naked eye detection also provides a very simple way to detect targeted analytes. [22-23] In this regard, a variety of fluorescence based sensing systems have been reported for the detection of Heparin with the help of certain fluorophores such as, conjugated polymers, [16-17, 24] small molecular probes, [13, 15, 18, 25-32] quantum dots, [33] and fluorophore labeled biomolecules [34-36] and nanocomposites [37].

However, a majority of the reported fluorescence-based sensing systems bear certain disadvantages, such as, "turn-off" mode of detection,[38] i.e. fluorescence quenching, which is generally associated with low sensitivity and is often affected by environmental fluctuations. [39] Additionally, while some of the reported fluorescence sensing systems also work through the "turn-on" mechanism, i.e. fluorescence enhancement upon interaction with Heparin, a majority of these probe molecules require time-consuming and tedious protocols for their synthesis. [39-40] Thus, commercially available fluorophores which will work through the "turn-on" mechanism are desired for the development of effective protocols for the simple, sensitive as well as specific detection of Heparin. Molecular rotors are one such class of molecules which work through the fluorescence turn-on mechanism, since they are initially non-emissive, in their free monomeric form, as their structures undergo large amplitude torsional movements causing efficient non-radiative de-excitation of their excited state. [41-43] Whereas, in the aggregated state, the torsional movements in their structure are restricted, leading to a huge emission enhancement. [44-46]

Thus, we intended to explore molecular rotor based cationic probe molecules for the effective sensing of Heparin. The entire approach for utilizing cationic fluorophores for Heparin sensing is based on the preamble that the anionic Heparin and the cationic fluorophore will undergo strong electrostatic interactions among each other, causing charge neutralization of the fluorophore, subsequently leading to aggregation of the fluorophore, resulting into huge fluorescence enhancement. In this regard, we have examined monocationic fluorophores, such as, Thioflavin-T (ThT); pseudoisocyanine (PIC) and a dicationic fluorophore, YOPRO-1 for the "turn-on" fluorescence detection of Heparin.

These probe molecules represent a wide range of desirable properties, such as, their cationic charge, molecular rotor nature, longer excitation and emission wavelength lying in the red region and their ability to work through turn-on fluorescence mechanism.

Therefore, this article aims to contribute to this growing area of Heparin sensing by summarizing the interesting photophysical properties of the mentioned fluorescent probe molecules. We envisaged that the interaction of the fluorophores with Heparin may lead to huge modulations in their photophysical properties, which will provide us an opportunity for, fluorimetric and colorimetric based sensitive detection of Heparin. Heparin induced large modulation in the photophysical properties of ThT, PIC and YOPRO-1 have been observed. Overall, our probe molecules, offer a simple, dual read-out, economic and specific, selective and rapid sensing of Heparin. Along with Heparin detection, the probe-Heparin complexes have also been utilized for the detection of Protamine, which is the only medically affirmed antitoxin of Heparin. We have employed a variety of photophysical methods for investigating the interaction between the fluorophores and Heparin, such as, steady-state fluorescence, ground-state absorption, time-resolved emission, circular dichroism measurements followed by molecular docking calculations. Finally, the performance of ThT, PIC and YOPRO-1 for Heparin sensing have been evaluated in the human serum matrix.

2. Experimental

2.1 Materials

All experiments were executed utilizing nano pure water. The fluorescent probes ThT and
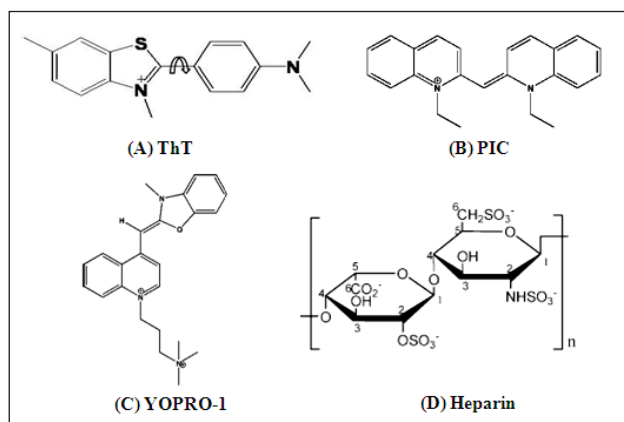
Scheme 1: *Chemical structures of (A) Thioflavin-T (ThT) (B) Pseudoisocyanine (PIC) (C) YOPRO-1 and (D) Dimer repeat unit of Heparin.*

PIC were obtained from Sigma Aldrich, whereas, YOPRO-1 was purchased from Thermo fisher scientific. The concentration of the probes was calculated using the molar absorptivity, viz. ThT ($\varepsilon_{412} \sim 31{,}600$ $M^{-1}cm^{-1}$), PIC ($\varepsilon_{491} \sim 42{,}700$ $M^{-1}cm^{-1}$) YOPRO-1 ($\varepsilon_{480} \sim 52{,}000$ $M^{-1}cm^{-1}$) and optical density. Heparin sodium salt, Protamine sulfate, Hyaluronic acid, Chondroitin sulfate, Dextrose, Mannitol, Galactose, Sucrose, Sodium acetate, Sodium sulfate, Calf thymus DNA and Sodium chloride were purchased from Sigma Aldrich. A cuvette with 1cm path-length was used to perform the measurements "unless otherwise stated. The pH of all the stock solutions was adjusted to ~7 and an optimum temperature of $25^{0}C$ was maintained while performing all the experiments.

2.2 Apparatus

Jasco spectrofluorimeter (model FP-8500) was used to carry out steady-state emission measurements and the ground-state absorption measurements were performed using a Jasco UV-vis spectrophotometer (model V-650). TCSPC measurements were carried out to collect fluorescent decay traces using an IBH instrument with a picosecond diode laser of excitation source 406 nm (~100ps, 1MHz) the details of which have been described elsewhere.[47-49] The instrument response function of the TCSPC setup was measured to be ~180 ps. All the measurements

were performed for 2-3 times in order to ensure the reproducibility.

2.3 Analysis

Data analysis of the obtained fluorescent decay traces was done using DAS-6 (a data analyzing software) with the help of single and multi-exponential decay models. The quality of the fits was judged by the χ_r^2 (reduced chi square) value which was approximately close to ~1.1 and the distribution of the weighted residuals was found to be random around the zero line along the data channels.

The multi-exponential function, used for fitting the decay process, is given as follows,[50]

$$I(t) = I(0)\sum \alpha_i \exp(-t/\tau_i) \tag{1}$$

The average excited-state lifetime was calculated with the help of the following equation,

$$<\tau> = \sum A_i \tau_i \tag{2}$$

Where $A_i = \alpha_i \tau_i / \sum \alpha_i \tau_i$ and α_i stands for the amplitude of the individual decay constants (τ_i).

2.4 Detection of Heparin in real samples

Human serum samples were procured from Sigma Aldrich and were utilized as it is. The serum samples were diluted using nano pure water. The compositions of human serum used for Heparin sensing were 1% for ThT assay, 3% for PIC assay and 20% for YOPRO-1 assay. Various Heparin concentrations were added into the serum samples to form Heparin spiked samples.

3. Results and Discussion

3.1. Thioflavin - T as a potential Heparin sensing probe:

Figure 1A presents the emission spectra of ThT in the presence of Heparin. Upon addition of Heparin to an aqueous solution of ThT, a largely red-shifted emission band appears at ~560 nm, which is in sharp contrast to a very weak emission

band for ThT at 490 nm (Figure 1A). Further addition of Heparin causes a gradual increase in the emission intensity of the red-shifted emission band and leads to a large emission enhancement of ~45 times at the saturation condition. ThT is virtually non-fluorescent in aqueous solution owing to its ultrafast molecular rotor property.[42] Ultrafast molecular rotors are characterized by their ability to twist around a single bond (Central C-C bond in ThT) [42, 51] This twisting motion constitutes a very efficient non-radiative process (k_{nr} ~10^{12} S^{-1}) for ThT, which leads to a quick dissipation of excitation energy, and leads to a very low emission yield. [42] However, this twisting motion is strongly affected by the rigidity of its micro-environment, which in turn immensely influences its emission yield. Owing to the immense sensitivity of the emission yield of ThT towards the rigidity in its surrounding environment, ThT is employed as a sensor for micro-viscosity in several chemical and biological environments, including amyloid fibrils.[42, 52]

Thus, although it can be argued that the increase in ThT emission, in the present case, is due to confinement of its monomeric form upon binding to Heparin, but according to the previous literature, the monomeric ThT emits at 490 nm. Thus, the presence of a strikingly large red-shifted emission band at 560 nm, in the present case, suggests that in the ThT molecules associated with Heparin are not in the usual monomer form, but rather ThT is present in a different molecular form. Very recently, a similar red-shifted emission band has been observed for ThT in the presence of highly negatively charged sulphated β-CD, and has been attributed to H-aggregates of ThT. [53] Since Heparin is known to bear the highest negative charge density for any known biological macromolecule, so it is very likely that Heparin will induce the formation of ThT aggregates. In the aggregated state, the torsional relaxation of ThT is strongly hindered [53] which leads to a turn-on emission in the presence of Heparin. The emission intensity increases in a linear fashion with the increasing concentrations of Heparin in a concentration range of 0 – 15μM, and the linear regression is I_{560}= 58+ 184.8 x [Heparin/μM] (R^2 = 0.996). The detection limit (LOD) of Heparin based on 3.3σ/s was calculated to be 18 nM, where σ represents the standard deviation of 10 blank measurements (ThT in aqueous solution), and s represents the slope of the fluorescence intensity (at 560 nm) with Heparin concentration (Figure 1A, inset). Importantly, H-aggregates of ThT formed on Heparin template displays emission in long-wavelength region, which offers the advantage of being relatively free from the intrinsic fluorescence by other biological contaminants such as DNA, RNA and proteins.

To further confirm about the molecular form of species responsible for the origin of this red-shifted emission, and to explore the possibility of detection of Heparin through colorimetry measurements, absorption spectra of ThT, in the presence of Heparin, was recorded. As displayed in Figure 1B, the addition of Heparin
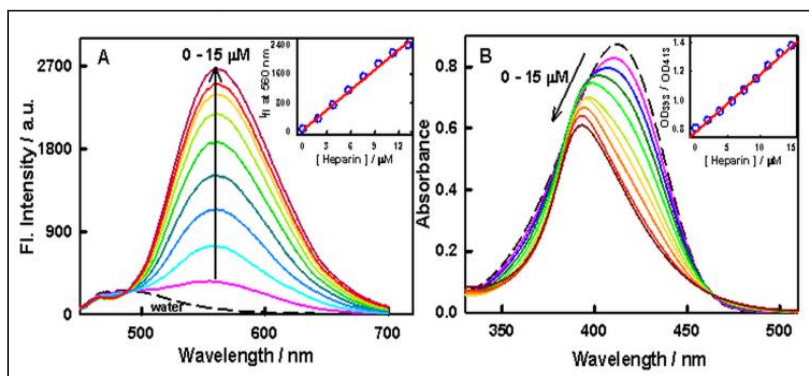
Figure 1. *(A) Steady-state fluorescence spectra (λ_{ex} = 400 nm) of ThT (24 μM) at varying concentration of Heparin. The emission spectrum of ThT in water is represented by the dashed line. Inset: Variation in the emission intensity of ThT with the increasing concentration of Heparin (B) Ground-state absorption spectra of ThT (24 μM) at varying concentration of Heparin. The dashed line represents the absorption spectrum of ThT in water. Inset: Variation in the absorbance ratio (OD_{393}/OD_{413}) of ThT with the increasing concentration of Heparin. [54]*

to an aqueous solution of ThT leads to a blue-shifted absorption band at 393 nm with a gradual decrease in absorbance. However, in aqueous solution, ThT displays an absorption maximum at 413 nm. The blue shift in the absorption spectra of ThT in the presence of Heparin is in sharp contrast to the association of monomeric ThT with the other negatively charged surfaces such as DNA, SDS micelles, etc,[52] where a red shift in the absorption spectra has been observed. This contrasting absorption spectral features of ThT in Heparin again indicates the association of ThT with Heparin, in a form other than monomeric form. Recently, a blue shift in the absorption spectra of ThT in the presence of negatively charged sulfated β-CD has been ascribed to H-aggregates of ThT.[53] Thus, the blue-shifted band presenting an absorption maximum at 393 nm for ThT in the presence of Heparin can be attributed to H-aggregation between ThT molecules on the highly negatively charged surface of Heparin. This blue shift can be understood in terms of molecular exciton theory. According to the molecular exciton theory,[53, 55] when chromophores adopt a head-to-head cofacial arrangement (H-aggregate), the transition from ground state to the higher energy exciton state is allowed, which results in the blue shift in the absorption spectra.

The excitonic interaction between the ThT molecules in the aggregated form is further confirmed by electronic circular dichroism (CD) measurements, which displays a clear bi-signate CD signal in the absorption region of ThT chromophores (Figure 2A). The bi-signate feature is characteristic of the aggregates,[53] and can be assigned to excitonic coupling between transition dipole moments of ThT.[53, 56]

Since the absorption maxima of monomer and H-aggregates of ThT are reasonably well separated (~20 nm), so we attempted to analyze our absorption titration data in terms of variation of absorbance at two different wavelengths, i.e., at 393 nm, corresponding to ThT H-aggregate, and at 413 nm, corresponding to the ThT monomer band. The ratio of the absorbance at these two wavelengths was found to increase linearly (Figure 1B, Inset) with the increasing concentration of Heparin in a concentration range of 0- 15 µM, and the linear regression was $OD_{393}/OD_{413} = 0.784 + 0.039 \times [Heparin/µM]$ ($R^2 = 0.995$). The calculated LOD of Heparin based on $3.3\sigma/s$ was 26 nM. Thus, the present system provides a unique advantage of dual read out of signal for Heparin, both in terms of colorimetry and fluorimetry.

Time-resolved emission measurements are crucial to gain insights into the excited state relaxation of dye molecules, and provides important clues for understanding the mechanism of enhanced emission of molecular rotors. In the aqueous solution, the monomer form of ThT decays very fast, which is within the limit of our equipment (the limit is 0.12 ns). It is reported to be ~ 1 ps in water,[42] which is assigned to the ultrafast twisting dynamics of ThT around the central C-C single bond in the excited state which quickly dissipates the excitation energy. On the contrary, the transient decay for ThT aggregates, in the presence of
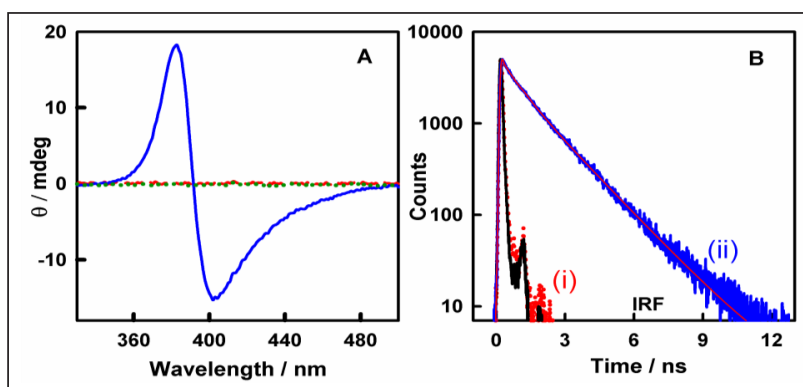

Figure 2. *(A)Circular dichroism spectrum of ThT in aqueous solution (dashed red line) and ThT in Heparin (blue solid line). The green dotted line represents Heparin in water without ThT(B) Excited-state decay trace for ThT in (i) aqueous solution and (ii) Heparin (λ_{ex} = 406 nm, λ_{em} = 560 nm). The solid black line represents instrument response function (IRF). [54]*

Heparin, (monitored at 560 nm) extends upto few nanoseconds (Figure 2B), with a multi-exponential decay kinetics.

The average excited-state lifetime for ThT in the aggregated state is calculated to be ~ 1.4 ns. The long lifetime indicates the presence of new aggregated species, and is also in conformity with the significantly reduced non-radiative processes (k_{nr} ~ 7.4 x 10^8 S-1 in Heparin as compared to k_{nr} ~ 10^{12} S-1 for ThT in water) of ThT aggregates in the presence of Heparin, leading to observed emission enhancement for H-aggregates of ThT. A similar long lifetime for the ThT aggregates has been also observed in presence of sulfated β-CD and its multi-

exponential decay nature has been attributed to the different conformational structure of the ThT in the excitonic or aggregated states.[53]

Selectivity is a very important parameter to evaluate the performance of a sensor. The structurally similar two glucosoaminogylcan analogues, Hyaluronic acid (HA) and Chondroitin sulfate (ChS) are often the main contaminants of clinical Heparin, thus, they were selected to evaluate the selectivity performance of ThT. The most intense fluorescence enhancement was observed for ThT in the presence of Heparin, while for Chs and HA, the fluorescence enhancement of ThT was found to be insignificant (Figure 3A). Thus, these results suggest that ThT displays very high selectivity for Heparin over its two structurally similar common contaminants. This selectivity for Heparin may be due to lower charge density and disadvantageous spatial orientation as well as more distant spatial distribution of anions on ChS and HA as compared to those of Heparin. On average, Heparin possesses three sulfate groups and one carboxylate group per disaccharide unit, among which one sulfate and carboxylate group reside at the same side of one saccharide ring, ChS carries one carboxylate and one sulfate group per disaccharide unit, whereas HA carries only one carboxyl group per disaccharide unit. The selectivity experiments for ThT were also extended to some mono- and disaccharides and various anions. None of these anions and molecules produce distinguished fluorescence enhancement for ThT (Figure 3B). These results demonstrate that our sensor system displays high selectivity towards Heparin.
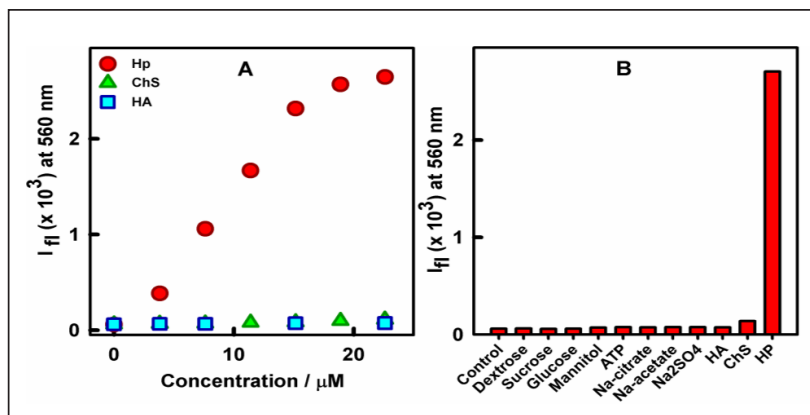
Figure 3. *(A) Variation in emission intensity (λ_{ex} = 400 nm, λ_{em} = 560 nm). of ThT at increasing concentrations of Hp, ChS and HA. (B) Selectivity analysis with various saccharides and anions.[54].*
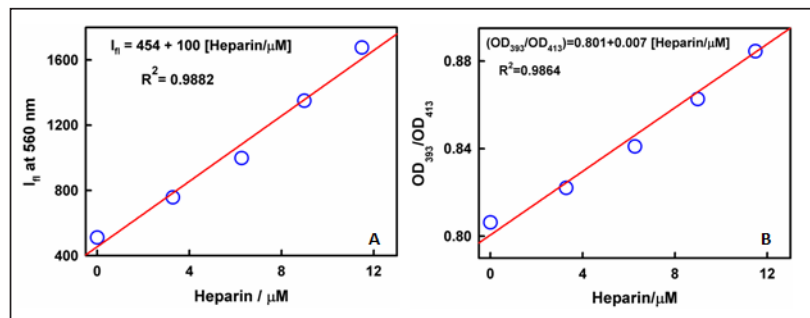
Figure 4. *(A) Variation in emission intensity of ThT (λ_{ex} = 400 nm, λ_{em} = 560 nm) with the increasing concentration of Heparin in 1% Human serum. The best-fit straight line (in red) represents linearity of the data. (B) Variation in the ratio of absorbance (OD_{393}/OD_{413}) of ThT with the increasing concentration of Heparin in 1% Human serum. The best-fit straight line (in red) represents linearity of the data. (The measurements were performed at a high concentration of dye in a thinner path-length cuvette).[54]*
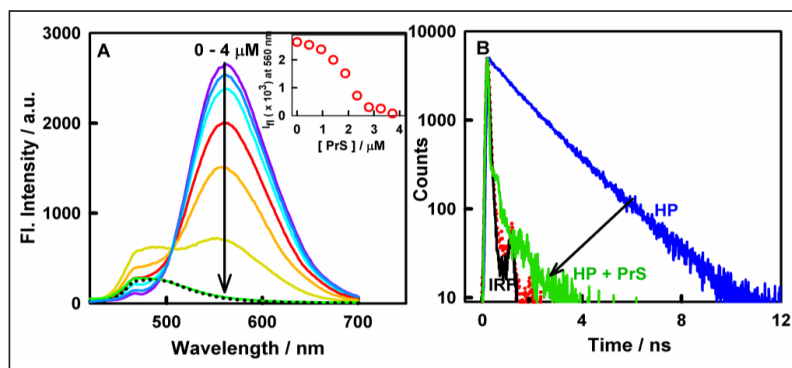
Figure 5. *(A) Steady-state emission spectrum (λ_{ex} = 400 nm) of ThT in Heparin at varying concentration of Protamine (PrS). ThT in only water is represented by the black dotted line. Inset: Variation in the emission intensity at 560 nm with increasing concentration of PrS (B) Transient decay trace for ThT in Heparin and ThT in Heparin with 3.7 µM PrS. The dotted red line represents the decay in water.[54].*

To evaluate the practical usefulness of our sensor system for Heparin in real biological samples, we attempted to detect the amount of Heparin in human serum samples using ThT. In diluted human serum samples containing ThT, the fluorescence intensity of ThT increased linearly with the increased concentration of Heparin (Figure 3A). We also analyzed the colorimetric response of ThT towards Heparin spiked human serum samples. The absorbance ratio at two wavelengths (OD_{393}/OD_{413}) increases linearly with the increasing concentrations of Heparin (Figure 3B). The calculated LOD for Heparin detection in human serum samples was

~90 nM. Thus, these results suggest that the developed ThT H-aggregate based detection method can be used to detect Heparin without significant matrix interference.

To reduce the risk of medical complications, in case of Heparin overdose,[24, 33] Protamine, the only clinically approved antidote for Heparin, is administered to reverse the anticoagulant effect of Heparin. [24] Here, we anticipated if we can monitor interaction of Protamine with Heparin, using the same system of ThT aggregates. Figure 5A shows that the fluorescence intensity of the ThT-Heparin complex decreases drastically with the gradual addition of Protamine. This decrease in emission intensity can be attributed to the disassembly of the ThT H-aggregates from Heparin surface, as a consequence of stronger electrostatic interaction of cationic Protamine with anionic Heparin. Since the free ThT is weakly emissive in nature, so the disassembly of the H-aggregates of ThT from the Heparin surface towards the monomeric form leads to a decrease in emission intensity. This dissociation of ThT aggregates was further supported by time-resolved emission measurements, where
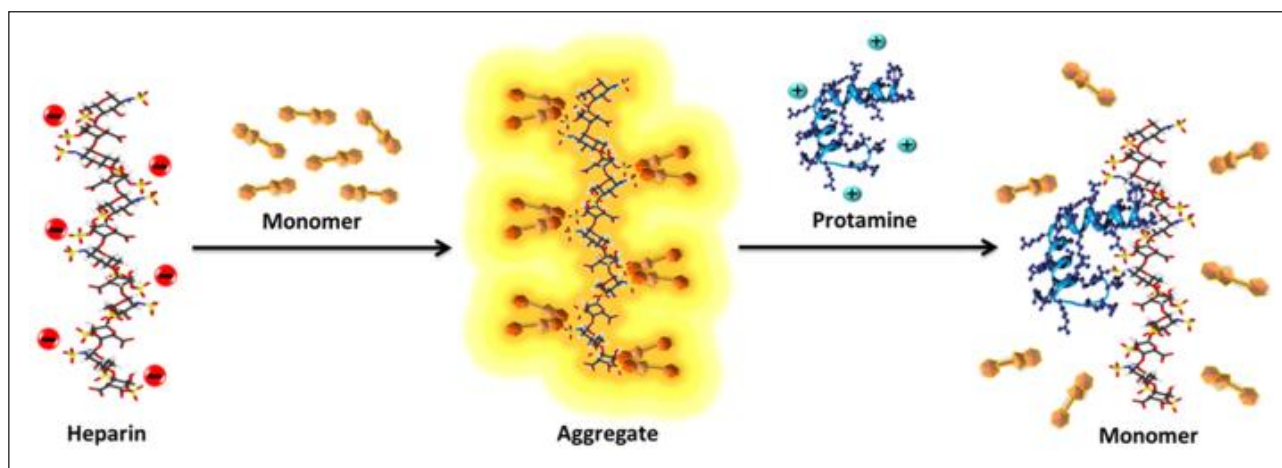
Scheme 2. *Schematic representation of Heparin induced ThT aggregates and its dissociation upon Heparin-Protamine interaction.[54].*

decay trace for ThT-Heparin complex reaches a situation similar to that of bulk water, upon addition of Protamine (Figure 5B).

Thus, this data suggests that H-aggregates of ThT formed on the Heparin surface can be used for investigating the interaction of Heparin with its only medically approved antidote Protamine. (Scheme 2)

In Summary, we have developed a turn-on sensor system for quick, economic and convenient detection of Heparin. This utilizes emission from "H-aggregates", which are otherwise considered as non-emissive and rather problematic in designing a biosensor. Hence our system provides a unique case for sensing a vital bio-molecule and a drug with extensive medical applications. Compared with the use of sophisticated fluorescent sensors, obtained through complicated and time-consuming synthetic steps, for identifying Heparin, the self-assembly induced, rather unusual H-aggregate emission reported here, exploits non-covalent interaction. Our sensor system offers several advantages including, label free approach, high sensitivity and selectivity, emission in the biologically is advantageous red-region, and most importantly constructed from in-expensive commercially available dye molecule, which is

expected to impart a large impact on the sensing field of Heparin. The assay shows reasonably good Heparin quantification range with very low LOD, even in 100 fold diluted human serum samples. Further, our system also represents one of the very few which can operate both through fluorimetry and colorimetry, providing great versatility to the sensing system. ThT can be also suitably used as a probe to explore the interaction of Heparin with its antidote, Protamine. Thus, our assay is expected to facilitate the Heparin related biochemical and biomedical research.

3.2 Pseudoisocyanine as a potential Heparin sensing probe

Herein, we have evaluated a monocationic cyanine based probe, known as Pseudoisocyanine, (PIC) which belongs to the class of molecular rotor and is a known molecule for assembling in the form of J-aggregates. Figure 6A represents the emission spectra of PIC in presence of Heparin. In aqueous solution, PIC does not show any detectable emission, however, in the presence of Heparin, PIC displays a large emission enhancement with an emission maximum at 571 nm. The increasing concentration of Heparin in the aqueous solution of PIC gradually increases its emission intensity, with an exceptional emission enhancement of 400 fold, at a concentration of ~35 μM of Heparin. The non-emissive nature of PIC in the aqueous solution (free monomer form) has been attributed to the torsional relaxation of intervening methine bridges of the PIC (see scheme-1 B), which is a major non-radiative process for the molecule and renders the molecule virtually non-emissive in bulk water.[57] However, enhanced emission for PIC, although very limited, has been achieved in the case of PIC aggregates.[58] PIC is known to form J-aggregates upon binding to negatively charged
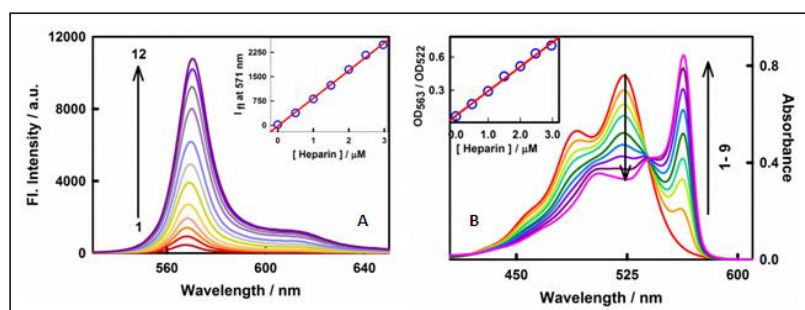
Figure 6. *(A) Steady-state emission spectra (λ$_{ex}$ = 520 nm) of PIC at different concentrations of Heparin (in μM) (1) 0.5 (2) 1 (3) 1.5 (4) 2 (5) 3 (6) 6 (7) 9 (8) 11.5 (9) 16 (10) 22 (11) 29 (12) 35. Inset: Changes in the fluorescence intensity of PIC with increasing concentration of Heparin. (B) Ground-state absorption spectra of PIC at varying concentration of Heparin (in μM) (1) 0 (2) 1 (3) 2 (4) 3 (5) 6 (6) 9 (7) 11.5 (8) 16 (9) 35. Inset: Variation in the ratio of absorbance (OD$_{563}$/ OD$_{522}$) of PIC with the increasing Heparin concentration.[31]*

synthetic polymers or polyelectrolytes, such as, carboxymethyl amylose, poly(styrene sulphonates), poly(acrylic acids) etc.[59-60] Since Heparin is the most negatively charged biological macromolecule, it is reasonable to expect that Heparin will also promote the formation of PIC aggregates. Thus, in the present case, the extra-ordinarily enhanced emission of PIC, with emission maximum at 571 nm, is assigned to the formation of J-aggregates of PIC taking place on the surface of Heparin. In this aggregated state, on the surface of Heparin, the tight packing of the PIC molecules prohibit the torsional relaxation of PIC, thus blocking the non-radiative process and consequently achieving large enhancement in the emission intensity. The PIC-heparin complex registers a quantum yield value of 0.024 which is very similar to the value reported for PIC in glycerol [61]. Note that the emission from the PIC J-aggregate, in the presence of Heparin, lies at a relatively red-region of the visible spectrum (571 nm) when compared to the reported fluorescence based probes [13-18, 62]. This constitutes a significant advantage for a bio-sensing probe, as this region of spectrum is relatively much less affected by the interference of auto-fluorescence of tissue components.

The titration data inferred that the linear regression was I_{571}= 5+ 857 x [Heparin/µM] with a correlation coefficient (R^2) of 0.996, for the linear increment in the emission intensity with an increasing concentration of Heparin, in a dynamic range of 0 –4 µM. The calculated detection limit of Heparin based on 3σ/s[63] was 2 nM, where σ represents the standard deviation of 10 blank measurements, and s represents the slope of the plot of emission intensity versus Heparin concentration. The observed detection limit for our sensor system is quite good when compared to the previously reported Heparin detection methods.[13, 15, 33, 64-66]

To inspect the possibility of Heparin detection by colorimetric method, the absorption spectra of PIC has been also measured in the presence of Heparin. Figure 6B represents the absorption spectra of PIC at varying concentrations of Heparin. PIC, in aqueous solution, presents an absorption maximum at 522 nm. The addition of Heparin to aqueous solution of PIC leads to dramatic changes in the absorption spectra of PIC with the evolution of a distinctly red-shifted sharp new absorption peak at 563 nm along with the concomitant reduction of monomeric absorption peak at 522 nm and with an isobestic point at 539 nm. This intense and sharp absorption band at a red-shifted wavelength is a characteristic of the J-type aggregate, where the dye molecules in the aggregate structure with interacts strongly with each other leading to new electronic excitations, which are coherently delocalized over many PIC molecules rather than being localized at individual PIC molecule. The delocalized excitation causes an intense and sharp absorption band for PIC J-aggregates. Similar spectral features have been reported for PIC J-aggregates in the system constituting of negatively charged synthetic polyelectrolytes.[59] Thus, the spectral features observed for PIC in the presence of Heparin can be ascribed to the formation of J-aggregates of PIC on the surface of Heparin. The appearance of distinct absorption maximum at 563 nm (in presence of Heparin), is significantly red-shifted by ~40 nm in comparison to PIC in aqueous

Figure 7. *(A) Change in emission intensity of PIC (λ_{ex} = 520 nm, λ_{em} = 571 nm) with varying concentrations of Heparin (HP), Chondroitin sulfate (ChS) and Hyaluronic acid (HA). (B). Fluorescence response of PIC towards various possible interfering polysaccharide and biomolecules.[31]*
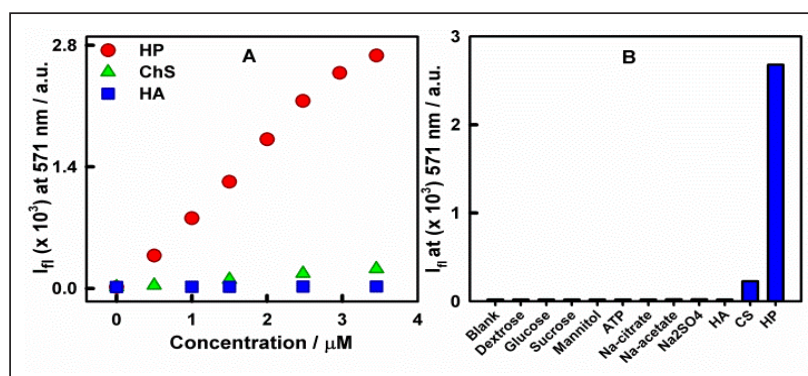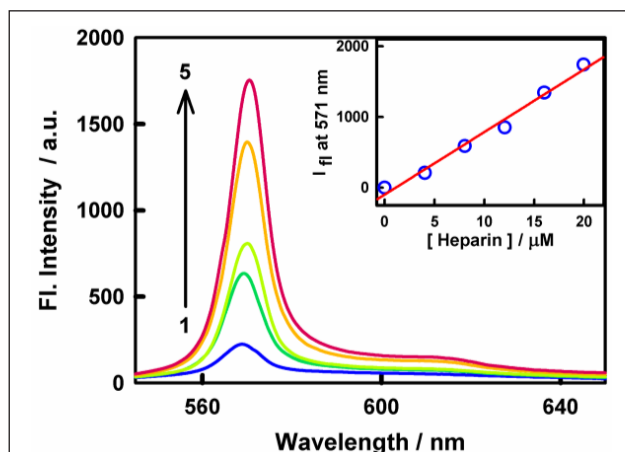
Figure 8: *Steady-state fluorescence spectrum (λ_{ex} = 520 nm) of PIC at varying concentration of Heparin in 3% human serum (1) 4 µM (2) 8 µM (3) 12 µM (4) 16 µM (5) 20 µM. Inset: The variation of emission intensity of PIC at 571nm with the increasing concentration of Heparin in 3% human serum. The best-fit straight line (in red) represents linearity of the data.[31]*

solution, facilitates visual color change of the experimental solution for the free and bound form of PIC.

We analyzed the spectrophotometeric titration data in a ratiometric fashion. For this purpose, we chose two wavelengths, i.e., 522 nm,
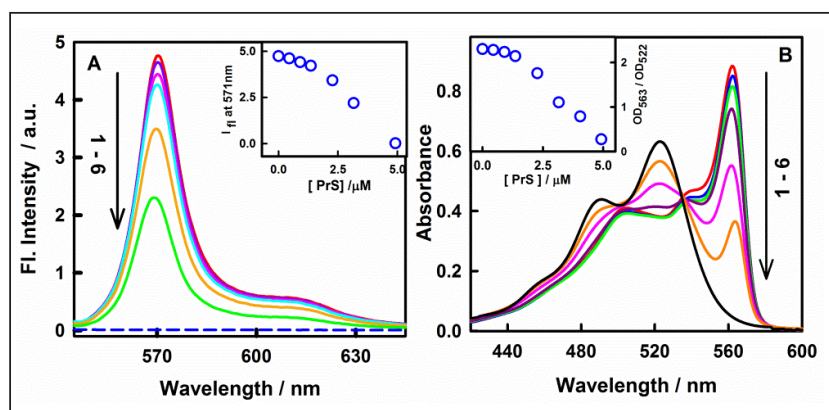
corresponding to monomeric species and 563 nm, corresponding to PIC J-aggregates. With a gradual increase in the concentration of Heparin from 0 to 5 µM, the ratio of optical density (OD) at these two wavelengths was observed to vary in a linear fashion, and the linear regression was OD_{563}/OD_{522}= 0.07 + 0.22 x [Heparin/µM] with a correlation coefficient (R^2) of 0.999. The limit of detection for Heparin calculated as 3.3σ/s was 9 nM. Thus, the present system of PIC offers an unique opportunity of dual read out of signal for Heparin i.e., both by fluorimetry and colorimetry.

We have also tested the selectivity of PIC towards Chondroitin 4-sulfate (ChS) and Hyaluronic acid (HA) (Figure 7A), in addition to some more possible interfering bio-analytes including several mono and disachharides such as glucose, mannitol, sucrose and dextrose, and some common anionic species, such as adenosine triphosphate, sodium citrate, sodium sulfate and sodium acetate. However, none of these species could induce the characteristic fluorescence response (Figure 7B) from PIC thus endorsing a very high selectivity of PIC towards detection of Heparin.

We next attempted to detect Heparin in human serum samples. In serum samples containing 12 µM PIC, the fluorescence intensity at 571 nm, was found to increase linearly in the concentration range of 0-20 µM of Heparin (Figure 8) and a linear correlation equation of I_{571}= 20+ 88.4 x [Heparin/µM] with a regression coefficient of 0.987. The LOD was found to be 11.4 nM. The linear detection range obtained in the serum matrix is also suitable for monitoring Heparin in the postoperative scenario or long term care (1.7-10 µM).[67] Thus, these results suggest that the induced emission response from the PIC J-aggregate has potential to sense Heparin in the serum

Figure 9. *(A) Steady-state fluorescence spectrum (λ_{ex} = 520 nm) of Heparin induced PIC J-aggregate system at varying concentration (in µM) of Protamine sulfate (PrS) (1) 0 (2) 0.5 (3) 1.0 (4) 1.4 (5) 2.3 (6) 5. Inset: Changes in the emission intensity at 571 nm with the varying concentration of PrS.(B) Ground-state absorption spectrum of PIC in Heparin at varying concentration of PrS (in µM) (1) 0 (2) 0.5 (3) 1.0 (4) 1.4 (5) 2.3 (6) 5. Inset: Changes in the ratio of absorbance (OD_{563}/OD_{522}) of PIC in Heparin with the increasing concentration of PrS.[31]*

matrix without significant interference from the matrix itself.

We have further investigated the binding of Protamine with Heparin and its impact on the fluorescence response of our sensor system, so as to utilize this variation for probing Protamine-Heparin interaction. Therefore, the fluorescence response of the PIC-Heparin complex was evaluated in the presence of the varying concentration of Protamine and the results have been presented in Figure 9. As evident from the figure, the addition of Protamine to the PIC-Heparin complex leads to a progressive decrease in the fluorescence intensity of the system in a concentration dependent fashion indicating gradual breakage of the PIC J-aggregate on the surface of Heparin. This observation is attributed to the fact that Protamine is an arginine rich positively charged peptide bearing very high binding affinity for Heparin and thus upon binding to Heparin, weakens the interaction of PIC with Heparin leading to disassembly of PIC J-aggregate from the surface of Heparin. The interaction of Protamine with Heparin was also monitored using steady-state absorption measurements and the results have been summarized in figure 9B. As evident from the figure, the addition of Protamine to the PIC-Heparin complex leads to a sharp and progressive decrease in the J-aggregate absorption band causing a reduction in the ratio of the absorbance (OD_{563}/OD_{522}) in a manner similar to that of the steady-state emission measurements. This decrease in the J-aggregate band of the PIC-Heparin complex can be assigned to the dissociation of PIC from the surface of Heparin due to stronger electrostatic interaction of positively charged Protamine with negatively charged Heparin. Thus, these results clearly suggest that, in addition to sensing Heparin, PIC can also be employed to monitor the interaction of Heparin with Protamine.

We would like to conclude with a brief discussion on the advances that we have made in the current work as compared to our previous work,[54] where we employed Thioflavin-T, a
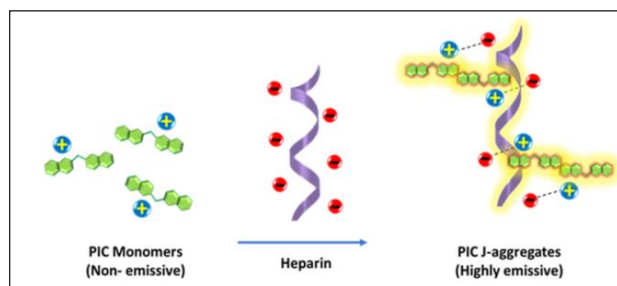
Scheme 3. *Schematic presentation of Heparin-induced PIC aggregates.[31]*

molecular rotor probe, as a sensor for Heparin. The fundamental difference in the strategy that we employed in the present case was the utilization of type of aggregation formed in the presence of Heparin. The type of aggregation has large bearing on the emission yield of the aggregate assembly. For example, it is known that H-type aggregate, where the chromophores are arranged head-to-head, are weakly emissive in nature whereas J-type aggregation (head-to-tail arrangement of chromophore) are, in general, highly emissive in nature. In the previous case of Thioflavin-T, we had H-type aggregates where we could achieve only limited enhancement of upto 45 fold.[54] In the present case, we have chosen Pseudoisocyanine (PIC) molecule, which has been reported to have a tendency to form J-aggregate in some other chemical environment, and to our expectation, we could observe an intense J-aggregate emission in presence of Heparin. Thus, in the present work, which employs Pseudoisocyanine (PIC) dye, we have been able to achieve an impressive emission enhancement of upto ~400 fold as compared to ~45 fold in our previous work that leads to ~ 8 fold improvement in the detection limit in an even higher concentration of serum matrix (11.4 nM for PIC in 3 % serum vs 90 nM for Thioflavin-T in 1 % serum). Apart from emission, the changes in the absorption spectra for our current probe molecule (PIC) are way more distinct and significant, in response to Heparin, as compared to our previous probe (ThT). In the case of PIC, a large red-shifted ($\Delta\lambda$~ 41 nm) sharp and distinct absorption band is observed specifically in the presence

of Heparin which leads to a colour change in the experimental solution that can be detected even with naked eyes. On the other hand, the changes in the absorption spectra for ThT are not that drastic. Another noteworthy advantage associated with our current sensing system (PIC) is that although the emission maximum for both the systems are not widely different (571 nm for PIC-Heparin vs 560 nm for ThT-Heparin), the long wavelength (red side) excitation for the PIC (λ_{ex} = 520 nm) is definitely an advantage over our

previous molecule, ThT (λ_{ex}=400 nm), from the viewpoint of reduced auto-fluorescence. Thus, although the working mechanism for both the dyes (turn-on emission) is similar, our present probe (PIC) offers many crucial advantages over our previous probe ThT, which are important from sensing perspective.

3.3. YOPRO-1 as a potential Heparin sensing probe

Since the whole idea of using cationic molecular rotor probe for Heparin sensing is to exploit the electrostatic interaction between the cationic probe and anionic Heparin, thus, employing a molecular rotor probe with a higher cationic charge will be a desirable advance in the field of Heparin sensing for better performance. Thus, in the present contribution, we introduce a dicationic unsymmetric cyanine based molecular rotor dye, commercially known as YOPRO-1 (See Scheme 1C), for the fluorescence based Heparin detection. Figure 10 A represents the steady-state fluorescence spectra of YOPRO-1 in the presence of Heparin. Heparin additions into the aqueous solution of YOPRO-1 results into a huge emission enhancement at 580 nm compared to a weak emission band, obtained at 510 nm, in case of aqueous solution of YOPRO-1. A large red shift of ~70 nm, in the emission maximum, and a ~55 fold enhancement in emission intensity is seen in the emission spectra of YOPRO-1 upon the addition of increasing concentrations of Heparin. The weak emission of free YOPRO-1 has been attributed to the molecular rotor nature of the
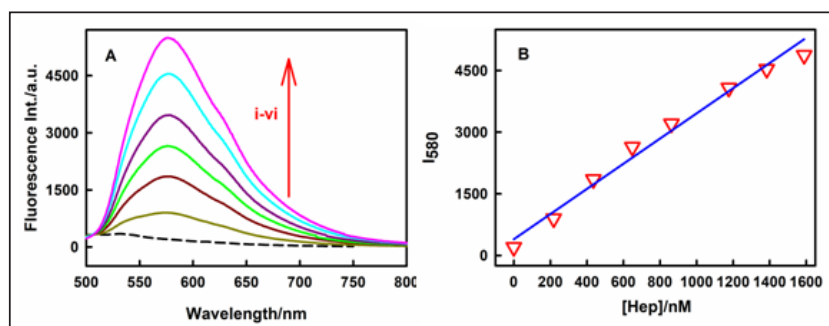
Figure 10. *(A) Steady-state fluorescence spectra of YOPRO-1 in water (λ_{ex}=440nm) at various Heparin concentrations (in nM) (i) 220 (ii) 430 (iii) 680 (iv) 960 (v) 1380 (vi) 2090. The steady-state fluorescence spectrum of YOPRO-1 in water is represented by a dashed black line. (B) Variation in the emission intensity at 580nm with increasing Heparin concentration. The data points are represented by red triangles whereas the linear fit to these data points is represented by a solid blue line.[72]*
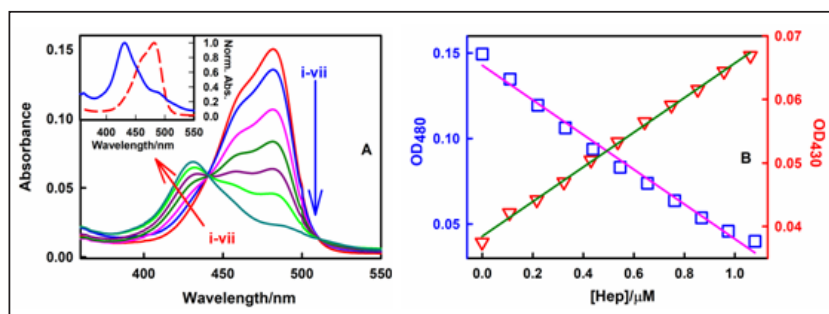
Figure 11. *(A) Ground-state absorption spectra of YOPRO-1 in water at varying Heparin concentrations (in µM) (i) 0 (ii) 0.11 (iii) 0.32 (iv) 0.54 (v) 0.76 (vi) 0.97 (vii) 1.60. Inset: Normalized absorption spectra of YOPRO-1 in water (dashed red line) and YOPRO-1 bound to 4.7 µM Heparin (solid blue line) (B) Variation in the absorbance at 480 nm and 430 nm respectively with increasing Heparin concentrations. The data points obtained for the absorbance at 480 nm are represented by blue squares and the linear fit to these data points is represented by a solid pink line, whereas, the data points obtained for the absorbance at 430 nm are represented by red triangles and the linear fit to these data points is represented by a dark green line.[72]*

probe. [68] Some of the unsymmetrical cyanine dyes, including YOPRO-1, are reported for turn on detection of double stranded DNA, [68-71] where the torsional motion of fragments of YOPRO-1 are heavily impeded in the presence of DNA, leading to large emission enhancement. Nevertheless, the exciting class of these cyanine dyes have never been utilized for Heparin detection. Thus, although it can be considered that the increase in emission intensity of YOPRO-1 in the present case, is due to the impediment of torsional relaxation in the monomeric form of the YOPRO-1 upon its interaction with Heparin, however, according to the existing literature, it is known that the monomeric form of YOPRO-1, emits at 510 nm, including in the DNA matrix. [68-69] Thus, the presence of a large red shift of ~70 nm (λ_{em}= 580nm) in the emission maximum suggests that the emission enhancement obtained, in the presence of Heparin, is not due to the monomeric form of the probe, but due to some other molecular form of the probe. Since Heparin is known as the most negatively charged biomolecule, it is expected to induce aggregation of the dicationic probe, YOPRO-1 due to the strong electrostatic interactions between them followed by charge neutralization of the probe molecule on the surface of Heparin. Similar red-shifted emission due to aggregation of molecular rotor based probe molecules has been also previously reported in literature. "The emission intensity is seen to increase linearly with a gradual increase in the concentration of Heparin in the range of 0-1600 nM with a linear regression equation of I580 (subscript)=3063 X[Heparin]/nM+393, R2 (superscript)=0.978, (Figure 10). The limit of Heparin detection was calculated, using the formula 3.3σ/s, and was found to be 0.48 nM."

For further investigations on the aggregated form of YOPRO-1 and to examine the prospect of colorimetric detection of Heparin, ground-state absorption measurements were carried out at various concentrations of Heparin and Figure 11A displays the results. Initially, the absorption maxima of the aqueous solution of YOPRO-1 appears at 480 nm, however, upon gradual addition of Heparin to the solution, impressive changes in the absorption spectra of YOPRO-1 are obtained, with a remarkable blue shift of ~50 nm that results into a new absorption maxima at 430 nm (See figure 11A, inset). This kind of blue shift in the absorption maximum of YOPRO-1 is in sharp contrast with that observed for the monomeric form of the dye, in presence of other negatively charged biomolecules, such as, DNA, where it registers a red-shift in the absorption maximum.[73] Thus, the distinct blue shift observed in the present case, suggests the presence of YOPRO-1 in a molecular form different from its more frequently encountered monomeric form. Such new absorption bands, blue-shifted from its free monomeric form, are indicative of the formation of H-aggregates of YOPRO-1 molecules. This can be understood by the excitonic theory,[74] according to which, when the transition dipoles of chromophores maintain a head-to-head arrangement, known as H-type aggregate, the transition from ground state to only higher energy exciton state is allowed, which leads to shift towards the higher energy (blue shift) of the

Figure 12. *(A) Transient decay traces of YOPRO-1 in water (λ_{ex} = 445, λ_{em} = 580) in the (1) absence (red line) and in the (2) presence of 0.65 µM Heparin (dark green line). The instrument response function is displayed by a black dotted line. (B) Response plot for ($\triangle I_{580}$) for various proteins at a concentration at 2.7 µM. The presented error bar is the standard error of the mean.[72]*
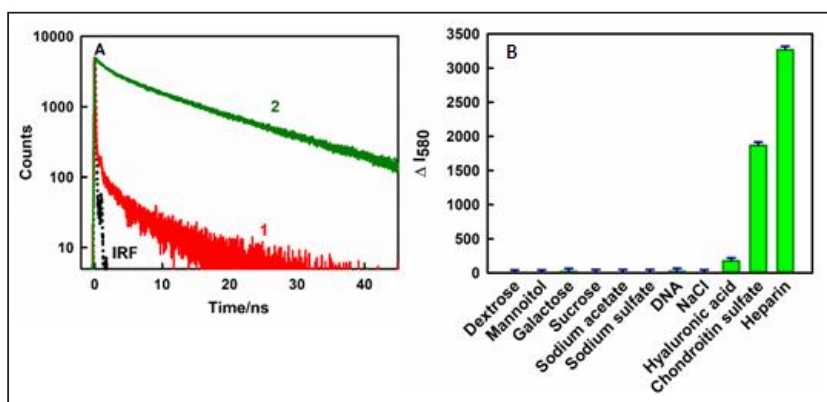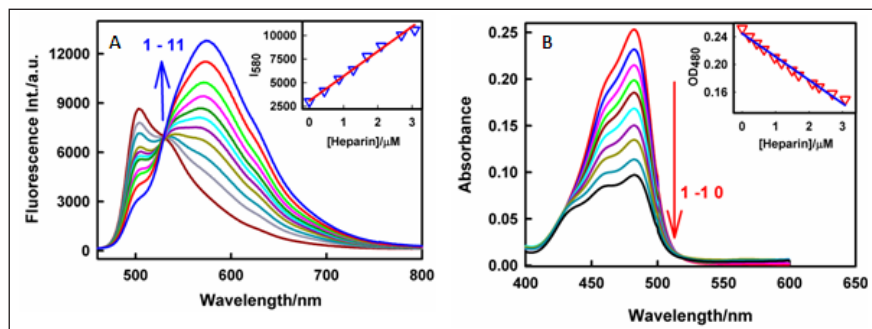
Figure 13. *(A) Steady-state fluorescence spectra of YOPRO-1 in 20 % Human serum matrix (λ_ex=440 nm) in presence of various concentrations of Heparin (in µM) (1) 0 (2) 0.11 (3) 0.54 (4) 0.86 (5) 1.28 (6) 1.49 (7) 1.69 (8) 2.30 (9) 2.69 (10) 3.82 (11) 6.58. Inset: Variation in the emission intensity at 580nm with increasing concentration of heparin. The blue triangles represent the data points whereas the solid red line represents the linear fit to these data points. (B) Ground-state absorption spectra of YOPRO-1 in 20 % Human serum matrix in presence of increasing concentrations of Heparin (in µM) (1) 0 (2) 0.44 (3) 0.86 (4) 1.28 (5) 1.69 (6) 2.30 (7) 3.08 (8) 3.82 (9) 5.25 (10) 6.58. Inset: Variation in the absorbance at 480nm with increasing concentration of Heparin. The red triangles represent the data points obtained for the emission intensity at 580 nm, whereas, the solid blue line represents the linear fit to the data points.[72]*

absorption maxima. Whereas, when the transition dipole arrangement is head-to-tail, the transition from ground-state to lower excitonic state is allowed, leading to a lower energy shift (red-shift) in the absorption spectra. Thus, the blue-shifted band for YOPRO-1, observed in the presence of Heparin, clearly indicates the H-type arrangement of molecular dipoles of YOPRO-1 in the aggregated state.

Since the absorption maxima of the monomer form and the H-aggregate form of YOPRO-1 is distinctly separated by ~50 nm shift, analysis of the titration data was performed at both the wavelengths i.e. at 480 nm corresponding to YOPRO-1 monomer, and at 430 nm, corresponding to YOPRO-1 H-aggregates (Figure 11B). The linear regression of the monomer form was OD_{480}=-0.101[Heparin]/µM+0.1427, R^2=0.986 and that of the H-aggregate form was OD_{430}=0.0267[Heparin]/µM+0.038, R^2=0.997. The LOD of the system (using absorbance data) was calculated using the formula of 3.3σ/s and was found to be 3.9 nM. Thus, the current framework offers a very good opportunity of read out of signal in dual-way for the quantification of Heparin, i.e.,

in terms of fluorimetry as well as colorimetry.

In order to further understand the mechanism of enhanced emission for molecular rotor class of molecules, carrying out time resolved emission measurements are crucial, as they provide important information on excited state relaxation of the probe molecules. Therefore, time-resolved emission measurements for YOPRO-1 in aqueous solution and, in the presence of Heparin, were carried out. As seen in figure 3A, in aqueous solution, YOPRO-1 records a very fast decay trace (within the limit of the instrument, IRF~180 ps). This suggests that the excited state of YOPRO-1 undergoes efficient non-radiative deexcitation on an ultrafast time scale. Infact, a lifetime of ~2 ps has been reported for YOPRO-1 in aqueous solution.[68] However, a dramatic slowdown in the transient decay traces is observed in the presence of Heparin (Figure 12A). The average excited state lifetime was determined to be ~12.8 ns. Note that such an enormous increment in the excited-state lifetime has not been noted before for YOPRO-1, even in the presence of DNA, for which they are known to be excellent binders.

Further, we have also tested the selectivity of YOPRO-1 towards Heparin in terms of fluorescence response, towards various related analytes. The selected analytes included the two structurally similar glycosaminoglycan analogs, Chondroitin sulfate and Hyaluronic acid, which are the main contaminants of clinical Heparin along with some coexisting analytes. The response of YOPRO-1 in terms of difference in the initial and final emission intensity ($\triangle I_{580}$) obtained at equal concentrations of tested analytes were recorded and the results are displayed in figure 12B. It is evident from the figure that YOPRO-1

shows maximum fluorescence response towards Heparin compared to the other biomolecules.

An assay for Heparin detection in complex human serum matrix was performed. Steady-state fluorescence measurements of YOPRO-1 in serum matrix were carried out and the results are displayed in 13 A. As evident from the figure, YOPRO-1 shows a sensitive response towards the spiked Heparin in the serum. A linear response in the concentration range of 0-3μM was obtained with a linear regression of I_{580}= 2671[Heparin]/μM+3071, R^2=0.992 and a LOD based on the formula 3.3σ/s was found to be 7.4 nM in terms of fluorescence measurements. We have also evaluated the response in serum matrix by using ground-state absorption measurements. (Figure 13B) and obtained a linear regression of OD_{480}=-0.033[Heparin]/μM+0.244 and a LOD of 12 nM.

Lastly, we have also employed YOPRO-1-Heparin complex to detect Protamine concentrations. Figure 14A displays the steady-state emission spectra of YOPRO-1-Heparin complex at various concentrations of Protamine. The emission intensity of the complex continuously decreases upon increasing concentrations of Protamine. This drop in the emission intensity can be ascribed to the displacement of YOPRO-1 H-aggregates from the surface of Heparin due to very strong electrostatic interactions between cationic Protamine and anionic Heparin. This strong binding of Protamine to Heparin leads to release of free YOPRO-1 in the solution which are weakly emissive and a decrease in the emission intensity is thus observed. The signal response for Protamine concentration was found to be in the range of 0-350 nM with a linear regression of I_{580}=-14788 [Prs]/μM+5187, R^2=0.982. The limit of detection of Protamine based on the formula 3.3σ/s was found to be 0.1 nM. Thus, it can be concluded that sensing scheme can also be employed for the detection of Protamine along with Heparin detection.

The possibility of Protamine detection through ground-state absorption measurements was also investigated for the current system. Figure 14B represents the ground-state absorption spectra of YOPRO-1-Heparin complex with increasing Protamine concentrations. The blue shifted absorption band at 430 nm,
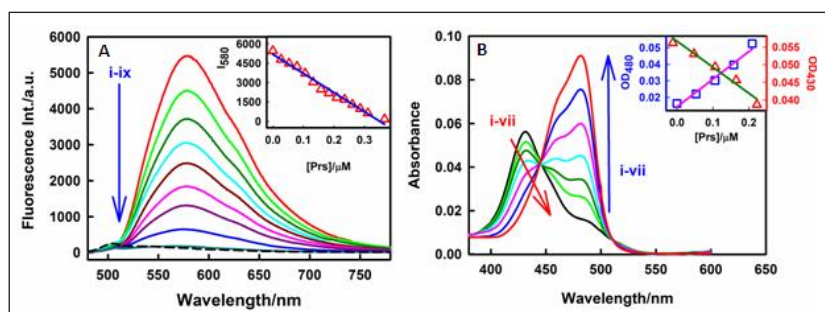
Figure 14. (A) *Steady-state fluorescence spectra of YOPRO-1-Heparin complex in aqueous solution (λ_{ex}=440 nm) at various Protamine concentrations (in μM) (i) 0 (ii) 0.05 (iii) 0.10 (iv) 0.13 (v) 0.15 (vi) 0.21 (vii) 0.26 (viii) 0.31 (ix) 0.36. The steady-state emission spectrum of YOPRO-1 in water has been displayed in black dashed line. Inset: Plot of changes in the emission intensity at 580 nm with increasing Protamine concentrations. (B) Ground-state absorption spectra of YOPRO-1-Heparin complex in presence of various concentrations of Protamine (in μM) (i) 0 (ii) 0.08 (iii) 0.13 (iv) 0.18 (v) 0.23 (vi) 0.28 (vii) 0.38. Inset: Plot of changes in the absorbance at 480 nm and 430 nm with increasing Protamine concentrations. The absorbance data obtained at 430 nm are represented in red triangles and the linear fit to the data points is represented in dark green line, whereas, the absorbance data obtained at 480 nm is represented in blue squares and the linear fit for the data points is represented in solid pink line.[72]*

associated with the formation of H-aggregates of YOPRO-1, is seen to gradually decrease alongside a corresponding increment in the monomer band at 480 nm. The strong interaction of Protamine and Heparin leads to the displacement of the H-aggregates of YOPRO-1 from the surface of Heparin towards the monomeric form of YOPRO-1 free in the aqueous solution. The reverse signals obtained in terms of absorbance of the monomer and the aggregate band can be successfully employed for Protamine detection through absorption measurements. Protamine detection could be carried out in a linear range of 0-0.2μM and LOD for Protamine
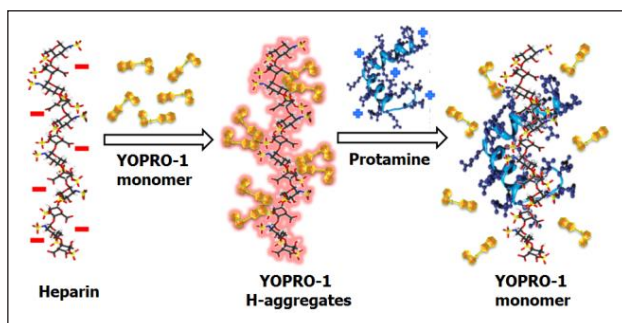
Scheme 4. *Schematic illustration of Heparin induced aggregate formation of YOPRO-1 and its subsequent dissociation by Protamine-Heparin interaction.[72]*

was calculated to be 6 nM based on 3.3σ/s. The linear regression for the signal variation at 480 nm (monomeric form) was OD_{480}=0.167[Prs]/μM+0.0142, R^2=0.974, while that at 430 nm, (aggregate form) was OD_{430}=-0.082[Prs]/μM+0.057, R^2=0.972. Thus, the current system provides a benefit of dual read out in terms of fluorimetry as well as colorimetry.

Overall, we have developed a turn on sensor for simple, economic, and dual read out system for the effective detection of Heparin. The sensing system utilized the emission of H-aggregates of a dicationic cyanine derivative, YOPRO-1 formed in the presence of Heparin. Interestingly, H-aggregates are usually considered to be non-emissive, problematic in biosensing applications, which, in contrast, here, helps in sensitive detection of Heparin. Moreover, the formation of emissive H-aggregates has never been reported for YOPRO-1 in any biological or chemical environment. Importantly, most of the reported fluorescent probes for Heparin are monocationic in nature, and provides only limited strength to the electrostatic interactions, thereby largely limiting their response in serum matrix. In the present case, YOPRO-1 is a dicationic probe, which significantly strengthens its interaction with Heparin which is evident from the response obtained in high percentage of human serum matrix (20%). YOPRO-1 is extensively utilized for DNA staining and detection, however for the first time, in this report, we demonstrate its application in sensing a very vital biomolecule, Heparin. The

probe also shows high selectivity for Heparin over its structurally similar analogs, Chondroitin sulfate and Hyaluronic acid. Our sensing system provides several advantages such as emission in the biologically beneficial red region, high sensitivity and selectivity and most importantly, the commercial availability of the probe molecule. Along with Heparin quantification, this sensor system can also be utilized for the detection of its medically approved antidote, Protamine with very low LOD in terms of both colorimetry and fluorimetry. Importantly, this sensing system shows a good response in the biologically complex, human serum matrix suggesting the potential application of this system in real life scenario.

4. Conclusions

Overall, we have identified various molecular rotor based cationic fluorophores ThT, PIC and YOPRO-1 for the detection of Heparin. The utilized fluorophores enable us to detect Heparin optically via fluorimetry as well as colorimetry. The sensing systems provide various advantages such as, high sensitivity and selectivity towards Heparin and most importantly, the sensing framework is developed with the use of commercially available probe molecules. The probe molecules were also utilized for the detection of Protamine, which is the only clinical antidote of Heparin. The performance of these fluorophores was also evaluated in real samples (human serum matrices). Although the monocationic probe molecules, viz. ThT and PIC could detect Heparin only in a limited concentration of serum, we have made a significant development by utilizing a dicationic probe molecule, YOPRO-1, which significantly strengthens its interaction with Heparin and is evident from the response obtained in high percentage of human serum matrix (20%). The developed assays for Heparin sensing are expected to contribute significantly to Heparin related biomedical and biochemical research.

References

1. I. Capila, R.J. Linhardt, Angew. Chem., Int. Ed., 41 (2002) 390.
2. G.J. Despotis, G. Gravlee, K. Filos, J. Levy, Anesthesiology, 91 (1999) 1122.
3. D.L. Rabenstein, Nat. Prod. Rep., 19 (2002) 312.
4. B. Girolami, A. Girolami, Semin. Thromb. Hemostasis., 32 (2006) 803.
5. T.E. Warkentin, M.N. Levine, J. Hirsh, P. Horsewood, R.S. Roberts, M. Gent, J.G. Kelton, N. Engl. J. Med., 332 (1995) 1330.
6. J.S. Ginsberg, N. Engl. J. Med., 335 (1996) 1816.
7. R.Y. Zhan, Z. Fang, B. Liu, Anal. Chem., 82 (2010) 1326.
8. K.L. Gemene, M.E. Meyerhoff, Anal. Chem., 82 (2010) 1612.
9. S. Beni, J.F.K. Limtiaco, C.K. Larive, Anal. Bioanal. Chem., 399 (2010) 527.
10. Z. Zhong, E.V. Anslyn, J. Am. Chem. Soc., 124 (2002) 9014.
11. R. Cao, B. Li, Chem. Commun., 47 (2011) 2865.
12. X. Fu, L. Chen, J. Li, M. Lin, H. You, W. Wang, Biosens. Bioelectron., 34 (2012) 227.
13. L. Cai, R. Zhan, K.-Y. Pu, X. Qi, H. Zhang, W. Huang, B. Liu, Anal. Chem., 83 (2011) 7849.
14. H. Szelke, S. Schubel, J. Harenberg, R. Kramer, Chem. Commun., 46 (2010) 1667.
15. Q. Dai, W. Liu, X. Zhuang, J. Wu, H. Zhang, P. Wang, Anal. Chem., 83 (2011) 6559.
16. W. Sun, H. Bandmann, T. Schrader, Chem. Eur. J., 13 (2007) 7701.
17. K.-Y. Pu, B. Liu, Adv. Funct. Mater., 19 (2009) 277.
18. A.T. Wright, Z. Zhong, E.V. Anslyn, Angew. Chem. Int. Ed., 44 (2005) 5679.
19. P. Mikuš, I. Valášková, E. Havránek, J. Pharm. Biomed. Anal. , 36 (2004) 441.
20. Q. Yang, X. Wang, H. Peng, M. Arabi, J. Li, H. Xiong, J. Chood, L. Chen, Sens. Actuators B Chem., 302 (2020) 127176.
21. K. Yin, F. Yu, D. Liu, Z. Xie, L. Chen, 223 (2016) 799.
22. Z. Zhang, H. Wang, Z. Chen, X. Wang, J. Choo, L. Chen, Biosens. Bioelectron., 114 (2018) 52.
23. T. Lou, Z. Chen, Y. Wang, L. Chen, ACS Appl. Mater. Interfaces, 3 (2011) 1568.
24. S.M. Bromfield, E. Wilde, D.K. Smith, Chem. Soc. Rev., 42 (2013) 9184.
25. L.-J. Chen, Y.-Y. Ren, N.-W. Wu, B. Sun, J.-Q. Ma, L. Zhang, H. Tan, M. Liu, X. Li, H.-B. Yang, J. Am. Chem. Soc., 137 (2015) 11725.
26. C.W. Chan, D.K. Smith, Chem. Commun., 52 (2016) 3785.
27. P. Jana, M. Radhakrishna, S. Khatua, S. Kanvah, , Phys. Chem. Chem. Phys., 20 (2018) 13263.
28. D. Kim, U. Lee, J. Bouffard, Y. Kim, Adv. Opt. Mater., 8 (2020).
29. L. Fan, D. Jia, W. Zhang, Y. Ding, Analyst, 145 (2020) 7809.
30. Z. Yang, X. Fan, W. Cheng, Y. Ding, W. Zhang, Anal. Chem., 91 (2019) 10295.
31. N.H. Mudliar, P.M. Dongre, P.K. Singh, Sens. Actuators B Chem., 301 (2019) 127089.
32. Z. Zhang, S. Li, P. Huang, J. Feng, F.-Y. Wu, Microchimica Acta, 186 (2019) 790.
33. Z. Liu, Q. Ma, X. Wang, Z. Lin, H. Zhang, L. Liu, X. Su, Biosens. Bioelectron., 54 (2014) 617.
34. D.-H. Kim, Y.J. Park, K.H. Jung, K.-H. Lee, Anal. Chem., 86 (2014) 6580.
35. H. Lee, B. In, P.K. Mehta, M.Y.L.N. Kishore, K.H. Lee, ACS Appl. Mater. Interfaces, 10 (2018) 2282.
36. P.K. Mehta, H. Lee, K.H. Lee, Biosens. Bioelectron., 91 (2017) 545.
37. Z. Yang, L. Fan, X. Fan, M. Hou, Z. Cao, Y. Ding, W. Zhang, Anal. Chem. , 92 (2020) 6727.
38. R.S. Aparna, A.J.S. Devi, R.R. Anjana, J. Nebu, S. George, Analyst, 144 (2019) 1799.
39. Y. Gao, K. Wei, J. Li, Y. Lic, J. Hu, Sens. Actuators, B., 277 (2018) 408.
40. J.O. Escobedo, O. Rusin, S. Lim, R.M. Strongin, Curr Opin Chem Biol. , 14 (2010) 64.
41. P.K. Singh, M. Kumbhakar, H. Pal, S. Nath, J. Phys. Chem. B, 113 (2009) 8532.
42. P.K. Singh, M. Kumbhakar, H. Pal, S. Nath, J. Phys. Chem. B 114 (2010) 2541.
43. A.A. Awasthi, P.K. Singh, J. Phys. Chem. B, 121 (2017) 6208−6219.
44. A.M. Desai, S.P. Pandey, P.K. Singh, Phys. Chem. Chem. Phys., 23 (2021) 9948.
45. G.S. Singh, S.P. Pandey, P.K. Singh, Phys. Chem. B, 125 (2021) 7033.
46. N.H. Mudliar, P.K. Singh, Chem. Euro. J, 22 (2016) 7394.
47. P.K. Singh, M. Kumbhakar, H. Pal, S. Nath, J. Phys. Chem. B, 112 (2008) 7771.
48. P. Verma, S. Nath, P.K. Singh, M. Kumbhakar, H. Pal, J. Phys. Chem. B, 112 (2008) 6363.
49. P.K. Singh, M. Kumbhakar, H. Pal, S. Nath, J. Phys. Chem. B, 113 (2009) 1353.
50. J.R. Lakowicz, Principle of Fluorescence Spectroscopy, Plenum Press, New York, 2006.
51. M.A. Haidekker, E.A. Theodorakis, J. Biol. Eng., 4 (2010) 11.
52. P.K. Singh, S. Nath, J. Phys. Chem. B, 117 (2013) 10370−10375.
53. N.M. Mudliar, P.K. Singh, Chem. Euro. J, 22 (2016) 7394.
54. N.H. Mudliar, P.K. Singh, Appl. Mater. Interfaces 8(2016) 31505.
55. F.C. Spano, Acc. Chem. Res., 43 (2010) 429.
56. D. Fedunova, P. Huba, J. Bagelova, M. Antalik, Gen. Physiol. Biophys., 32 (2013) 215.
57. R.F. Khairutdinov, N. Serpone, J. Phys. Chem. B, 101 (1997) 2602.
58. H. Fidder, Chem. Phys., 341 (2007) 158.
59. C. Peyratout, E. Donath, L. Daehne, J. Photochem. Photobio., A, 142 (2001) 51.
60. O.-K. Kim, J. Je, G. Jernigan, L. Buckley, D. Whitten, J. Am. Chem. Soc., 128 (2006) 510.
61. H.-P. Dorn, A. Muller, Chem. Phys. Lett., 130 (1986) 426.
62. S. Wang, Y.-T. Chang, Chem. Commun. (2008) 1173.
63. IUPAC Compendium of Analytical Nomenclature: Definitive Rules, Pergamon Press, Oxford, 1981.
64. H. Liu, P. Song, R. Wei, K. Li, A. Tong, Talanta, 118 (2014) 348.

65. Y. Ling, Z.F. Gao, Q. Zhou, N.B. Li, H.Q. Luo, Anal. Chem., 87 (2015) 1575.

66. S.-N. Ding, C.-M. Li, N. Bao, Biosens. Bioelectron., 64 (2015) 333.

67. K.-Y. Pu, B. Liu, Macromolecules, 41 (2008) 6636.

68. T.L. Netzel, K. Nafisi, M. Zhao, J.R. Lenhard, I. Johnson, J. Phys. Chem. B, 99 (1995) 17936.

69. K. Uno, T. Sasaki, N. Sugimoto, H. Ito, T. Nishihara, S. Hagihara, T. Higashiyama, N. Sasaki, Y. Sato, K. Itami, Chem. Asian J., 12 (2017) 233.

70. G. Cosa, K.-S. Focsaneanu, J.R.N. McLean, J.P. McNamee, J.C. Scaiano, Photochem., 73 (2001) 585.

71. M. Levitus, S. Ranjit, Q. Rev. Biophys., 44 (2011) 123.

72. S.P. Pandey, P. Jha, P.K. Singh, J. Mol. Liq., 328 (2021) 115327.

73. R.W. Sabnis, Handbook of Fluorescent Dyes and Probes, John Wiley & Sons, Inc., New Jersey, 2015.

74. M. Kasha, Radiat. Res., 20 (1963) 55.

Miss Shrishti Pandey *is currently a Ph.D. (Biotechnology) Student at Amity University Mumbai, under the Lady TATA Memorial Trust's- Junior Research Scholarship. Her research interest involves developing fluorescence-based sensors for various important bio-analytes, which include amino acids, protein aggregates, Heparin, Protamine, etc. Till date, Miss Shrishti has authored 18 publications in high impact international journals including 5 in Sensors and Actuators B: Chemical, 5 in Journal of Molecular Liquids and in other prestigious journals, such as, Journal of Physical Chemistry, International Journal of Biological Macromolecules, Dyes and Pigments, etc. Recently, she has received the Lady Tata Memorial Trust's - Award of Scientific Research Scholarship. She has also been awarded the Best oral presentation award for students by the Japanese Photochemistry Association in the year 2021.*

Dr. Prabhat K. Singh *is currently working as Scientific Officer (F) at Radiation and Photochemistry Division of Bhabha Atomic Research Centre, India. His research interests include crafting of self-assembled materials and their applications in designing optical sensors for chemo-sensing and bio-sensing applications. Till date, Dr. Singh has published 104 research articles in peer-reviewed international journals. He is recipient of the Young Scientist Award by Department of Atomic Energy (DAE), Indian Science Congress Association (ISCA) and National Academy of Sciences, India (NASI). He has been selected as the Member of the India's first Young Academy, i.e., Indian National Young Academy of Sciences (INYAS) under the flagship of INSA, as well as, the Member of NASI. He has also served as Associate of Indian Academy of Science (IASc), Bangalore and Young Associate of Maharashtra Academy of Science (MASc.). In 2020, He has been selected as the member of the prestigious Global Young Academy. In 2021, Dr. Singh is listed in the single year category of World's Top 2% Scientists published by Stanford University (USA) in Elsevier.*

Preferential solvation of 5-aminoquinoline in 1,4-dioxane-water binary mixture

Abhoy Karmakar[ǂ], Avinash Kumar Singh[ǂǂ]*, Anindya Datta[*]

Department of chemistry, Indian institute of technology Bombay , Powai
Mumbai, India, 400076
Email: adutta@iitb.ac.in, asingh8@uottawa.ca

Abstract

Steady state absorption and fluorescence spectroscopic data indicates preferential solvation of 5AQ in 1,4-dioxane -water binary mixture. Deviations from linearity are observed in fluorescence spectra when plotted as a function of both water mole fraction (x_w) and Onsager's dielectric function ($F(\varepsilon)$). Hydrogen bonding ability of the polar component of binary mixture also contributes to the preferential solvation.

Introduction:

Solvents are central to the discipline of chemistry.[1] Their profound impact on the reaction pathways warrants understanding the process of solvation and solvation dynamics.[2] Among the molecular systems used for exploring the phenomenon of solvation dynamics, quinoline and quinoline derivatives have long intrigued researchers owing to the diverse excited state dynamics of these molecules.[3-6] The origin of these wide-ranging exited state properties can be broadly attributed to three factors (i) the unique structure of quinoline backbone itself where a homocyclic and a heterocyclic ring are fused together (ii) the nature of substituent and its position on the quinoline backbone[6,7] and (iii) the solvent.[8] The effect of positional isomerism on the excited state dynamics of quinoline class of molecules has been studied by various research groups for aminoquinolines.[9] The position of amino group on the homocyclic and the heterocyclic part of quinoline moiety alters fundamentally the dynamics of the molecule upon excitation with light. Specifically, when the amino group is present on the homocyclic part of the molecule (for example 5- Aminoquinoline (5AQ)), the solvation in hydrogen bonding solvent leads to large red shifts in the emission spectra accompanied by quenching of the

fluorescence.[10] In neat alcoholic solvents, the large red shift observed for 5AQ is attributed to the solvation of a highly polar intramolecular charge transfer (ICT) state by polar protic solvents. The lowering of the ICT state energy makes the intersystem crossing to a triplet state feasible leading to the quenching of the fluorescence.[10] Further investigations in our group in the excited state dynamics of 5AQ in solvent mixtures, for instance, hexane-alcohol and acetonitrile-alcohol point indicate preferential solvation of the 5AQ molecule by polar protic alcohol molecules.[11] The extent of preferential solvation was revealed to be dependent upon the difference in polarity between the two components of the solvent mixture and became more profound when the polar solvent was protic as well. Time resolved area normalized emission spectroscopy (TRANES) performed on 5-aminoquinoline in diethyl ether (DEE) and methanol reveals a distinct second state understood to be formed by solvation of solute molecules by methanol molecules.[12] The availability of a plethora of solvents with varying properties like polarity and hydrogen bonding ability provides an opportunity to understand the phenomenon of preferential solvation merely by changing the components and composition of the solvent mixture.[13-15]

In this study, we report the excited state dynamics of 5AQ in dioxane-water mixture. Steady state and time resolved spectroscopy techniques were used to understand the behavior of 5AQ in dioxane-water binary mixture by varying the mole fraction of water. Many solvatochromic studies has pointed towards the anomalous solvent properties of 1, 4-dioxane.[16,17] Although dioxane is considered nonpolar with a dielectric constant of 2.25, Kamlet-Taft analysis reveal a polarizability () of 0.55.[18,19] Also, dioxane is a moderate hydrogen bond acceptor (). Also, the proximity of 1,4-Dioxane properties to that of water and their miscibility at all proportions makes it an interesting system.[20] Previous solvation dynamics studies performed on systems like 4-aminophthalimide and coumarin 153 show the absence of preferential solvation in 1,4-dioxane-water binary mixtures.[20] In this study we show that the excited state dynamics of 5AQ in 1,4-dioxane-water mixture, is a complex interplay of preferential solvation and hydrogen-bonding. We have also performed Stern-Volmer analysis for fluorescence quenching in 5AQ with increasing mole fraction of water to understand the quenching accompanied by the red shift upon increasing mole fraction of water.

Experimental
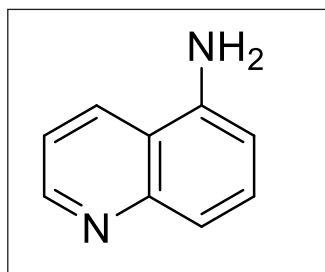
Scheme 1: Structure of 5-aminoquinoline (5AQ)

5-Aminoquinolines (5AQ) was purchased from Sigma Aldrich and was used without further purification. 1,4-dioxane was spectroscopic grade and was purchased from Spectrochem, Mumbai. Deionized water was used for preparing the 1,4-dioxane-water binary mixture. The steady state absorption spectra were recorded on a

JASCO V530 spectrometer. Perkin Elmer LS55 fluorimeter and Fluoromax-4 fluorimeter were used for recording the emission spectra. Time correlated single photon counting (TCSPC) decays were recorded on a IBH Horiba Jobin Yvon (FluoroCube) TCSPC setup for the excited state lifetime measurements. The fluorescence decays were collected with an emission polarizer set at magic angle of 54.7^0 with respect to the excitation light. Fluorescence decay traces were fitted using sum of exponentials by the process of iterative reconvolution method using IBH DAS 6.0 software using the following equation

$$I(\lambda, t) = I_0(\lambda) \sum_i a_i e^{-t/\tau_i} \qquad (1)$$

Where τ_i and a_i are the lifetime and the associated amplitude of the ith component. The relative fluorescence quantum yield (Φ_f) was calculated using standard quinine sulfate dissolved in 0.5M H_2SO_4 (ϕ_f =0.55) as the reference.

The nonradiative rate constants are calculated by using the formula $k_{NR} = (1 - \Phi_f)/\tau_f$, where Φ_f is fluorescence quantum yield and is radiative lifetime. For all the fluorescence measurements the absorbance of the solutions was kept below around 0.1. at the excitation wavelength.

Results and discussion

Steady state emission spectra of 5AQ shows a steady red shift with increasing mole fractions of water in the 1,4-dioxane-water mixture (Figure 1). The emission peak maximum was observed at 470 nm in neat 1,4-dioxane and at 510 nm in the 1,4-dioxane-water mixture when the mole fraction of water was 0.60. Although 5AQ has a net dipole moment of zero similar to that of hexane, the emission peak maximum is remarkably red shifted to that in hexane (418 nm)[10] This observation points toward the so-called "pseudopolar" behaviour of 1,4-dioxane.[18] Addition of water further shifts the emission maximum to longer wavelengths. For the lower

concentrations of water, the shift is rapid, however, for = 0.2, the shift becomes constant at approximately 510 nm (Table 1, Figure 2). The deviations from the linear behavior are apparent in the emission spectrum. Even for small mole fraction values of water (x_w < 0.4), the deviations are obvious. However, it has been established that the deviation of the fluorescence spectra only is not definitive evidence of preferential solvation. Scarlata and Suppan has argued that the actual dielectric constant of the binary mixtures is a more accurate parameter for examining the hypothesis of preferential solvation.[21-25] To this effect, we have analyzed the absorption and emission peak maxima as a function of water mole fraction (x_w) and the Onsager's function $F(\varepsilon)$ (Figure 3). The nonlinear behavior of fluorescence peak maxima is evident when it is plotted against the Onsager's dielectric function. This observation is in contrast from the case of coumarin 153 where Huppert and coworkers found a small nonlinear dependence of fluorescence peak maxima on the water mole fraction in 1,4-dioxane-water mixture (x_w < 0.5). and linear dependence on the Onsager's dielectric function.[18] They attributed their observation to dielectric enrichment which is a dominant phenomenon when the difference in the ground and excited state dipole moments as well as the difference between Onsager's dielectric functions are large.

Now, It is important here to consider the factors contributing towards the nonideality observed in $F(\varepsilon)$ vs x_w (Figure 3) reported in this
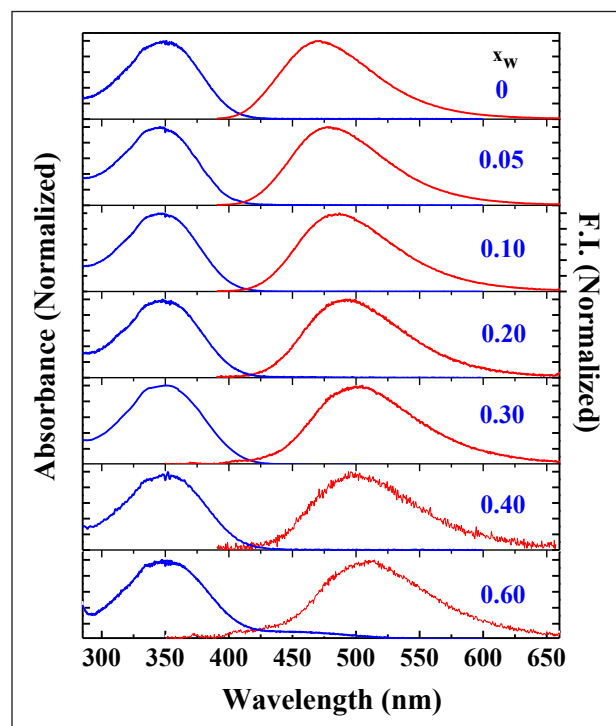
Figure 1: Absorption (red) and emission (blue) spectra of 5AQ in 1,4-dioxane-water mixture with increasing mole fraction of water. The signal to noise ratio in emission spectra for x_w = 0.40 and x_w = 0.60, is slightly worse due to quenching of fluorescence.

paper. Onsager's function F, represents polarity of a solvent as a function of dielectric constant using the following relation

$$F(\varepsilon) = 2(\varepsilon - 1)/(2\varepsilon + 1) \qquad (2)$$

For a binary mixture consisting of one nonpolar and one polar solvent and dielectric

Table 1: The spectral and temporal parameters for 5AQ in 1,4-dioxane-water mixture

Mole Fraction (x_w)	$F(\varepsilon)$	$\lambda_{abs.}^{max}$ (cm^{-1})	λ_{em}^{max} (cm^{-1})	Δv (cm^{-1})	Φ_f	k_{NR}*10^8 (s^{-1})	<τ> (ns)
0.00	0.455	28571	21231	7340	0.30	0.42	16.74
0.05	0.480	28653	20833	7820	0.28	0.48	15.14
0.10	0.507	28653	20534	8119	0.16	0.62	13.65
0.20	0.560	28736	20202	8534	0.09	0.97	9.41
0.30	0.613	28653	20040	8613	0.06	2.26	4.15
0.40	0.665	28818	19960	8858	0.03	2.79	3.47
0.60	0.770	29069	19646	9423	0.02	3.30	2.97
1.00	0.980	30030	18726	11303	-	-	0.007

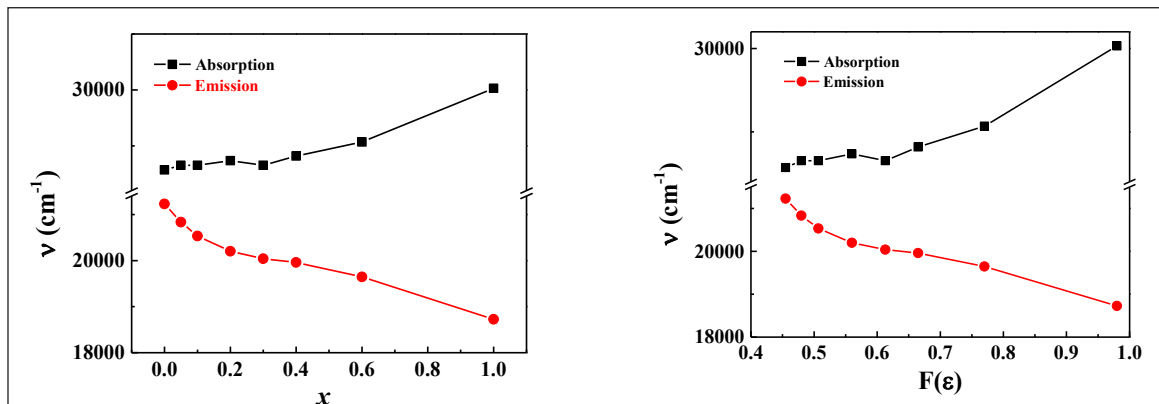*Figure 2. Absorption and emission peak maxima plotted as a function of water mole fraction (x_w) (left panel) and Onsager's dielectric function (right panel).*

constants ε_N of ε_P and respectively, the Onsager's function is linear combination of their respective mole fractions

$$F_{linear\ bulk} = x_N F_N + x_P F_P \qquad (3)$$

For an ideal solution the value of F(ε) should vary linearly with mole fraction of water present in the mixture. However, for 1,4-dioxane water mixtures the deviations observed in the value of F(ε) with increasing water mole fraction are remarkable. [18] For a molecule exhibiting charge separation in excited state, the peak shift is usually a good way to examine the local environment. For a binary mixture where the F(ε) changes linearly with the mole fraction of the polar solvent, the peak shift is also linear. [26] However, in a binary mixture of a polar and nonpolar solvent the local environment around a highly dipolar solute is complex in nature. The bulk mole ratio of a binary solvent composed of moles of a nonpolar solvent and moles of a polar solvent is defined as

$$X = {}^{x_N}/_{x_P} \qquad (4)$$

The mole ratio near the solute is different than the bulk mole ratio and is defined as

$$Y = {}^{y_N}/_{y_P} \qquad (5)$$

Bulk and mole ratio-near solute are related to each other as

$$Y = X e^{-Z} \qquad (6)$$

Z represents a parameter that takes into account "preferential solvation" of the solute. For a solute molecule of dipole moment μ, Suppan defined, Z as[24]

$$Z = \frac{C M \mu^2 \Delta F_{N,P}}{4 \pi \varepsilon_0 2 \delta R T r^6} \qquad (7)$$

Where, $\Delta F_{N,P} = F_P - F_N$ is the difference between the Onsager's function defined above for the polar and nonpolar components of the binary mixture, M is the mean molar weight of the polar and nonpolar solvents, δ is mean density of the two solvent components, T is temperature and R is gas constant. For Z > 0, the polar solvent relative concentration is higher around the solute. Using the parameters for 1,4-dioxane-water mixture, M = 53 g/mol, [18] δ = 1.02 g/cm³,[18] Δμ = 2.48 D[27] and r = 5.2 angstroms[18], Z can be determined to be 0.3 indicating dipolar enrichment upon excitation of 5AQ. In this case, deviation of the fluorescence peak maxima from the linear behavior with water mole fraction is expected and indeed we observe a marked deviation from linearity (Figure 2).

Another important parameter, that needs to be introduced here is nonlinearity ration represented by ' ρ_{exp}. ρ_{exp}. is an experimentally determinable parameter and is defined by

$$\rho_{exp} = \frac{2 \int_0^1 (E_{exp} - E_{linear,bulk}) dx_p}{\Delta E_{N,P}} \quad (8)$$

Where E_{exp} is experimental peak maximum, $E_{linear,bulk}$ is theoretically determined peak energy and $\Delta E_{N,P}$ is the peak energy difference when solute is present in pure polar and nonpolar solvent.

The parameter called nonlinearity ratio ρ_{exp}, is a sum of contributions from both factors namely preferential solvation (ρ_{ps}) and dielectric nonlinearity (ρ_{ni})

ρ_{ni} can be determined from experimental parameters as follows

$$\rho_{ni} = \frac{2 \int_0^1 (E_{exp} - E_{linear,bulk}) dx_p}{\Delta F_{N,P}} \quad (9)$$

Where $\Delta F_{N,P}$ is difference in Onsager's function of the two components. The determination of ρ_{ps} is rather straight forward. Kauffman and coworkers have proposed that for $\rho_{ps} < 1$, ρ_{ps} and Z are related as[28]

$$\rho_{ps} = 0.31 Z_{ps} \quad (10)$$

Using Coumarin 153 as a solute, Huppert and coworkers have determined the ρ_{ni} to be 0.28 for 1,4-dioxane-water binary mixtures.[18] Using the values of ρ_{exp} experimentally measured quantities for absorption spectra in table 1, the value of was calculated using equation 1 and was found to be -0.22. According to the relation $\rho_{exp} = \rho_{ps} + \rho_{ni}$, and $\rho_{ni} = 0.28$, $\rho_{ps} = -0.3$, Z_{ps} determined to be ~ -1. For emission spectra $\rho_{ps} = -0.2$ and Z_{ps} was determined to be -1.7. The calculated values of Z_{ps} indicate preferential solvation which we observe clearly even at water mole fractions less than 0.4.

The molecular structure of 5AQ also contributes towards its complex photophysics in binary mixtures. With one ring nitrogen and one amino group, there is always a possibility of ground state complexation with strongly hydrogen bonding solvents as shown in numerous reports.[29, 30] The fluorescence of 5AQ is heavily quenched in the protic solvents. We observed similar trend with increasing mole fraction of water in the binary mixture (Table 1). TCSPC decay traces correlate to the quenching of the fluorescence (Figure 3). For comparison, it is important to mention that the excited state lifetime of 5AQ in 1,4-dioxane is 16 ns while in the case of water it is 7 ps. It has been proposed that hydrogen bonding facilitates intersystem crossing in 5AQ and loss of fluorescence quantum yield.[10] In our experiments we observed a slow but steady blue shift with subsequent addition of water in the binary mixture. In neat water the absorption peak maxima was observed to be at 333 nm compared to 350 nm in neat 1,4-dioxane. In the previous investigations reported by our group we have noted that the extent of preferential solvation depends on the physical properties of the components of the binary mixture.[12] These physical properties include the polarity of the solvent as well as the hydrogen bond accepting and donating capability of the solvent molecule.[11,]
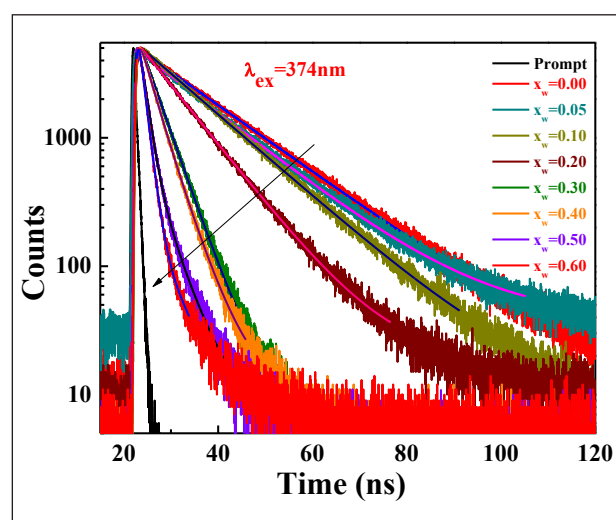

Figure 3. *Time resolved fluorescence decays of 5AQ in various mile fractions of water, x_w of dioxane-water mixture.*

[12] For instance, the extent of preferential solvation in a diethyl ether- acetonitrile system is less than the preferential solvation present in a diethyl ether-methanol system.[12] If one of the components is polar as well as protic, specific solute-solvent interactions also come into play.

Conclusion:

Deviations from linearity in the fluorescence peak maxima and the Onsager's dielectric function when plotted as a function of water mole fraction show that preferential solvation is operative in 1,4-dioxane-water mixture. Transient 1,4-dioxane-water clusters might contribute to the dynamics but the dominating factor is H-bonding capability of the polar counterpart of the binary mixture as shown from steady state and time resolved data.

Acknowledgements:

References

1. Reichardt, C., Solvents and Solvent Effects: An Introduction. *Organic Process Research & Development* **2007,** *11* (1), 105-113.

2. Roytman, V. A.; Singleton, D. A., Solvation Dynamics and the Nature of Reaction Barriers and Ion-Pair Intermediates in Carbocation Reactions. *Journal of the American Chemical Society* **2020,** *142* (29), 12865-12877.

3. Nimlos, M. R.; Kelley, D. F.; Bernstein, E. R., Spectroscopy and structure of 2-hydroxyquinoline. *The Journal of Physical Chemistry* **1987,** *91* (27), 6610-6614.

4. Bach, A.; Leutwyler, S., Proton transfer in 7-hydroxyquinoline·(NH3)n solvent clusters. *The Journal of Chemical Physics* **1999,** *112* (2), 560-565.

5. Singh, A. K.; Ghosh, S.; Kancherla, R.; Datta, A., Engineering the Excited-State Dynamics of 3-Aminoquinoline by Chemical Modification and Temperature Variation. *The Journal of Physical Chemistry B* **2016,** *120* (50), 12920-12927.

6. Schulman, S. G.; Sanders, L. B., Fluorescence and phosphorescence of 5- and 8-aminoquinoline. *Analytica Chimica Acta* **1971,** *56* (1), 83-89.

7. Schulman, S. G.; Abate, K.; Kovi, P. J.; Capomacchia, A. C.; Jackman, D., Photoluminescence of 6- and 7-aminoquinolines. *Analytica Chimica Acta* **1973,** *65* (1), 59-67.

8. Panda, D.; Datta, A., The role of the ring nitrogen and the amino group in the solvent dependence of the excited-state dynamics of 3-aminoquinoline. *The Journal of Chemical Physics* **2006,** *125* (5), 054513.

9. Driscoll, E. W.; Hunt, J. R.; Dawlaty, J. M., Photobasicity in Quinolines: Origin and Tunability via the Substituents' Hammett Parameters. *The Journal of Physical Chemistry Letters* **2016,** *7* (11), 2093-2099.

10. Singh, A. K.; Das, S.; Karmakar, A.; Kumar, A.; Datta, A., Solvation and hydrogen bonding aided efficient non-radiative deactivation of polar excited state of 5-aminoquinoline. *Physical Chemistry Chemical Physics* **2018,** *20* (34), 22320-22330.

11. Das, S.; Singh, A. K.; Biswas, D. S.; Datta, A., Dynamics of Preferential Solvation of 5-Aminoquinoline in Hexane–Alcohol Solvent Mixtures. *The Journal of Physical Chemistry B* **2019,** *123* (48), 10267-10274.

12. Das, S.; Singha, P. K.; Singh, A. K.; Datta, A., The Role of Hydrogen Bonding in the Preferential Solvation of 5-Aminoquinoline in Binary Solvent Mixtures. *The Journal of Physical Chemistry B* **2021,** *125* (46), 12763-12773.

13. Dutta, R.; Pyne, A.; Mondal, D.; Sarkar, N., Effect of Microheterogeneity of Different Aqueous Binary Mixtures on the Proton Transfer Dynamics of [2,2'-Bipyridyl]-3,3'-diol: A Femtosecond Fluorescence Upconversion Study. *ACS Omega* **2018,** *3* (1), 314-328.

14. Crosio, M. A.; Silber, J. J.; Moran Vieyra, F. E.; Falcone, R. D.; Borsarelli, C. D.; Correa, N. M., Deciphering Solvation Effects in Aqueous Binary Mixtures by Fluorescence Behavior of 4-Aminophthalimide: The Comparison Between Ionic Liquids and Alcohols as Cosolvents. *The Journal of Physical Chemistry B* **2021,** *125* (48), 13203-13211.

15. Kumar Behera, P.; Kumar Mishra, A., Static and dynamic model for 1-naphthol fluorescence quenching by carbon tetrachloride in dioxane–acetonitrile mixtures. *Journal of Photochemistry and Photobiology A: Chemistry* **1993,** *71* (2), 115-118.

16. Åkerlöf, G.; Short, O. A., The Dielectric Constant of Dioxane–Water Mixtures between 0 and 80°. *Journal of the American Chemical Society* **1936,** *58* (7), 1241-1243.

17. Goates, J. R.; Sullivan, R. J., Thermodynamic Properties of the System Water-p-Dioxane. *The Journal of Physical Chemistry* **1958,** *62* (2), 188-190.

18. Molotsky, T.; Huppert, D., Solvation Statics and Dynamics of Coumarin 153 in Dioxane–Water Solvent Mixtures. *The Journal of Physical Chemistry A* **2003,** *107* (41), 8449-8457.

19. Laurence, C.; Nicolet, P.; Dalati, M. T.; Abboud, J.-L. M.; Notario, R., The Empirical Treatment of Solvent-Solute Interactions: 15 Years of .pi.*. *The Journal of Physical Chemistry* **1994,** *98* (23), 5807-5816.

20. Mukherjee, S.; Sahu, K.; Roy, D.; Mondal, S. K.; Bhattacharyya, K., Solvation dynamics of 4-aminophthalimide in dioxane–water mixture. *Chemical Physics Letters* **2004,** *384* (1), 128-133.

21. Zurawsky, W.; Scarlata, S., ASSESSMENT OF DIELECTRIC ENRICHMENT AROUND TWO FLUOROPHORES IN BINARY SOLVENTS. *Photochemistry and Photobiology* **1994,** *60* (4), 343-347.

22. Zurawsky, W. P.; Scarlata, S. F., Preferential solvation of 6-propionyl(N,N-dimethylamino)naphthalene in binary, polar solvent mixtures. *The Journal of Physical Chemistry* **1992,** *96* (14), 6012-6016.

23. Suppan, P., Invited review solvatochromic shifts: The influence of the medium on the energy of electronic states.

Journal of Photochemistry and Photobiology A: Chemistry **1990,** *50* (3), 293-330.

24. Suppan, P., Local polarity of solvent mixtures in the field of electronically excited molecules and exciplexes. *Journal of the Chemical Society, Faraday Transactions 1: Physical Chemistry in Condensed Phases* **1987,** *83* (2), 495-509.

25. Lerf, C.; Suppan, P., Hydrogen bonding and dielectric effects in solvatochromic shifts. *Journal of the Chemical Society, Faraday Transactions* **1992,** *88* (7), 963-969.

26. Khajehpour, M.; Kauffman, J. F., Dielectric Enrichment of 1-(9-Anthryl)-3-(4-N,N-dimethylaniline) Propane in Hexane−Ethanol Mixtures. *The Journal of Physical Chemistry A* **2000,** *104* (30), 7151-7159.

27. Bridhkoti, J. P.; Gahlaut, R.; Joshi, H. C.; Pant, S., Effect of positional substitution of amino group on excited state dipole moments of quinoline. *Journal of Luminescence* **2011,** *131* (9), 1869-1873.

28. Khajehpour, M.; Welch, C. M.; Kleiner, K. A.; Kauffman, J. F., Separation of Dielectric Nonideality from Preferential Solvation in Binary Solvent Systems: An Experimental Examination of the Relationship between Solvatochromism and Local Solvent Composition around a Dipolar Solute. *The Journal of Physical Chemistry A* **2001,** *105* (22), 5372-5379.

29. Driscoll, E. W.; Hunt, J. R.; Dawlaty, J. M., Proton Capture Dynamics in Quinoline Photobases: Substituent Effect and Involvement of Triplet States. *The Journal of Physical Chemistry A* **2017,** *121* (38), 7099-7107.

30. Steck, E. A.; Ewing, G. W.; Nachod, F., Absorption Spectra of Heterocyclic Compounds. II. Amino-Derivatives of Pyridine, Quinoline and Isoquinoline. *Journal of the American Chemical Society* **1948,** *70* (10), 3397-3406.

Abhoy Karmakar *completed his B.Sc. (Hons, Chemistry) from St. Xavier's College (Kolkata) in 2014. In 2016, he complicated his M.Sc. (Chemistry) from IIT Bombay, where he worked on ultrafast dynamics of aminoquinoline molecules under the supervision of Prof. Anindya Datta. In 2021, he obtained his Ph.D. (Chemistry) from the University of Alberta and worked on metal halide perovskites using solid-state NMR spectroscopy under the supervision of Prof. Vladimir K. Michaelis.*

Avinash Kumar *Singh is a postdoctoral fellow at Department of Physics, University of Ottawa where he works in the area of ligh-matter strong coupling in terahertz regime. Previously he has worked at the Ames laboratory of the United states department of energy in the area of coherent Raman imaging techniques. He obtained his PhD under the supervision of Prof. Anindya Datta at the department of Chemistry, IIT Bombay in 2017, where he worked on understanding the excited state dynamics of molecules and novel materials.*

Anindya Datta is *a professor of chemistry at IIT Bombay. His group explores excited state phenomena in complex systems. The principal tools of trade are Femtosecond Transient absorption, Femtosecond Optical Gating and Time Correlated Single Photon counting, along with steady state absorption and fluorescence spectroscopy. Prof. Datta obtained his PhD from Jadavpur University and was a postdoctoral fellow in Iowa State University.*

Ultrafast Exciton Dynamics in Polyacene Nanoaggregates and Thin Films

Rajib Ghosh*, Biswajit Manna and Amitabha Nandi

Radiation and Photochemistry Division, Bhabha Atomic Research Centre, Mumbai-400 085, India
Email: rajib@barc.gov.in

Abstract

Polyacene based organic semiconducting materials find potential application in organic solar cell and organic light emitting diode. A thorough understanding of photophysics and exciton dynamics is imperative for effective utilization of these materials in optoelectronics. In this article, we describe ultrafast exciton dynamics of a series of anthracene derivatives in nanoaggregate (NA) and thin film (TF) measured by femtosecond transient pump-probe spectroscopic techniques. In contrast to strong emissive behaviour in solution, polyacenes in solid state exhibits quenching of fluorescence due to various exciton relaxation channels. In diphenylanthracene derivatives, photoinduced exciton state relaxes to excimer state. The contribution of excimer relaxationis shown to depend on the position of phenyl substitution. Exciton diffusion parameters in these molecules are observed to correlate with packing efficiency in nanocrystalline state. On the other hand, phenylethynyl derivative of anthracene undergoes ultrafast singlet fission (SF) to triplet state. Phenylethynyl substitution at 9,10 position of anthracene changes the singlet and triplet level ordering favourable (i.e., singlet level at twice energy of the lowest triplet level) for dissociation of singlet excitons to a pair of triplets. Energy level perturbation by phenylethynyl substitution is exploited to induce faster SF in tetracene derivatives. Importance of intermolecular coupling on singlet fission dynamics is exemplified in triisopropylsilyl derivative of anthracene, which does not exhibit efficient SF process due to weak intermolecular coupling in solid state. Implication of different excitation relaxation pathways on potential optoelectronic application is discussed.
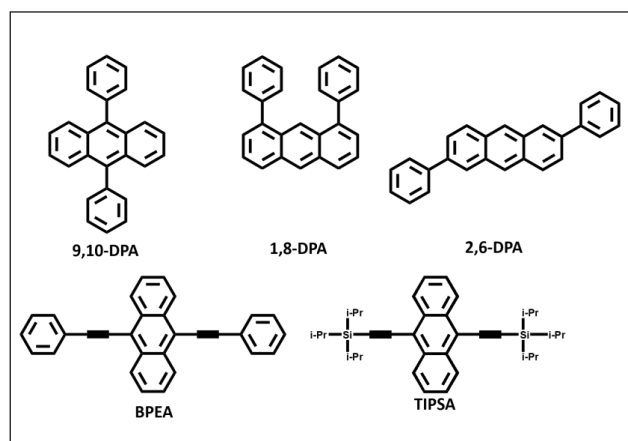
1. Introduction

Small molecular organic semiconductor materials have drawn great attention for various optoelectronic and photovoltaic applications in the recent past.[1-3] Efficiency of these devices extensively relies upon the excitonic properties e.g. exciton lifetime, exciton diffusion length of the light absorbing materials.[4] Knowledge of the effect of molecular structure and molecular packing on the exciton dynamics and diffusion properties provides important physical insights about the applicability of these materials in the organic photovoltaic or light emitting devices.[5-7] Thus, it is imperative to understand exciton dynamics and excitonic diffusion properties of organic semiconducting materials.

Anthracene and its derivatives are endowed with strong near UV absorption and blue emission with high quantum yield, which make these materials suitable candidate for potential application in optoelectronic devices, particularly in blue organic light emitting diodes. To understand the true potential in these applications, it is necessary to unravel the effect of substituent and morphology on the photophysics in solid state. Modified structure on inclusion of various substituents causes changes in the electronic energy levels and molecular packing efficiencies in the solid forms which may greatly influence photoinduced exciton dynamics of organic semiconducting materials in solid state. Thus it is imperative to study

steady state photophysics and exciton diffusion, relaxation and deactivation properties to unravel the structure-morphology dynamics in solid state of potential blue light emitting materials.

In recent past, we conducted extensive photopysical and ultrafast spectroscopic investigation on different polyacene derivatives in solid state to understand structural and molecular packing influence on exciton relaxation behaviour.[8-13] In this article, we present the summary of our understanding on exciton diffusion and deactivation pathways in several phenyl and phenylethynyl derivatives of anthracene. We show how electronic and structural perturbation by the substituent's affect excited state properties of anthracene derivatives. Diphenyl substitution at different position of anthracene is shown to impact exciton diffusion and exciton-to-excimer relaxation. On the other hand, perturbation of electronic levels by phenylethynyl substituents introduces a new deactivation channel, namely singlet fission (SF) which led to production of two triplets per absorbed photon.[14-17] This potentially increases the possibility to overcome Schokley-Quisser limit of organic photovoltaic efficiency.[18,19] The favourable influence of phenylethynyl substitution meeting energetic and kinetic criteria of SF process is exemplified with different derivatives of anthracene and tetracene.

2. Materials and Methods

High purity (>99%) polyacene derivatives reported in this articlewere purchased from commercial sources. Nanoaggregates (NA) were prepared by flash-precipitation method. Typically, 100 µl of 2 mM of sample solution in tetrahydrofuran was injected in the 5 ml aqueous PVA solution (1 mg/ml) under vigorously stirring condition and left undisturbed for a few hours before carrying out spectroscopic measurement. Thin films (TF) of anthracene and tetracene derivatives of about 100 nm thickness were deposited on glass substrates by thermal vapour deposition method. The morphological characterization of the NA and TF were carried out by using dynamic light scattering (DLS) and atomic force microscopy (AFM), respectively. A representative DLS and AFM data is shown in figure 1. Optical measurements were conducted by UV-visible absorption and room temperature photoluminescence experiments. Ultrafast dynamics of excitons in NA and thin film of the samples were carried out by fluorescence upconversion and transient pump-probe spectroscopy.
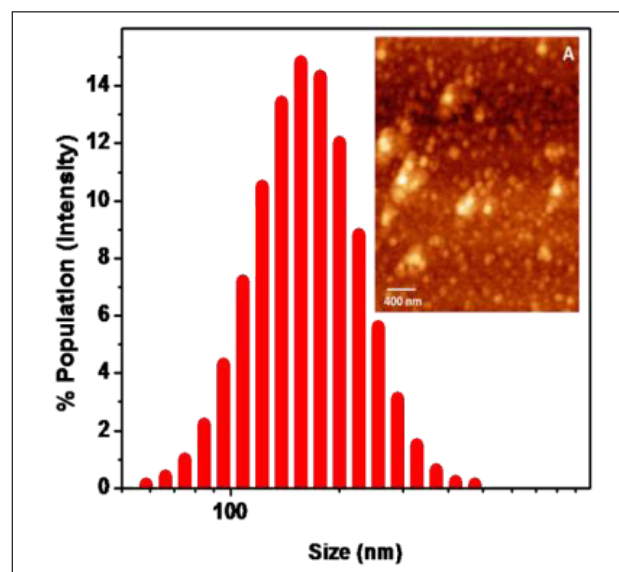
Figure 1: *Representative DLS and AFM data of 9,10-DPA nanoaggregate prepared by flash-precipitation method. Nanocrystals of diameter in the range of few hundred nanometers (average size of ~ 500 nm) is readily formed for all the polyacene derivatives prepared by this method.*
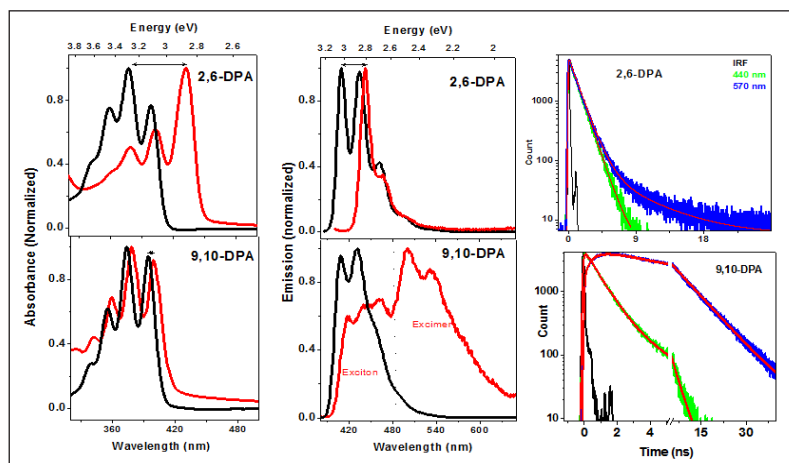

Scheme 1: *Molecular Structure of different anthracene derivatives investigated to understand structural and molecular packing effect on exciton dynamics.*

Figure 2: *Steady state absorption and emission spectra of monomer (black) vs. nanoaggregate (red) of two different DPA derivatives. Figures in right column show the transient emission decay traces of nanoaggregates at two selected wavelengths.*

3. Results and Discussion

A. Exciton-excimer relaxation in diphenylanthracene derivatives

Diphenylanthracenes (DPA) exhibits strong absorption and fluorescence in solution and has been extensively used for upconverted luminescence applications. However, in nanoaggregated state, photophysics of DPAs is remarkably altered due to excitonic interaction. Depending on position of phenyl substitution, dihedral angle between anthracene and phenyl ring differs. From quantum chemical calculation and reported crystal structure[10,20,21], dihedral angle is ~80° for 9,10-DPA, 55° for 1,8-DPA and ~28° for 2,6-DPA. The influence of difference in dihedral angle on molecular packing and consequent photophysical properties are described below.

Steady state absorption and emission behaviour of monomer and nanoaggregate of 2,6- and 9,10-DPA are shown in figure 2. Comparison of peak normalized absorption spectra recorded in THF solution with their corresponding absorption spectrum of NAs show red shift upon aggregate formation, indicating J-type intermolecular interaction. However, the extent of red shift for the lowest energy vibrational progression due to aggregation is quite different

in these two DPA derivatives (Figure 2) suggesting different degree of inter-molecular interaction in NAs. Lower spectral red shift in 9,10-DPA NA indicates weaker intermolecular interaction as compared to 2,6-DPA NA. This indicates that perpendicular disposition (dihedral angle of ~80°) of two phenyl rings at 9 and 10 position of anthracene impede intermolecular interaction between adjacent molecules. Larger red shift in the absorption spectra in 2,6-DPA NA is in line with the less twisted conformation (dihedral angle of ~28°) which provides favourable situation for better intermolecular interaction. consistent with large red shifted absorption spectra in its NA. 1,8-DPA (dihedral angle ~55°) displays intermediate shift in absorption band edge. Thus, torsional conformation of phenyl substituents in anthracene depending on the position influences intermolecular interaction which is reflected in the extent of shift in absorption spectra of their NA.

Emission properties of DPAs also drastically changes from monomer to nanoaggregate state. Emission quantum yield significantly quenched in solid state with appearance of low energy emission band in some of the DPA derivatives (Figure 2 and Table 1). Room temperature emission behaviour of the nanoaggregates also reflects systematic influence of molecular structural change on the emission property of NA samples. 9,10-DPA NAs show both excitonic and excimeric emission covering 400-600 nm wavelength region and contribution of excimer emission dominates over excitonic emission. On the other hand, in 2,6-DPA NA, long wavelength excimer emission is negligible and emission spectra mainly consists of excitonic emission covering 425-500 nm wavelength range. In 1,8-DPA, excimer emission contribution is less as compared to excitonic emission. The differences in emission characteristics of the

three DPA aggregates can be explained from their differences in intermolecular distance and relative orientation in crystal structure.

Table 1: *Photophysical parameters (emission quantum yield and exciton lifetime) of three DPA derivatives in monomer and nanoaggregate.*

System	Φ_f monomer	Φ_f NA	$<\tau>_{exciton}$ ns	$<\tau>_{excimer}$ ns
9,10-DPA	0.95	0.40	0.8	15 ns
1,8-DPA	0.64	0.16	0.6	13 ns
2,6-DPA	0.49	0.05	1.15	-----

Like anthracene, three DPA derivatives discussed in the present work, form monoclinic crystal structure in their most thermodynamically stable polymorph. In crystalline anthracene, minimum intermolecular distance in the direction of closest approach of two anthracene molecules is 6.04 Å. However, efficient excimer formation demands closer intermolecular interaction, most favourable for intermolecular distance < 5 Å.[22] Consequently, crystalline anthracene does not exhibit significant excimer emission. In case of 2,6-DPA, minimum intermolecular distance is about 6.24 Å and hence excimer formation is not facilitated. In case of 9,10-DPA, the excimer emission dominates over the singlet excitonic emission due to interaction of phenyl substituents of adjacent molecules. We propose that, the transition dipole associated with the lowest energy electronic transition in 9,10-DPA is oriented in the same direction with that of the attached phenyl substitutions. Even though, intermolecular distance between anthracene cores is large in 9,10-DPA, phenyl substituents of two neighbouring 9,10-DPA molecules are in close proximity (~3Å) which facilitates excimer formation. In 1,8-DPA, small contribution of excimer emission arises from the contribution of noncrystalline phase. This contrasts with 9,10-DPA, where excimer dominates in most stable α-crystalline phase. Dominance of excimer emission in α-crystalline phase of 9,10-DPA was confirmed by comparing the emission behaviour

of NA of different sizes. As we increase size of nanoaggregate from few hundred nanometer to micrometer, excimer emission contribution drastically increases. Further, grinding of single crystal of 9,10-DPA results in decrease in excimer emission due to increased contribution of amorphous phase. Thus, depending upon the position of phenyl substituents and their conformation, crystalline packing of DPA molecules differ, which influences emission properties of these materials in NA state.

Time resolved emission measurement (Figure 2) revealed dynamics associated with relaxation of exciton to excimer state. In solution, three DPA derivatives exhibit single exponential decay with singlet lifetime of 3.75 ± 0.25 ns in THF solution. However, NA of 9,10- and 1,8- DPA exhibits wavelength dependent nonexponential decay kinetics due to presence of both exciton and excimer emission. In 9,10-DPA, excitonic state decays with a lifetime of 0.8 ns with concomitant growth of excimer emission in longer wavelength which decays with a lifetime of about 9 ns. In case of 2,6-DPA NA, the temporal profile recorded at excitonic emission maxima (e.g. 440 nm) fit exponentially with a lifetime of about 1.15 ns. Only a small contribution (<5%) of long lived component appears at longer wavelength. This suggests formation of excimer state is not favoured in 2,6-DPA and whole emission spectral feature of 2,6-DPA NA is primarily dominated by exciton state. However, we note that even though 2,6-DPA NA does not relax to excimer state, exciton emission yield is much smaller as compared to other two derivatives which suggest Presence of other unknown nonradiative deactivation channel.

B. Exciton diffusion parameters:

Knowledge of exciton diffusion parameters in organic semiconducting materials are very important from photovoltaic application perspective.[4] Large exciton diffusion length is desirable for efficient diffusion of exciton to donor-acceptor interface for efficient charge carrier generation. In most organic semiconductors,

exciton diffusion is limited to a few tens of nanometers depending on molecular packing and crystal morphology. We have employed pump-fluence dependent exciton-exciton annihilation kinetics to measure exciton diffusion parameters of three DPA derivatives to understand the impact of molecular packing on exciton diffusion. At high exciton density, ultrafast bimolecular exciton – exciton annihilation dominates due to diffusional encounter of two excitons leading to nonradiative decay of one exciton back to the ground state. Thus, excitation fluence dependent exciton – exciton annihilation kinetics can be analysed to extract exciton diffusion coefficient (D) and diffusion lengths (L_D) which are related bimolecular decay rate constants of exciton (k_2), exciton decay lifetime (τ or k_1^{-1}) and exciton annihilation radius (R_a) by equation 1 and 2.[8,23,24]

$$k_2 = 8\pi R_a D \qquad (1)$$

$$L_D = (6D\tau)^{1/2} \qquad (2)$$

To determine exciton diffusion parameters, nanoaggregates and thin films of different DPA derivatives were excited at different excitation intensities and exciton decay kinetics were recorded. For all samples, exciton decay gets faster with increase in excitation intensity (representative kinetic traces of 9,10-DPA NA at three different excitation fluencies are shown in figure 3) which indicates involvement of bimolecular exciton annihilation dynamics in early time scale. However, exciton decay at longer time scale is independent of excitation fluence and thus represents unimolecular natural decay of the excitons at low exciton density. Combined unimolecular and bimolecular decay channels (equation 3) leads to equation 4 and thus experimental decay traces can be fit to an analogous equation (equation 5) to extract exciton annihilation rate constants (k_2)[8].

$$\frac{d[S_1]}{dt} = -k_1[S_1] - \frac{k_2[S_1]^2}{2} \qquad (3)$$

$$[S_1]_t = [S_1]_0 \frac{[exp(-k_1 t)]}{(1 + k_2' t)} \qquad (4)$$

$$I_t = I_0 \frac{[exp(-k_1 t)]}{(1 + k_2' t)} + R \qquad (5)$$

Here, I_0 and I_t and are the transient signal (photoluminescence intensity or differential absorbance by excitonic state) at time zero and time t. R represents the residual signal, representing long lived transient such as excimer or triplet state. The temporal profiles recorded were fitted following equation 5 and k_2' *values have been extracted from the fitting of temporal profiles recorded for different singlet exciton densities* ($[S_1]_0$). The onset of annihilation of singlet exciton densities have been estimated from the intercept along x-axis of the k_2' *vs.* $[S_1]_0$ linear plot which has further been used to calculate the exciton annihilation radius. Then, exciton diffusion coefficient and diffusion length were estimated from equation 1 and 2 respectively, and these parameters for different samples are provided in Table 2. Exciton diffusion length of all three molecules is in the range of 10 nm, typical of small molecular organic semiconducting systems. However, we find a systematic change in estimated diffusion parameters for three NAs investigated in the present work (Scheme 2). As NA system changes form 9,10-DPA to 1,8-DPA and finally to 2,6-DPA, diffusion parameters show systematic increase. Different dihedral angle of phenyl groups in different DPA derivatives causes variation in intermolecular distance in their NA, which in turn results in difference in exciton hopping rates leading to changes in diffusion coefficient and diffusion length of the singlet excitons generated by photoexcitation. The dihedral angle between phenyl substituent and anthracene moiety of these three derivatives apparently displays inverse trend of diffusion parameters. From the crystal structure parameter of the three derivatives, we note that the shortest unit cell parameter decreases from 9,10-DPA to 2,6-DPA. As exciton diffusion occurs by incoherent exciton hopping by resonance energy transfer mechanism, changes in intermolecular distance critically influence the exciton diffusion parameters. Consequently, near planar 2,6-DPA
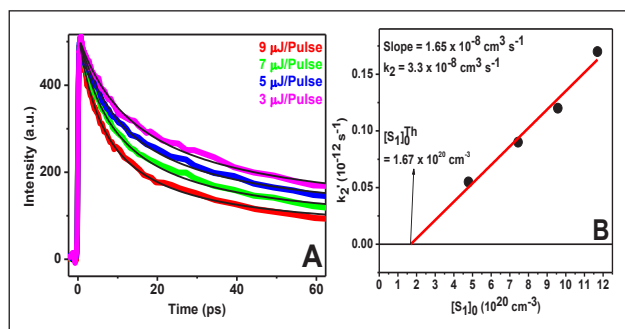
Figure 3: *(A) Fluence dependent temporal kinetics of exciton relaxation of 9,10-DPA NA measured at 430 nm. (B) k_2' vs. $[S_1]_0$ plot.*

NA appears as most promising fast exciton transporter in the present series.

Table 2: Exciton diffusion parameters of three DPA derivatives evaluated from ultrafast exciton-exciton annihilation kinetics.

Nanoaggregate	k_2 (cm^{3}s^{-1})	D (cm^{2}s^{-1})	L_D (nm)
9,10-DPA	0.33×10^{-9}	1.11×10^{-4}	7.3
1,8-DPA	1.66×10^{-9}	2.90×10^{-4}	10.2
2,6-DPA	2.22×10^{-9}	3.54×10^{-4}	15.6

C. Singlet fission dynamics in phenylethynyl derivatives of anthracene and tetracene

Photoinduced singlet fission to a pair of triplet state in organic semiconductor has opened up the possibility to increase photovoltaic efficiency by overcoming the Shockley-Quiesser
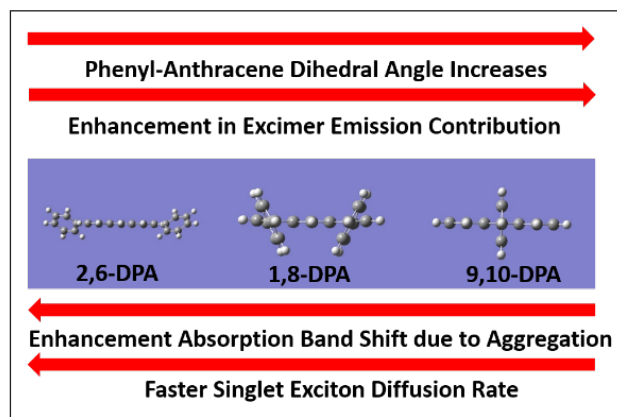
Scheme 2: *Systematic diagram representing effect of molecular structure on the photophysics and exciton diffusion properties of different DPA nanoaggregates.*

limit[18,19]. However, very specific thermodynamic ($2 \times E_{T1}$) and kinetic requirements (strong intermolecular coupling) led to very limited number of molecular systems reported to exhibit efficient SF process.[14-17] Chemically stable, low cost, blue absorbing SF materials are scarce. In anthracene, ethynyl substitution in 9, 10 position is computationally predicted to have T_1 level at half of the singlet energy level and thus meets thermodynamic criterion of SF process.[25,26] To explore experimental feasibility of SF in anthracene derivative we conducted detailed photophysics and ultrafast dynamics of 9,10-bis(phenylethynyl)antharcene derivative, abbreviated as BPEA[25].
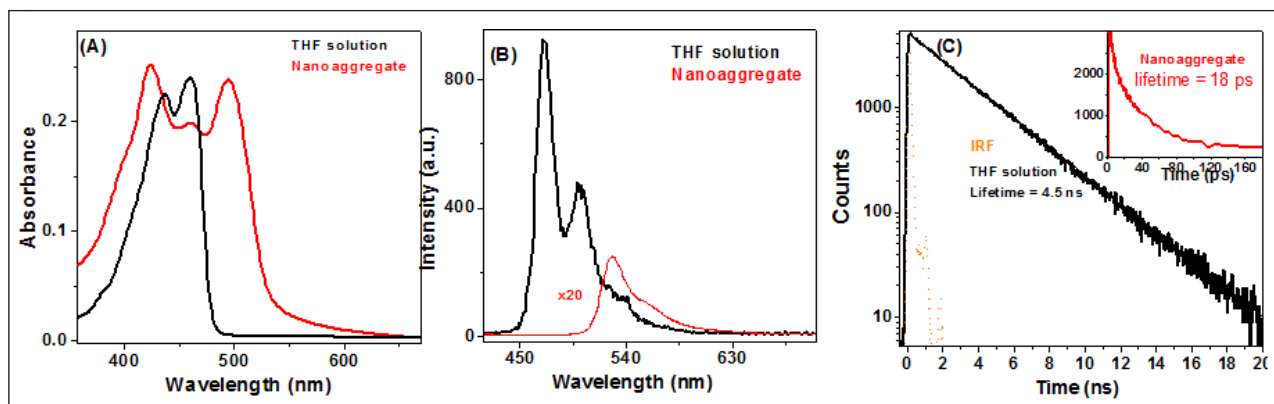

Figure 4: *Steady state and time resolved emission results of BPEA nanoaggregate.*

Unlike DPA derivatives presented in previous section, emission of BPEA in nanoaggregate (NA) and thin film (TF) quenches several orders of magnitude with a significant red shift of emission maximum (Figure 4B). Efficient intermolecular interaction in solid state is reflected from large spectral shift in absorption spectrum. Strong emission quenching suggests fast singlet exciton deactivation mechanism in BPEA NA. Fluorescence upconversion measurement indeed revealed ultrafast exciton quenching with a lifetime of 20 ps as compared to 4.5 ns lifetime in solution (Figure 4C). To underpin fast nonradiative relaxation mechanism in BPEA NA and TF, we performed detailed ultrafast spectroscopic measurement of this sample. Ultrafast pump-probe spectroscopic measurement revealed clear signature of ultrafast and efficient singlet fission in BPEA nanoaggregate and thin film. Figure 5A shows the femtosecond transient spectral evolution of BPEA nanoaggregate upon 390 nm femtosecond laser excitation. Decay of singlet exciton excited state absorption (ESA) signal at 600-700 nm region and recovery of ground state bleach in first few picoseconds time scale is assigned to

exciton-annihilation common to the behaviour of DPA derivatives described in previous section (confirmed by pump fluence dependent study). Interestingly, in tens of picosecond timescale, rise of triplet signal at 480 nm region and concomitant increase of bleach signal at 520 nm region (Figure 5B) gave a direct spectroscopic signature of SF process generating a pair of triplet excitons by interacting with a neighboring ground state molecule. Triplet character of long-lived excitons was confirmed by triplet sensitization experiment. Microsecond lifetime together with 160% triplet yield unequivocally established dominant SF mechanism responsible for singlet exciton deactivation in BPEA nanoaggregate. Very similar results were obtained in thin film sample of BPEA. We attributed efficient singlet fission to thermodynamically favourable energy level ordering ($E_{S1} > 2 \times E_{T1}$) of singlet and triplet level in BPEA.[25,26] As singlet fission was not observed in diphenyl derivatives of anthracene, positioning of phenylethynyl groups at 9 and 10 position is attributed to crucial to induce SF in this anthracene derivative. In addition, planar structure of BPEA allows close packing in solid state which provide necessary intermolecular
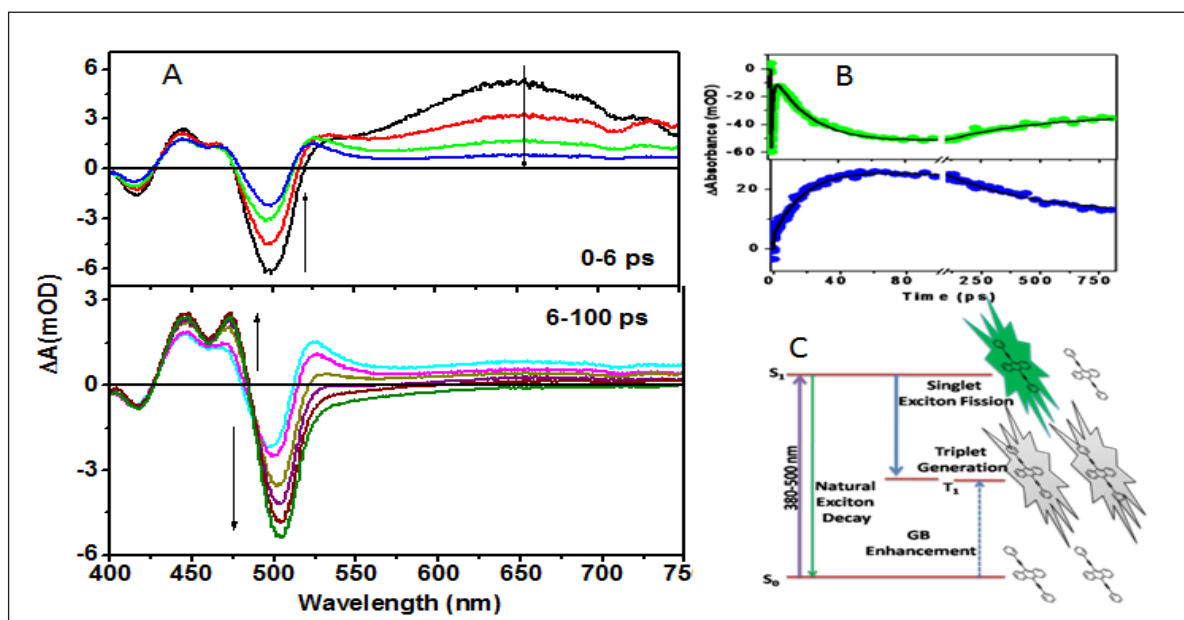

Figure 5: *Ultrafast pump-probe dynamics of BPEA nanoaggregate. (A) Transient spectral evolution, (B) Kinetic traces at two selected wavelengths, (C) Schematic showing dominant SF process as derived from ultrafast pump-probe experiments.*

coupling required for ultrafast SF, outcompeting other nonradiative decay channels. It is important to note that in thin film and nanoaggregate of BPEA, SF efficiency is not quantitative (i.e. triplet yield is <200%) due to presence of noncrystalline phase which partially traps of exciton localization

as excimer state. Moreover, polymorphism in BPEA crystal structure is reported to show different SF rates in differently treated thin film.[27] Our recent measurement on single crystalline sample of BPEA has shown faster and quantitative SF with 200% triplet yield (unpublished results).

Creation of two triplet excitons per absorbed photon by means of SF mechanism is proposed to a potential gateway of improving photovoltaic efficiency utilizing BPEA types of efficient singlet fissile materials.
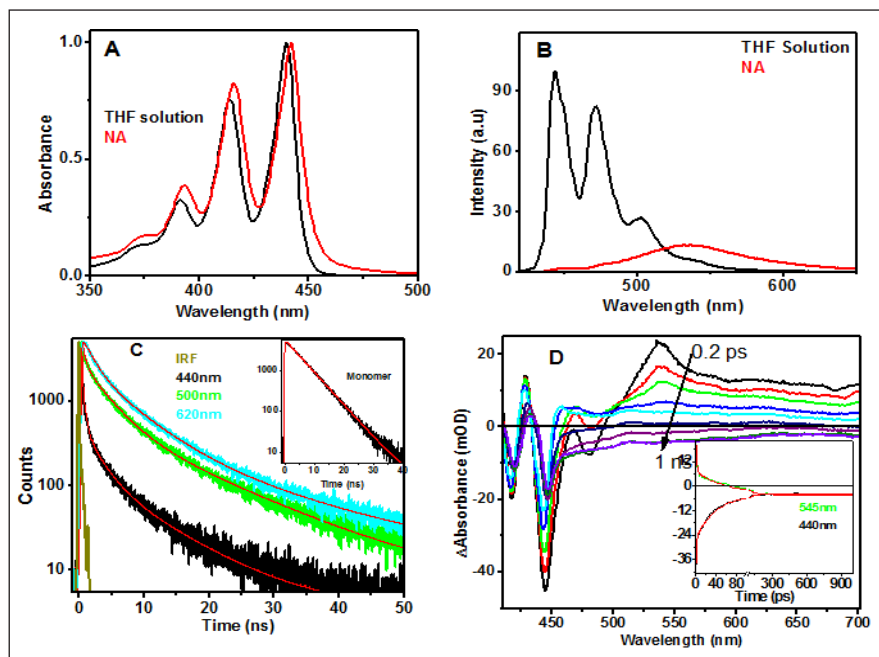

Figure 6: *Steady state absorption (A), emission (B) and transient emission (C) properties of TIPSA monomer and nanoaggregate. (D) pump-probe dynamics of TIPSA nanoaggregate.*
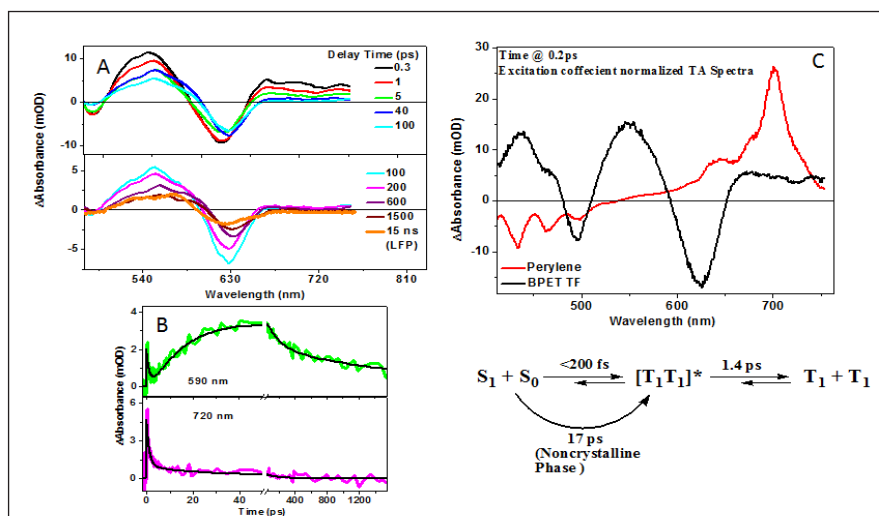
To further probe the effect of molecular packing on SF dynamics, a structurally analogous molecule, namely, 9,10-bis(triisopropylsilyl) anthracene (abbreviated as TIPSA) were subjected to photophysical and ultrafast spectroscopic investigation. Due to bulkier and nonplanar triisopropyl substitution, intermolecular interaction is anticipated to be affected which may hamper experimental feasibility of SF process. Indeed, while SF is computationally predicted to be thermodynamically favorable in TIPSA[26], our spectroscopic investigation does not find signature of efficient triplet formation in TIPSA. As shown in figure 6A, absorption spectrum of TIPSA is very similar in monomer and nanoaggregate. Similarly, emission spectrum (Figure 6B) is only moderately quenched in TIPSA as compared to hundred fold quenching in BPEA. However, emission

Figure 7: *Ultrafast pump-probe dynamics of BPET thin film. (A) Transient spectral evolution, (B) Kinetic traces at two selected wavelengths, (C) Comparison of early time transient signal of BPET film with a non singlet fission material. (D) Schematic showing dominant SF process as derived from ultrafast pump-probe experiments.*

peak in TIPA NA is red shifted and spectrally broad, similar to the behaviour of 9,10-DPA. This broad and red shifted emission is attributed to formation of long lived excimer state, charcaterized by more than ten nanosecond lifetime (Figure 6C). Ultrafast transient pump-probe measurement displayed in Figure 6D shows that that evolution of exciton absorption band to a negative stimulated emission band in 100 ps timescale confirming relaxation of exciton state to excimer state. However, we have only observed very weak signature of triplet state absorption at 430 nm region. We attribute this to inefficient intermolecular coupling leading to slow SF rate and thus other relaxation mechanism such as excimer formation becomes dominant relaxation channel of singlet exciton state. Our results support that kinetic feasibility of SF process requires strong intermolecular interaction in solid state.

To confirm favourable influence of planar phenylethyl substitution towards SF dynamics and generality of this approach, we further investigated exciton dynamics of a phenylethynyl derivative of tetracene, namely, 5,12-bis(phenylethynyl)tetracene (abbreviated as BPET).[ref] Tetracene is known to undergo singlet fission, however, due to endothermic nature, singlet fission is slower in this material (occurs in tens of picoseconds). Hints of fast nonradiative deactivation of singlet exciton in BPET nanoaggregate and thin film came from static absorption and fluorescence experiments. Like BPEA, BPET film exhibits strong perturbation of absorption spectrum and almost three orders of magnitude quenching of emission, making it virtually nonemissive species which is in sharp contrast to its highly emissive behaviour in solution.[28] Detailed ultrafast pump-probe experiment on thin film of BPET revealed that singlet excitons in BPET undergo ultrafast triplet pair formation in <200 fs timescale, which is an order of magnitude faster than tetracene. Figure 7 shows that transient spectral evolution of BPET thin film. In early timescale, transient spectrum

of BPET film exhibits signature of triplet excited state. While there is a slow rise component in the triplet ESA and concomitant growth of bleach signal, characteristics of SF process, observation of triplet signal in early timescale (within 300 fs of laser excitation) hints to an ultrafast component of triplet generation in this material. As time-resolution of our pump-probe spectrometer was limited to 200 fs, we adopted an indirect approach to assess possibility of ultrafast SF process in this material. Under identical experimental condition (same pump fluence and sample absorbance), comparison of bleach signal with a non-singlet-fission material in solution such as perylene led us to extract formation of 1.6 times of excited state per photon absorption, which implies 80% SF yield occurring in <200 fs. Slower component of triplet rise (with a lifetime of about 20 ps) is attributed to originate from non-crystalline phase in thin film which does not provide strong enough electronic coupling for ultrafast singlet fission. Detailed analysis of ultrafast pump-probe data led us to conclude ultrafast SF to correlated triplet pair state in <200 fs, followed by triplet pair separation in 1.4 ps in the crystalline phase of BPET sample. In essence, ultrafast SF in BPET also leads to better triplet yield (~180%) as compared to that in tetracene thin film (~150%).

Conclusion

In conclusion, solid state photophysics of polyacene molecules is remarkably altered as compared to well documented properties in solution. Depending on the structure of molecule, photogenerated excitons in anthracene derivatives can relax to excimer state in picoseconds time scale or may dissociate to triplet pair state by singlet fission (SF) process. Structural control of exciton and excimer emission in diphenyl derivatives of anthracene may be used to tune the emission colour and bright white light emissive system can be formulated with suitable doping.[29] On the other hand, changes in energy ordering of singlet and triplet levels in phenylethynyl derivative of anthracene favourable for singlet fission led to the possibility of carrier multiplication potentially

important for improving photovoltaic efficiency. The favourable influence of phenylethynyl functionalization on singlet fission has also been reported for tetracene derivative. Importance of intermolecular interaction in SF kinetics is exemplified by comparing pump-probe spectroscopy of BPEA and TIPSA nanoaggregate. In summary, structural influence on exciton diffusion and exciton relaxation behaviour in anthracene and tetracene based polyacene nanoaggregates and thin films have been discussed in detail.

Acknowledgement

References

1. Hedley, G. J.; Ruseckas A.; Samuel, I. D. *Chem. Rev.* **2017**, *117*, 796-837.
2. Ostroverkhova, O.*Chem. Rev.* **2016**, *116*, 13279-13412.
3. Salehi, A.; Fu, X.; Shin, D. H.; So, F. *Adv. Funct. Mater.* **2019**, *29*, 1808803.
4. Mikhnenko, O. V.; Blom, P. W. M.; Nguyen, T. Q. *Energ. Environ. Sci.,* **2015**, *8*, 1867-1888.
5. Serevičius, T.; Komskis, R.; Adomėnas, P.; Adomėnienė, O.; Jankauskas, V.; Gruodis, A.; Kazlauskas, K.; Juršėnas, S.*Phys. Chem. Chem. Phys.,* **2014**, *16*, 7089-7101.
6. Zambianchi, M.; Benvenuti, E.; Bettini, C.; Zanardi, C.; Seeber, R.; Gentili, D.; Cavallini, M.; Muccini, M.; Biondo, V.; Soldano, C.; Generali, G.; Toffanin, S.; Melucci, M. *J. Mater. Chem. C***2016**, *4*, 9411-9417.
7. Bhui, P.; Siddiqui, Q. T.; Muneer, M.; Agarwal, N.; Bose, S. *J. Chem. Sci.***2018**, *130*, 167.
8. Manna, B.; Ghosh, R.; Palit, D. K. *J. Phys. Chem. C.***2015**, *119*, 10641-10652.
9. Nandi, A.; Manna, B.; R. Ghosh, *Phys. Chem. Chem. Phys.,***2019**, *21*, 11193-11202.
10. Manna, B.; Nandi, A.; Nath, S.; Agarwal, N.; Ghosh, R.*J. Photochem. Photobiol. A.,***2020**, *392*, 112700.
11. Manna, B.; Palit, D. K. *J. Phys. Chem. C,***2020**, *124*, 24470-24487
12. Manna, B.; Nandi, A.*J. Phys. Chem. C.,***2019**, *123*, 21281-21289.
13. Manna, B.; Nandi, A.*J. Photochem. Photobiol. A,***2020**, *392*, 112407
14. Smith, M. B.; Michl, J. *Chem. Rev.,***2010**, *110*, 6891-6936.
15. Felter, K. M.; Grozema, F. C.*J. Phys. Chem. Lett.,***2019**, *10*, 7208-7214.
16. Smith, M. B.; Michl, J. Annu. *Rev. Phys. Chem.,***2013**, *64*, 361-386.
17. Thompson, N. J.; Congreve, D. N.; Goldberg, D.; Menon, V. M.; Baldo, M. A. *Appl. Phys. Lett.* **2013**, 263302, 103
18. Shockley, W.; Queisser, H. J. *J. Appl. Phys.,***1961**, *32*, 510-518.
19. Rao, A.; Friend, R. H. *Nat. Rev. Mater.,***2017**, *2*, 17063.
20. Salzillo, T.; Valle, R. G. D.; Venuti, E.; Brillante, A.; Siegrist, T.; Masino, M.; Mezzadri, F.; Girlando, A. *J. Phys. Chem. C.***2016**, *120*, 1831-1840.
21. Kusukawa, T.; Kojima, Y.; Kannen, F. *Chem. Lett.***2019**, *48*, 1213-1216.
22. Bains, G. K.; Kim, S. H.; Sorin, E. J.; Narayanaswami, V. *Biochemistry*, **2012**, *51*, 6207-6226.
23. Jortner, J.; Rice, S. A.; Katz, J. L.*J. Chem. Phys.,* **1965**, *42*,309.
24. Simpson, O. *Proc. – R. Soc. Edinburgh, Sect. A: Math. Phys. Sci.,* **1965**, *238*, 402.
25. Manna, B.; Nandi, A.; R. Ghosh, R. *J. Phys. Chem. C,* **2018**, *122*, 21047-21055.
26. Bhattacharyya, K.; Datta, A.; *J. Phys. Chem. C***, **2017**, *121*, 1412–1420
27. Bae, Y. J.; Kang, G.; Malliakas, C. D.; Nelson, J. N.; Zhou, J.; Young, R. M.; Wu, Y. Y.-L.; Duyne, R. P. V.; Schatz, G. C.; Wasielewski, M. R. *J. Am. Chem. Soc.***2018**, *140*, 15140-15144.
28. Nandi, A.; Manna, B.; Ghosh, R.*J. Phys. Chem. C.***2021**, *125*, 2583-2591
29. Manna, B.; Nandi, A.;Ghosh, R. *Photochem. Photobiol. Sci.,***2019**, *18*, 2748-2758

Dr. Rajib Ghosh is a scientific officer at Bhabha Atomic Research Centre, Mumbai, India. After completing M. Sc. in chemistry from University of Burdwan, he joined Bhabha Atomic Research Centre in 2007. He received his Ph. D. degree in 2015 from Homi Bhabha National Institute, Mumbai, for his work on ultrafast structural dynamics in charge transfer molecules in solution. Dr. Ghosh pursued postdoctoral research on ultrafast coherent spectroscopy in Max-Planck Institute for Structure and Dynamics of Matter, Hamburg, Germany. Dr. Ghosh is recipient of University Gold Medal and Homi Bhabha Gold Medal and conferred with young scientist award by the Department of Atomic Energy in 2015and by the National Academy of Sciences, India in 2018. His current research interest includes ultrafast spectroscopy, exciton dynamics and coherent spectroscopy of organic and inorganic materials of optoelectronic interest.

Dr. Biswajit Manna did his M. Sc. in chemistry from Indian Institute of Technology, Bombay. Subsequently he joined Bhabha Atomic Research Centre in 2011. He obtained Ph. D. in 2017 from Homi Bhabha National Institute, Mumbai. He is working in the field of photochemistry and ultrafast spectroscopy. His main research interests are exciton dynamics of organic nanostructure materials.

Mr. Amitabha Nandi obtained his B.Sc (Phys) from University of Calcutta and M.Sc (PhyS) from Indian Institute of Technology, Kanpur. He joined RPCD, BARC in 2013 and recently submitted his thesis in HBNI on ultrafast spectroscopy of organic material for Ph.D. degree. His research interest is morphology dependent excited state dynamics of organic material having application in photovoltaic application.

Coumarin based colourful sensors for ionic species

Satya Narayan Sahu

School of Chemistry, Sambalpur University, Jyoti Vihar, Burla-768 019, Odisha, India
Email: snsahu.chem@gmail.com; snsahu@suniv.ac.in

Abstract

The design of chromofluorescent molecular sensor for the selective and sensitive detection of analyte of chemical, biological and environmental relevance is an innovative approach that offers tremendous applications. Contrary to potentiometric/electrochemical sensing techniques, the dual mode optical sensing provides a direct visualization tool toward a particular analyte without a sophisticated analytical instrument. In this regard, coumarin molecules have found a special place to act as an excellent chromogenic and fluorogenic unit. We have developed a coumarin functionalized organic molecule which could optically discriminate the presence of fluoride and cyanide ions amongst the other anions in a solution phase. Further, the same molecule could able to show brilliant aggregation induced emission (AIE) characteristic which can be employed to sense heavy metal ions like copper in almost 100% water medium *via* a fluorescence colour change.

1. Introduction

Developing specific molecular probes for solution phase analysis of ionic analytes in a mixture of competitive species is undoubtedly a challenging task.[1,2] Amongst the various analytes, the detection of biologically and environmentally relevant fluoride, cyanide and copper ions is of most significant.[3-5] Though several methods, including atomic absorption, electrochemical, voltammetric, potentiometric and ion-exchange chromatography techniques have been explored[6] but these practices do not offer a cost-effective, rapid and real time-monitoring system for detection of ions. In this regard, optical chemosensors possessing a chromofluorogenic unit are emerged as a powerful tool for the sensing of ionic analytes.[7-9] The ionic analytes bind to the probe molecules *via* non-covalent interactions and thereby trigger a perturbation in their photo physical properties to elicit a colour and/or fluorescence change in the probe solution.[7-9]

Recently, salicylidine Schiff base derivatives have been emerging as a potential candidate for anion sensors.[10,11] The uniqueness of this molecule is the presence of phenolic OH proton which can act as hydrogen bond donor for anionic species and the azomethine linkage that facilitates to undergo addition type reaction by a nucleophilic anion. Besides, Schiff bases show excellent photophysical properties *via* excited-state intramolecular proton transfer (ESIPT), photochromism and thermochromism processes.[12] In recent studies, salicylidene based Schiff bases have been emerged as potential molecules to show AIE characteristics in highly aqueous medium.[13] The uniqueness of salicylidene based Schiff base molecule is the presence of phenolic 'O' and azomethine 'N' which can act as electron donor for binding metal ions. Thus, attachment of a chromogenic and/or fluorogenic moiety as signalling subunit with the azomethine bond via π-conjugation could provide interesting optical response through efficient charge transfer during ion binding. Further, the chelating nature of ligands with metal ions strongly influences the fluorescence intensity of the metal-ligand complexes through modulating the energy levels of the ligand and metal ions.[14] It is therefore envisaged that attachment of a salicylidine unit with a coumarin derivative can lead up to

the development of chromofluorogenic sensor where the interaction between the ionic species with sensor molecule may trigger a colour and fluorescence change in the sensor medium. This prompted us to develop a coumarin-thiazolyl functionalized salicylidine Schiff base probe (**3**) which can trigger an optical output in the sensor medium upon interaction with ionic species. In this study, we have demonstrated the chromofluorogenic response of probe **3** with anions and cations through a fascinating colour change visible to naked eye.

2. Experimental

2.1. *General procedure for synthesis of probe 3*

A solution of salicyladehyde (0.305 gm, 2.5 mmol) in ethanol (5 mL) was added slowly in dropwise manner over 15 minutes to the solution of amino-thiazolyl derivative **2** (0.488 gm, 2.0 mmol) dissolved in 30 mL ethanol under reflux condition (Scheme 1).[15] Then the solution was allowed to reflux for 8 h with stirring till complete precipitation is formed. The precipitate obtained was then filtered under hot condition and washed with hot ethanol for several times to remove the unreacted salicyladehyde. The solid product obtained was dried in vacuum to get

the pure compound **3** as yellow colour powder in quantitative yields (92 %).

2.2. Instrumentation

^{1}H NMR was recorded on an Avance III–400 MHz Bruker spectrometer. Chemical shifts are reported in parts per million from tetramethylsilane with the solvent (DMSO-d_6: 2.5 ppm) resonance as the internal standard. Data are reported as follows: chemical shifts, multiplicity (s = singlet, d = doublet, t = triplet, m = multiplet), coupling constant (Hz). UV–visible absorption spectra were recorded on a Shimadzu UV-2450 spectrophotometer. Fluorescence emission spectra were recorded on a Hitachi F-7000 fluorescence spectrophotometer. pH readings were measured on UTECH CON-700 digital pH meter. Hydrodynamic diameters of the aggregates were measured using Malvern Zetasizer instrument. Transmission electron microscopy (TEM) experiment was performed on FEI Tecnai G^2 20 Twin instrument. HRMS experiment was performed on a Bruker ESI-MS microTOFQ instrument. Chromatographic purification was done using 60–120 mesh silica gels. For reaction monitoring, manually coated silica gel-300 mesh TLC plates were used.
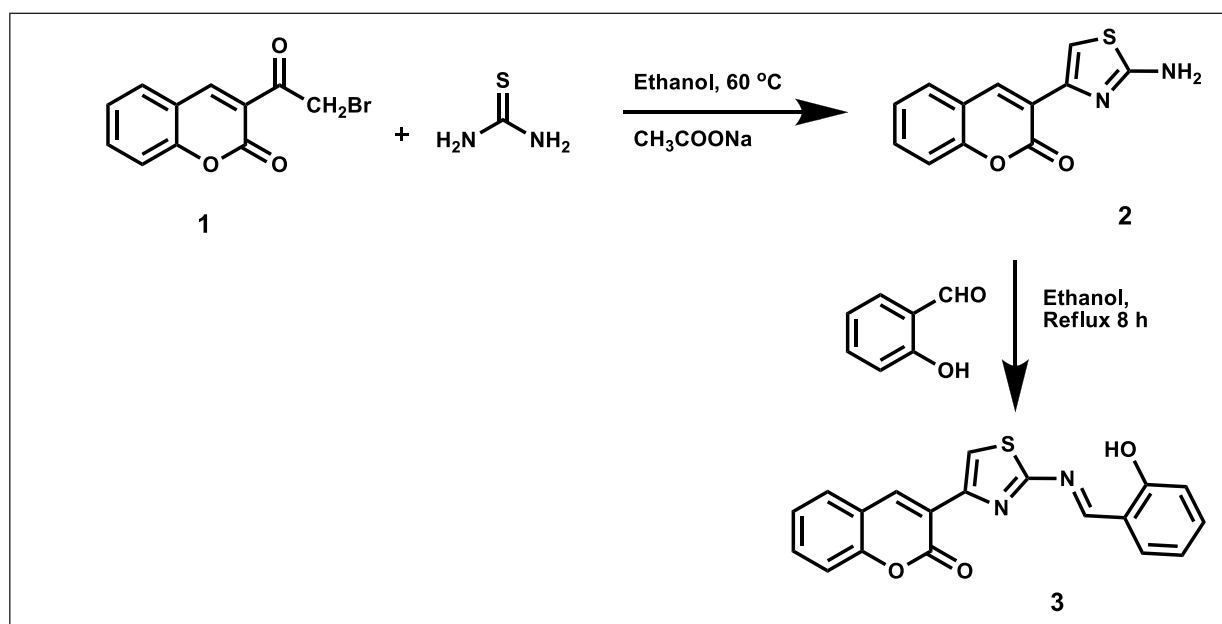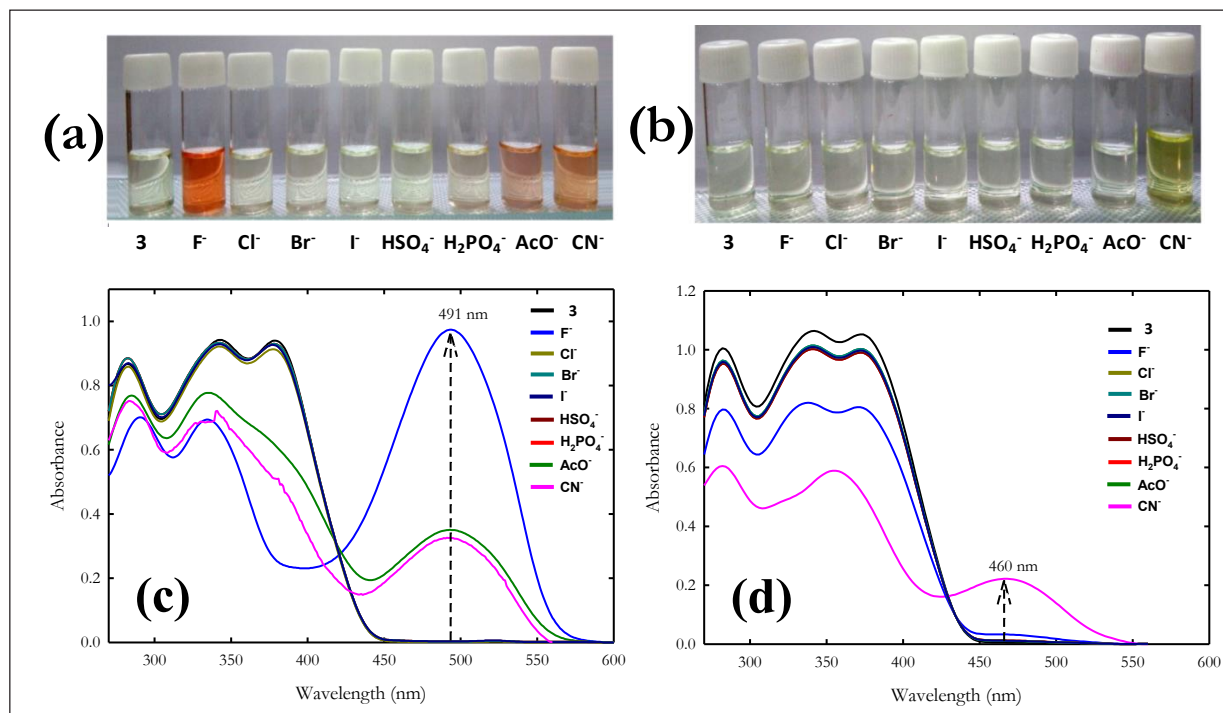

Scheme 1: *Synthesis of probe **3**.*

Figure 1: *Colour change in probe **3** in (a) organic and (b) aqueous solution (50µM) with the addition of 10 equivalents of various anions. The corresponding absorption spectra of probe **3** upon addition of 10 equiv. of F⁻, Cl⁻, Br⁻, I⁻, $H_2PO_4^-$, HSO_4^-, AcO⁻ and CN⁻ ions in (c) organic and (d) aqueous medium (50 µM).*

*2.3. Analytical characterization of probe **3***

M.P. = 230 ℃. ¹H NMR (400 MHz, *DMSO-d₆*) δ (ppm) = 7.00 (2H, m, Ar-H), 7.40 (1H, t, *J* = 8 Hz, Ar-H), 7.47 (2H, m, Ar-H), 7.64 (1H, t, *J* = 8 Hz, Ar-H), 7.90 (1H, d, *J* = 8.0 Hz, Ar-H), 7.97 (1H, d, *J* = 8 Hz, Ar-H), 8.37 (1H, s, coumarinyl-H), 8.88 (1H, s, thiozolyl-H), 9.38 (1H, s, aldimine-H), 11.53 (1H, s, Ar-OH, D₂O exchangeable). ¹³C NMR (100 MHz, *DMSO-d₆*) δ (ppm) = 115.9, 116.9, 119.1, 119.5, 119.8, 120.0, 124.8, 129.1, 131.1, 132.1, 135.2, 139.8, 145.7, 152.6, 158.8, 160.3, 164.3, 170.4. FT-IR (KBr) ν (cm⁻¹) = 3132, 3041, 1735 (>C=O), 1724, 1625, 1610 (>C=N), 1571, 1508, 1475, 1367, 1288, 1170, 1095, 1016, 904. UV-visible (acetonitrile, 50 µM) = λ_{max}(nm) 346, 378 (n-π*). Fluorescence emission (acetonitrile, 50 µM) λ_{em} = 535 nm at λ_{ex} 375 nm.

3. Results and discussion

*3.1. Colorimetric analysis of probe **3** upon interaction with anions*

The visual response of probe **3** against various anions (such as F⁻, Cl⁻, Br⁻, I⁻, $H_2PO_4^-$, HSO_4^-, AcO⁻ and CN⁻) was first monitored through colorimetric analysis in organic (acetonitrile, ACN) medium. It was found that the probe **3** exhibited a prominent and instant colour change from colourless to deep red only with fluoride ions while no significant colour response was observed on treatment with Cl⁻, Br⁻, I⁻, $H_2PO_4^-$ and HSO_4^- ions under analogous condition (Figure 1a). On the other hand, interaction of **3** with AcO⁻ and CN⁻ ions exhibited a faint colour change in comparison to that observed with fluoride ions (Figure 1a). When a similar set of colorimetric analysis was carried out in aqueous medium (H₂O-ACN, 1:1 v/v), it was interesting to note that the probe **3** exhibited a instantaneous colour change from colourless to deep yellow only with cyanide ions while no optical response was observed on treatment with F⁻, Cl⁻, Br⁻, I⁻, $H_2PO_4^-$, HSO_4^-, AcO⁻ ions as shown in Figure 1b.

Moreover the colorimetric analysis of the interaction of **3** with CN⁻ ions was tested in different percentage of aqueous acetonitrile

mixture ranging from 95/5 to 5/95 (ACN-H$_2$O v/v) which exhibited that the detection of cyanide ions could be possible through visual colour change in aqueous medium as high as 50% by volume of water.

3.2. UV-visible and Fluorescence study of probe 3 with anions

Based on the results obtained from the colorimetric analysis, UV-visible spectroscopic investigations of **3** upon interaction with fluoride and cyanide ions were performed at 50 µM concentration. Addition of fluoride ions to **3** in organic medium exhibited a newly developed longer wavelength absorption peak at 491 while no change was observed in the UV-visible spectrum upon addition of Cl$^-$, Br$^-$, I$^-$, H$_2$PO$_4^-$ and HSO$_4^-$ ions as depicted in Figure 1c. Conversely, addition of F$^-$, Cl$^-$, Br$^-$, I$^-$, H$_2$PO$_4^-$, HSO$_4^-$, AcO$^-$ and CN$^-$ ions to **3** in aqueous medium exhibited a longer wavelength absorption peak at 460 nm only in the presence of cyanide ions as shown in Figure 1d.

It was further observed that, gradual addition of a standard solution of fluoride ions (TBAF) to 50 µM solution of **3** in organic medium resulted in progressive increase in the absorption peak centred at 491 nm with simultaneous decrease in the absorption band at 378 nm in the UV-visible spectra with the appearance of an isobestic point at 421 nm (Figure 2). When the concentration of fluoride addition approached to one equivalent with respect to **3**, a colour change from colourless to reddish was observed in the probe solution and this colour became deeper on further addition of fluoride ions with concomitant increase in the intensity of absorption band at 491 nm. The observed colorimetric changes in probe solutions reached its limiting value on addition of two equivalents of fluoride ions.

Experimental observations indicate that the appearance of new absorption band at a higher wavelength (491 nm) during probe-fluoride interaction could be either due to the formation of hydrogen bonds with the phenolic –OH or its deprotonation by fluoride ions which results in a visual colour change possibly through efficient intramolecular charge transfer (ICT). UV-visible titration experiments of probe **3** with cyanide ion in organic medium (50 µM) exhibited a concurrent increase in the absorption peak at 491 nm, however, with lesser intensity as shown in Figure 3a. On the other hand, titration of cyanide ion with **3** in aqueous medium showed gradual increase of an absorption peak at 460 nm with a visual colour change from colourless to yellow in the probe solution (Figure 3b). Analysis of the titration profiles of cyanide ion with **3** in organic and aqueous medium indicates that the intensity of the absorption peaks at 491 and 460 nm
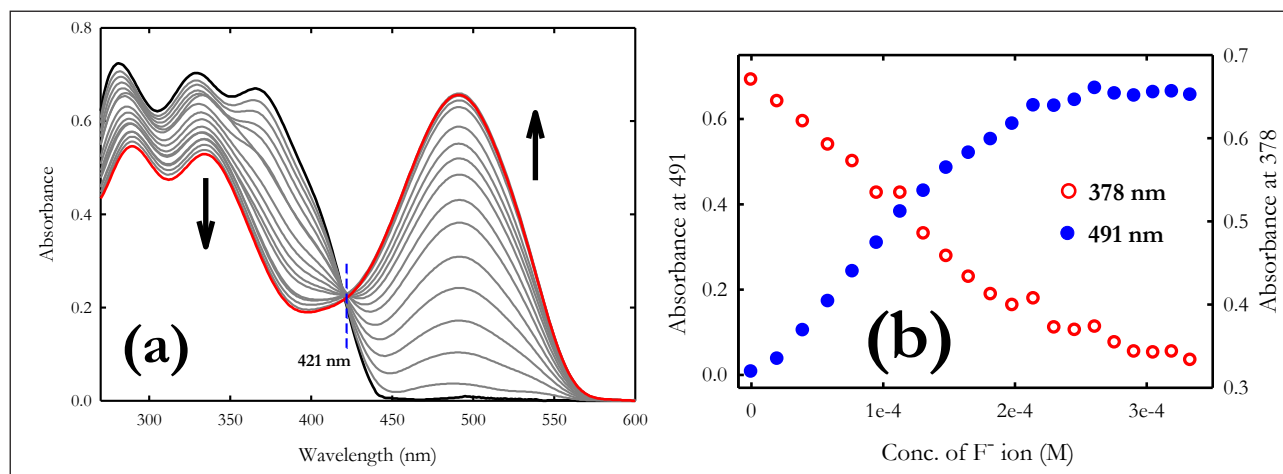

Figure 2: *(a) UV-visible titration spectra of probe **3** (50 µM) with 0–5 equiv. of TBAF in organic medium, (b) Change in absorbance at 378 and 491 nm with various concentrations of F$^-$ ions.*
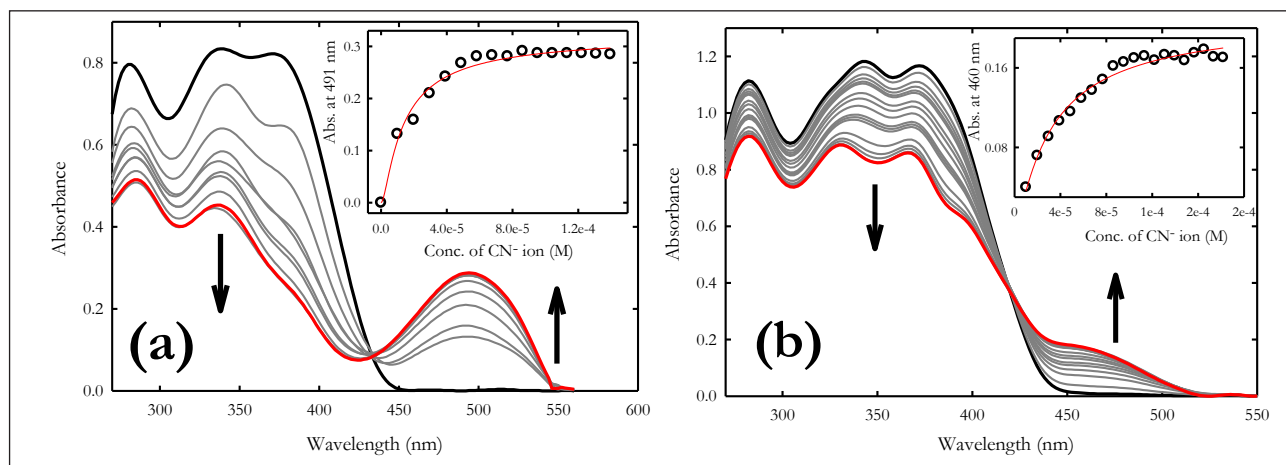
Figure 3: *(a) UV-visible titration spectra of probe **3** (50 μM) with 0–5 equiv. of CN⁻ ion in (a) organic, (b) aqueous medium. Inset shows change in absorbance at 491 nm (a) and 460 nm (b) for **3** with varying conc. of CN⁻ ion.*
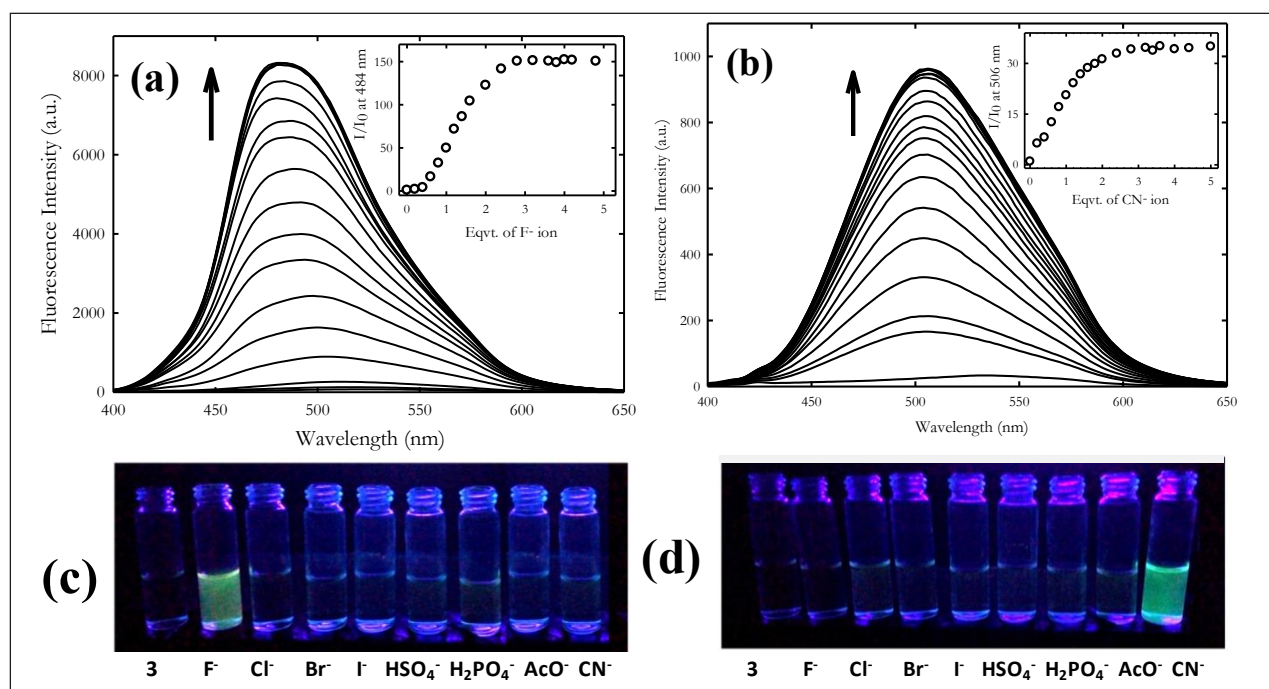

Figure 4: *(a) Fluorescence spectra of probe **3** (50 μM) with 0–5 equiv. of TBAF in organic medium. Inset shows change in fluorescent intensity (I/I_0) at 484 nm for **3** with varying equivalents of F⁻ ion. λ_{ex} = 375 nm, λ_{em} = 484 nm. (b) Fluorescence spectra of probe **3** (50 μM) with 0–5 equiv. of CN⁻ in aqueous medium. Inset shows change in fluorescent intensity (I/I_0) at 506 nm for **3** with varying equivalents of CN⁻ ion. λ_{ex} = 375 nm, λ_{em} = 506 nm. Fluorescent "turn on" behaviour of **3** (50 μM) for (c) fluoride ion in organic medium (d) cyanide ion in aqueous medium over other anions (10 equivalents) under UV light (365 nm).*

respectively reached the limiting value beyond two equivalents of cyanide addition. Similarly the titration experiments of **3** with acetate ion (TBAAcO) in organic medium showed analogous results as that of cyanide ion with a gradual increase in the absorption peak at 491 nm.

The interaction of probe **3** with the anionic species was further investigated by fluorescence technique in organic and aqueous mediums. It was observed that, addition of 10 equivalents of various anions such as F⁻, Cl⁻, Br⁻, I⁻, $H_2PO_4^-$, HSO_4^-, AcO⁻ (as TBA salts) and CN⁻ (as KCN)

to **3** in organic medium resulted in an intense emission peak at 484 nm only in presence of fluoride ions. In a similar experiment, addition of various anions to 50 µM probe solution in aqueous medium showed a significant increase in the fluorescence intensity at 506 nm only in the presence of cyanide ions. This indicated that the probe is quite selective and specific towards CN⁻ ion in aqueous medium. In absence of anions, the probe exhibited a low intensity emission peak at 535 nm in organic medium. On gradual addition of fluoride ions from 0 to 5 equivalents, a hypsochromically shifted ($\Delta\lambda$ = 51 nm) peak was increased at 484 nm that became saturated beyond two equivalents of fluoride ions with a fluorescence 'turn on' behavior by intensity enhancement of 150-folds (Figure 4a). In a similar experiment in aqueous medium, probe **3** showed an emission peak at 506 nm ($\Delta\lambda$ = 29 nm) upon incremental addition of CN⁻ ions up to two equivalents with 37-fold increase in the fluorescence intensity (Figure 4b).

The fluorescence "turn-on" signal in probe **3** could be a result of intramolecular charge transfer through anion-probe interaction which may suppress the n-π* transitions to facilitate the π–π* transitions that mostly responsible for the emissive behavior of the probe.[16] Probe **3** is fluorogenically selective for fluoride and cyanide ions in organic and aqueous mediums respectively (Figure 4c,d), which were in good agreement with the UV-visible experiments. Our result is worthy to note as it exhibits a fluorescence "turn on" behavior in comparison to earlier reports[17,18] which showed fluorescence quenching rather than enhancement on fluoride binding. While probe **3** exhibited a significant fluorescence change from colourless to green selectively with cyanide ions in comparison to other anions in aqueous medium (Figure 4d).

3.3. Aggregation-induced emission (AIE) studies of probe 3

The aggregation induced emission characteristics of **3** was investigated at 50 µM concentration in DMSO solution with addition of different fraction of water (f_w) ranging from 0 to 99.5% (v/v) buffered by 10 mM HEPES at pH 7.4. Figure 5a represents the AIE character of **3** under UV-lamp at 365 nm. Monomeric solution of **3** in 100% DMSO is almost colourless for visual detection. However, upon increasing the water fraction, the probe emits yellow colour fluorescence beyond 60%. The corresponding fluorescence spectra of **3** exhibit a weak emission band at 506 nm in 100% DMSO solution (50 µM) which decreases upon gradual addition of water fraction and new band at a longer wavelength of 544 nm appeared (Figure 5b). The intensity at 544 nm corresponding to the yellow fluorescence of probe **3** increases from 60% water fraction and exhibits a highest value at 80% (f_w) (Figure 5c). Further addition of higher water fraction (f_w >80%) results in reduction of emission intensity
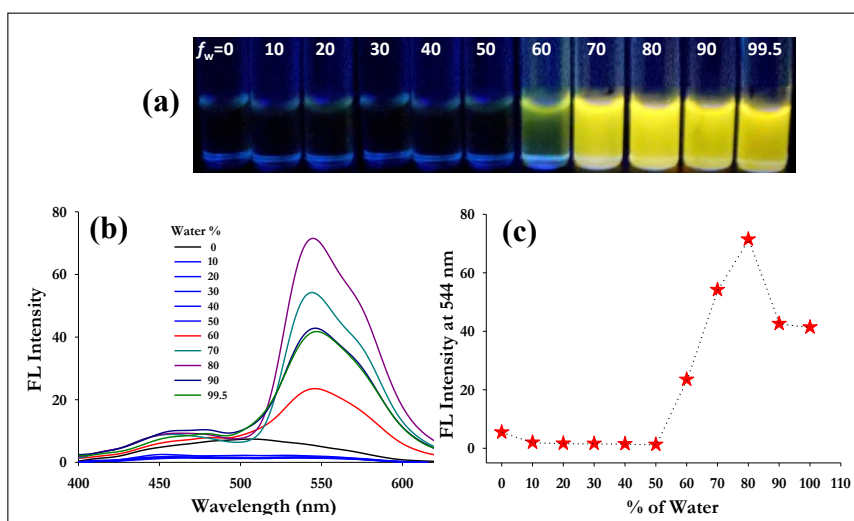

Figure 5: (a) Visual fluorescence response of 50µM probe 3 under an UV-lamp at 365 nm at varying DMSO-Water (buffered by 10 mM HEPES at pH 7.4) fraction. (b) Fluorescence response for 50µM of probe 3 at varying DMSO-Water (buffered by 10 mM HEPES at pH 7.4) fraction (λex = 362 nm).(c) Change in fluorescence intensity of probe 3 at 544 nm as a function of different percentage of water fraction (% fw).
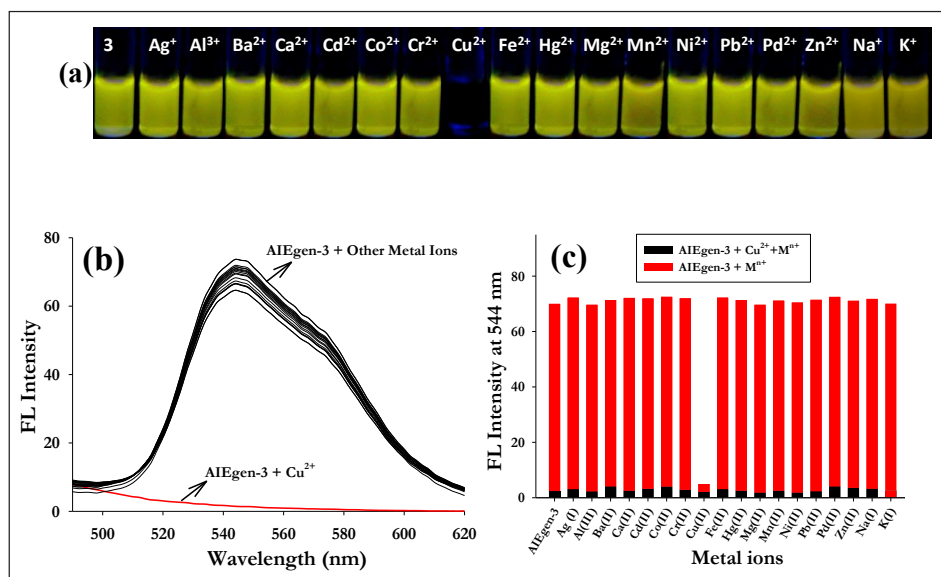
Figure 6: *(a) Visual fluorescence response under UV-Lamp at 365 nm; (b) Emission spectra of* **AIEgen-3** *(50 µM) upon addition of 10 equiv. of various metal ions; (c) Histogram showing fluorescent intensity of* **AIEgen-3** *at 544 nm with 10 equiv. of various metal ions (red bars) and with 10 equiv. of various metal ions plus of 10 equiv. of Cu^{2+} ions (black bars) [λ_{ex} = 362 nm].*

which could be possibly due to formation of larger molecular aggregates that precipitate out quickly resulting in a decrease in emission intensity. Besides, dynamic light scattering (DLS) studies of probe **3** in different water fractions in DMSO (f_w 60%, 80% and 99.5%) also showed a decrease in average particle size (Z_{av}) on addition of higher water volumes (Z_{av} at f_w 60% = 801 nm; at f_w 80% = 372 nm and at f_w 99.5% = 175 nm) indicating the formation larger aggregates that precipitates out from the solution phase. However, the emission intensity at 544 nm for **3** is significantly increased to 10 fold at 80% water fraction, and even in the 99.5% water fraction, the fluorescence intensity is still much higher (~ 7 fold) than that in pure DMSO.

Interestingly, the Stokes shift in aggregated probe **3** at 80% water fraction ($\Delta\lambda$=170 nm) is found to be much higher than that in pure DMSO ($\Delta\lambda$=132 nm) which is possibly because of the collective effect of ESIPT and AIE process.[19] It is believed that, at lower water fractions (in good solvent condition), the molecule (**3**) undergoes free rotation of the salicylidine aromatic unit around the C=N bond resulting in suppression

of ESIPT *via* non-radiative decay of excited states. However, as the volume of water fraction increases beyond 60%, the probe **3** suffers restriction in its free rotation possibly due decrease in solubility resulting to close packing/aggregation of the hydrophobic molecules through inter- and intra-molecular hydrogen bonding. This restriction of intramolecular rotation (RIR) in aggregated probe **3** perhaps facilitates the radiative release of the photo-excited energy through suppression of non-radiative decay.[20] All the above findings clearly suggest that compound **3** is an AIE active fluorophore in aqueous medium.[21] For the investigation of metal ion interactions, the aggregated fluorophore **3** was taken at 20:80 (v/v) DMSO:HEPES buffer medium at pH 7.4 which is termed as **AIEgen-3** solution on subsequent discussion.

3.4. Fluorescence and UV-visible studies of AIEgen-3 with metal ions

The fluorogenic response of **AIEgen-3** (50 µM) was investigated against 10 equivalents of various metal ions (such as Na^+, K^+, Ag^+, Al^{3+}, Ba^{2+}, Ca^{2+}, Cd^{2+}, Co^{2+}, Cr^{2+}, Cu^{2+}, Fe^{2+}, Hg^{2+}, Mg^{2+}, Mn^{2+},
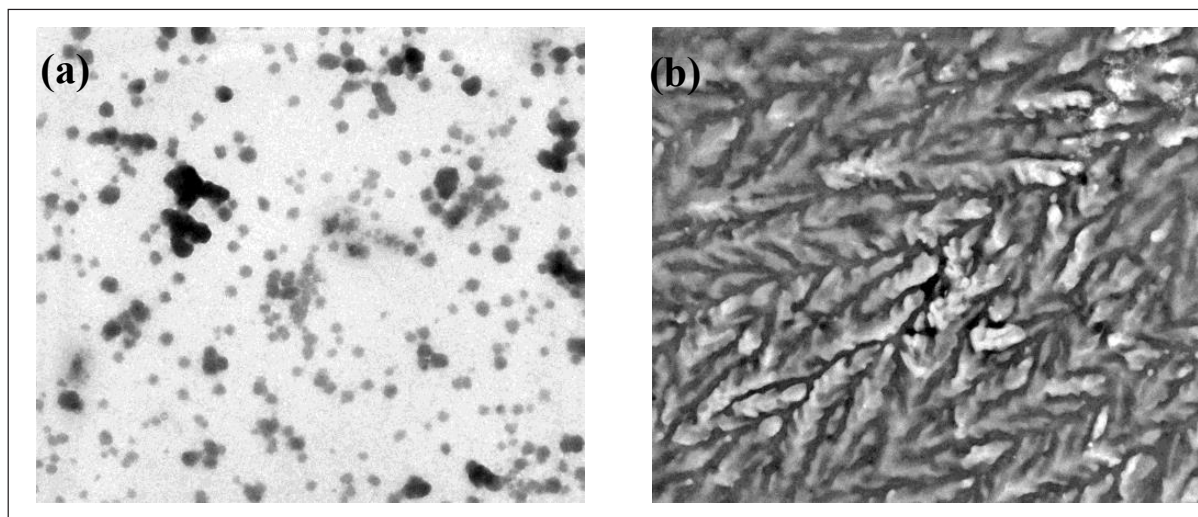
Figure 7: *TEM micrograph of (a)* **AIEgen-3** *(b)* **AIEgen-3** + *Cu^{2+}*

Ni^{2+}, Pb^{2+}, Pd^{2+} and Zn^{2+} taken in HEPES buffered medium at pH 7.4) through visual fluorescence analysis under an UV-Lamp at 365 nm. It was observed that **AIEgen-3** exhibited a diagnostic colour change from bright yellow fluorescence to non-fluorescent (colourless) only in presence of Cu^{2+} ions while no significant fluorescence response was observed in presence of other metal ions under the identical conditions (Figure 6a).

The emission spectra of **AIEgen-3** with various metal ions exhibited quenching of the AIE band at 544 nm only in presence of Cu^{2+} ions (Figure 6b). The competitive metal ion interaction study of **AIEgen-3** in presence of 10 equivalents of various metal ions clearly demonstrates that the fluorescence intensity of **AIEgen-3** at 544 nm gets completely quenched by Cu^{2+} ions even in the presence of other interfering metal ions. This result indicates a very high level of selectivity of **AIEgen-3** toward Cu^{2+} ion. The selectivity

behaviour was again monitored by UV-visible spectroscopy by addition of various metal ions to **AIEgen-3** solution (50 µM). The results indicated that the absorption maxima at 374 nm significantly decreases in presence of Cu^{2+} ion while other metal ions could not produce any detectable change in its UV-visible spectrum.

The mechanism of interaction of probe **3** with copper ions has also been studied by dynamic light scattering (DLS), transmission electron microscopy (TEM) and ESI-Mass spectrometry (ESI-MS) experiments. For instance, the aggregation behavior of probe **3** in poor solvent (water) in the absence and presence of Cu^{2+} ions have been examined from the particle size measurements by DLS experiments. The results showed that the average particle size (Z_{av}) of **AIEgen-3** (f_w 80%) in the absence of copper ions is estimated to be 372 nm. However, in presence of 2.0 equivalents of Cu^{2+} ions the

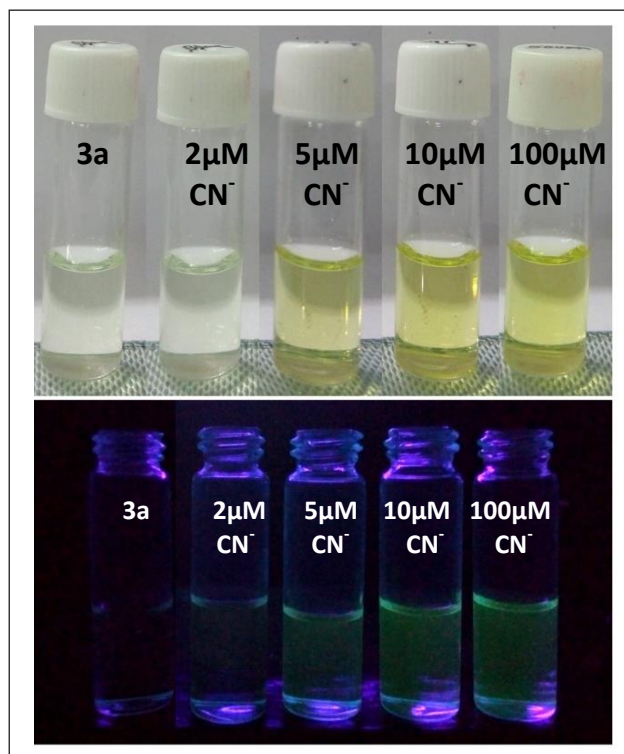| Table 1: Estimation of Cu^{2+} ion by AIEgen-3 in real samples using fluorescence assay					
Sample	**Cu^{2+} added (µM)**	**F.I. at 544 nm (a.u.)**	**Cu^{2+} found (µM)**	**RSD (%)***	**Estimation (%)**
AIEgen-3 (50 µM) (Blank)	0	59.85	--	--	--
Tap water sample-1	5	52.47	4.69	1.25	93.8
Tap water sample-2	10	46.31	9.58	1.31	95.8
Lycopene syrup -1	--	47.63	8.67	1.62	--
Lycopene syrup -2	5	43.47	12.44	1.19	91.0
*RSD (%) = percent relative standard deviation					

Figure 8: *Visual colour (top) and fluorescence change (bottom under UV light 365 nm) of **3** (50 µM) with the addition of various concentration of CN⁻ ion in tap water.*

average particle size dramatically increases to 656 nm which indicated an obvious effect of Cu^{2+} ions on the aggregation pattern of the probe. Further, the morphology of **AIEgen-3** aggregates has been investigated by TEM analysis which clearly indicates the formation of discrete aggregated nanoparticles in the range of 300-400 nm (Figure 7a). The addition of Cu^{2+} ions to **AIEgen-3** modulates the aggregation pattern of the probe that result in the formation of pinnate leaf type aggregates (Figure 7b). Moreover, the formation of **AIEgen-3**-Cu^{2+} complex was also analysed by ESI-MS that showed a strong peak at m/z 245.03 which could be attributed to the dimeric complex $[2(AIEgen\text{-}3).2Cu.ClO_4.CH_3CN. H_2O.H]^{4+}$ (calculated m/z 245.24).

All these findings clearly suggest that the aggregated **AIEgen-3** interact with Cu^{2+} ions resulting in swelling up of the aggregates *via* copper ion intercalation leading to the formation of larger particles. The aggregated copper complex possibly quenches the AIE fluorescence

signal of **AIEgen-3** at 544 nm *via* Cu^{2+} mediated PET mechanism.

4. Analytical applications

Considering the important applications of cyanide in industry, the detection of cyanide in natural environment by visual and fluorescence method in aqueous medium by probe **3a** has been investigated. Moreover to verify the possible interference of other components and ions present in real samples in the detection of cyanide ion, we have taken the town supply tap water as the medium of analysis. Different amounts of potassium cyanide were added to tap water in order to make the final concentrations of cyanide ion between 2 to 100 µM. A 50 µM probe solution was prepared in aqueous medium (H_2O-Acetonitrile 1:1 v/v) and different concentrations of cyanide ion in tap water were added to the probe solution. The observed visual and fluorescence colour change was depicted in Figure 8 which indicated that the probe could be applied for the detection of cyanide ion at micromolar range in environmental samples.

Further, the detection and estimation of copper ions by **AIEgen-3** has been investigated in natural environment by fluorescence measurement using town supply tap water as the medium of analysis. The extent of fluorescence quenching in **AIEgen-3** (50 µM) with known concentrations Cu^{2+} ions have been calibrated and found to be in excellent linear correlation (R^2 = 0.99) over the range 5 µM to 50 µM. Now solutions of Cu^{2+} ions in varying concentrations were prepared in tap water and estimated by **AIEgen-3** (50 µM) using the calibration plot. The results (Table 1) indicated that **AIEgen-3** could be applied for the detection and estimation of Cu^{2+} ions in environmental samples. In addition, **AIEgen-3** is also capable of estimating the amount of Cu^{2+} ions present in a pharmaceutical syrup sample (Lycopene syrup) without any pretreatment of the syrup solution. This will definitely open up new opportunities to estimate Cu^{2+} ions directly in pharmaceutical formulations.

5. Conclusions

In summary, a chromofluorescent salicylidine probe **3** functionalized with thiazolyl-coumarin derivatives has been synthesized through simple condensation reaction in quantitative yield. Interestingly probe **3** could optically discriminate the presence of fluoride and cyanide ion in organic and aqueous mediums respectively through a significant colorimetric and fluorescence "turn-on" change in the probe solution. Moreover probe **3** shows aggregation induced emission (AIE) characteristics at different water fraction in DMSO medium to elicit a bright yellow fluorescence under UV-illumination at 365 nm. The aggregated probe **AIEgen-3** selectively discriminates Cu^{2+} ions over a series of other interfering metal ions by a fluorescence "on-off" strategy *via* CHEQ process in DMSO-HEPES buffer (2:8 v/v) at a physiological pH of 7.4. The practical application of the probe was analyzed in various samples present in tap water and pharmaceutical formulations. The probe could be applied for the detection of copper and cyanide ion in aqueous environmental samples and as well as estimation copper ion in a pharmaceutical syrup (Lycopene).

Acknowledgment

References

1. N. Busschaert, C. Caltagirone, W. Van Rossom, P. A. Gale, Chem. Rev. 115 (2015) 8038-8155.
2. Singh R., Das G. In: Singh D., Das S., Materny A. (eds) Advances in Spectroscopy: Molecules to Materials. Springer Proceedings in Physics, 236 (2019) 57-65. Springer, Singapore.
3. P. B. Pati, Sens. Actuators, B: Chem. 222 (2016) 374–390.
4. M. Cametti, K. Rissanen, Chem. Commun. 20 (2009) 2809–2829.
5. V. K. Gupta. I. Ali, H. Y. Aboul-Enein, Developments in Environmental Science 2007), Vol 5, Chapter 3, 33-56.
6. A. Dhillon, M. Nairb, D. Kumar, Anal. Methods, 8 (2016) 5338-5352.
7. F. Wang, L. Wang, X. Chen, J. Yoon, Chem. Soc. Rev. 43 (2014) 4312-4324.
8. Y. Zhou, J. F. Zhang, J. Yoon, Chem. Rev. 114 (2014) 5511-5571.
9. D. Udhayakumari, S. Naha, S. Velmathi, Anal. Methods, 9 (2017) 552-578
10. L. Zang, D. Wei, S. Wang, S. Jiang, Tetrahedron. 68 (2012) 636-641.
11. Y. J. Na, G. J. Park, H. Y. Jo, S. A. Lee, C. Kim, New J. Chem. 38 (2014) 5769-5776.
12. E. Hadjoudis, I. M. Mavridis, Chem. Soc. Rev. 33 (2004) 579-588.
13. J. Mei, N. L. C. Leung, R. T. K. Kwok, J. W. Y. Lam, B. Z. Tang, Chem. Rev. 115 (2015) 11718-11940.
14. A.T. Afaneh, G. Schreckenbach, J. Phys. Chem. A, 119 (2015) 8106-8116.
15. S. K. Padhan, M. B. Podh, P. K. Sahu, S. N. Sahu, Sens. Actuators B Chem. 255 (2018) 1376-1390.
16. D. S. Kim, K. H. Ahn, J. Org. Chem. 73 (2008) 6831–6834.
17. V. Thiagarajan, P. Ramamurthy, D. Thirumalai, V. T. Ramakrishnan, Org. Lett. 7 (2005) 657–660.
18. C. Yang, J. Xu, W. Chen, M. Lu, Y. Li, X. Wang, J. Mater. Sci. 49 (2014) 7040–7048.
19. D. Xua, M. Liua, H. Zoua, J. Tiana, H. Huanga, Q. Wana, Y. Daia, Y. Wena, X. Zhanga, Y. Wei, Talanta, 174 (2017) 803-808.
20. T. Han, Y. Hong, N. Xie, S. Chen, N. Zhao, E. Zhao, J. W. Y. Lam, H. H. Y. Sung, Y. Dong, B. Tong, B. Z. Tang, J. Mater. Chem. C, 1 (2013) 7314-7320.
21. S. K. Padhan, N. Murmu, S. Mahapatra, M. K. Dalai, S. N. Sahu, Mater. Chem. Front., 3 (2019) 2437-2447.

Dr. Satya Narayan Sahu *earned his M.Sc. degree in Chemistry from Utkal University, Odisha, in 2001 and received his M.Tech. degree in Modern Methods of Chemical Analysis in 2003 and Ph.D. degree in Organic Chemistry in 2009 from Indian Institute of Technology, Delhi. After completion of his Ph.D. he joined Sambalpur University, Odisha, as an Assistant Professor in Chemistry, and then moved to Bielefeld University, Germany for post-doctoral work after receiving the BOYSCAST fellowship in 2010 from the Department of Science and Technology, Government of India. His current research interest focuses on the synthesis of chromofluorescent molecular sensors for ionic and molecular recognitions.*

INDIAN SOCIETY FOR RADIATION AND PHOTOCHEMICAL SCIENCES

(Reg. No. 617/1985, GBBSD, Bombay; Trust No. F-10965)

Radiation & Photochemistry Division

Bhabha Atomic Research Centre, Mumbai - 400 085

Member Enrolment Form

1. Name in Block Letters:

2. Date of Birth:

3. Highest Academic Qualification:

4. Present Position:

5. Addresses:

Office	Residence
Telephone	Telephone
E-mail	E-mail

6. Address for Correspondence: Office / Residence

7. Category of Membership Applied for: Annual / Life /Corporate member

8. Remittance: DD in favour of 'ISRAPS' payable at MUMBAI
    For Bank Transfer:
    A/c No.10536133801, SBI, BARC Branch, IFSC SBIN0001268
    (e-mail the money transfer details along with the details requested above to
    israps.secretary@gmail.com and CC to jyotim@barc.gov.in)

Category	Fees	Admission fee	Total Amount
Annual	Rs 200/-	Rs 100/-	Rs 300/-
Life Member	Rs 1500/-	Rs 100/-	Rs 1600/-
Corporate Member	Rs 20000/-	Rs 1000/-	Rs 21000/-

9. Brief Resume of activities and research interests:

10. List of memberships of other professional bodies, if any:

11. List of prizes/awards/fellowships received, if any:

12. Number of Publications:

I agree to abide by the constitution and bye-laws, and rules and regulations of the SOCIETY.

Place: Signature

Date:

Photograph

Contents